THE INTERACTIVE EFFECTS OF CLIMATE, LAND COVER CHANGE AND DAMMING ON THE FLOW REGIME AND FINE SEDIMENT DYNAMICS OF A TROPICAL RIVER

BY

ZOE LUM XIN YI

Thesis submitted to The University of Nottingham for the degree of Master of Research in Biology and Biochemistry

May 2021

Abstract

Tropical river ecosystems are being increasingly modified by the accelerated construction of hydropower dams. Dams are known to have detrimental effects on downstream flows and sediment transport, with long-lasting implications for fluvial processes, habitats and ecosystems. The tropics are also experiencing high rates of deforestation and forest degradation. These types of land use change can alter components of the hydrological cycle through the modification of terrain characteristics, evapotranspiration and fine sediment runoff. Moreover, predictions of increased temperatures and changes in precipitation in tropical regions may further modify the hydrological cycle and, in turn, river flows.

The state of Sarawak, Malaysia, is witnessing the construction of 12 mega-dams as part of the Sarawak Corridor of Renewable Energy. The compounding effects of these dams, land use change and climate change pose a significant threat to the hydrology and overall functioning of rivers in Sarawak, but this threat has received little scientific attention. Baleh river was chosen as the study site because it is a typical Malaysian river surrounded by intact forest and its catchment is a headwater region with clear hydropower potential that will soon be realized. Thus, it is an area which can provide highly valuable new information on how large dams interact with landcover and climate change to alter river dynamics. This study therefore aimed to assess how damming, land cover and climate change interact and influence runoff of water and sediment in the River Baleh, a naturally forested tropical catchment in Sarawak. It incorporates two main components: (i) long-term land cover change assessment, and (ii) hydrological modelling of the impacts of the dam, climate and land cover change on flows and sediment loads in the Baleh. The land cover change assessment involved processing multi-temporal satellite images in Google Earth Engine (GEE) and carrying out supervised classification in ArcGIS. Besides providing empirical data on the magnitude and nature of land cover change across the Baleh catchment, the classified image outputs from this component formed input data for the second component - the catchment hydrological modelling. For the hydrological modelling, the Soil and Water Assessment Tool (SWAT) was used to simulate discharge and fine sediment loads for the whole of the catchment. The model was calibrated and validated using observed flow data. The performance of SWAT on daily and monthly time-steps was good (NSE > 0.62). Baseline conditions in the catchment were established with SWAT before running the future climate, land cover and dam scenarios; baseline models runs used the most recent five-year period. The future scenarios modelled the influence of land cover change with both low and high deforestation rates as well as climate models that involved increased temperature and decreased rainfall. Two operational scenarios were devised for the dam: a non-hydropower regime simply balancing dam outflow and inflows, to maintain lake levels and avoid dam spilling, while a hydropower regime was created which involved the dam operating at specific percentages of its capacity over the course of the year.

Analysis of satellite images indicated that there has been very minimal land cover change in the Baleh catchment over the last two decades (<2% reduction in forest cover) but a significant expansion of logging roads; these roads may promote future deforestation. SWAT models suggested that even high deforestation rates (loss of 5% per year) will not cause major hydrological changes in the Baleh River, but the models indicated dramatic increases in sediment yield from sub-catchments and, in turn, increases in the total amount of sediment exported by the catchment (up to 736% increase by 2050, compared to baseline). Modelling of climate scenarios suggested a counter-acting effect, with predicted lower rainfall and high temperature decreasing flow and sediment loads. SWAT simulations suggest that the dam will

have a greater impact on flow and sediment loads in the Baleh catchment than the future land cover and climate change scenarios that were modelled. The presence of the dam has the greatest impact on flow and sediment at the dam site, reducing sediment loads by approximately 95% and reducing discharge variability. Simulations suggest that impacts on flow are still evident almost 100 km downstream, despite tributary inputs. Impacts on sediment loads at the catchment outlet are more difficult to understand, because of how the river might adjust to cumulative alterations in flow, competence and supply over decadal timescales. Preliminary analysis for the first five years of dam operation suggests that sediment yield at the basin outlet may differ from baseline much less than it does at the dam site but further work on this is needed, particularly because of the sensitivity to exact dam operational regimes (which at present are unclear). The high sediment yield from the upper sub-catchments has implications for the operation of the Baleh dam due to siltation, but the large size of the reservoir means that even by 2050 its storage capacity will have been reduced by only around 5%.

Overall, this study demonstrates how models such as SWAT can be used to provide insights into the complex interacting effects of anthropogenic stressors in tropical catchments. It is recommended that a period of 10-30 years is used for SWAT studies of the downstream effects of dams, to capture the sequences of transient states which will evolve in response to altered flow regimes and sediment supply. The traits of tropical rivers such as the Baleh (high discharge and sediment loads relative to catchment area) and the numerous tributaries create the potential for more rapid downstream 'recovery' than in other hydroclimatic settings, but this is confounded by ongoing climate and land cover changes which modify boundary conditions. Modelling assessments of the type presented here should be complemented by empirical studies of fluvial adjustment, to fully understand the habitat and ecological changes that follow impoundment.

Acknowledgements

The completion of this thesis was only possible with the support from many people.

I would like to first thank my supervisor, Professor Christopher Gibbins, whose guidance and expertise were invaluable in forming the main framework for this study. Your feedback helped me not to lose sight of the bigger picture and developed my critical thinking skills. My co-supervisors, Dr Alex Lechner, Professor Ramon Batalla and Dr Damia Vericat were also extremely helpful in improving the research method and suggesting new ideas.

I would also like to extend my gratitude to Sarawak Energy Berhad (SEB), who funded my Master's and allowed me to pursue this research project. Many thanks to Karen Lee from SEB and Celine Chong, my colleague at the University of Nottingham, for assisting me in the data collection phase.

I would like to thank my husband, parents, and friends for their endless support and encouragement throughout this long process. Finally, I thank God for sustaining me with His strength, joy and peace. I give Him all the glory for the completion of this thesis.

Table of contents

CHAPTER 1. INTRODUCTION

1. Chapter 1 Introduction

1.1 Context

The construction of dams has been accelerated in recent years by rising global demand for renewable energy (Zarfl et al., 2015). This is largely due to the high effectiveness and relatively low cost of planning and development of hydroelectricity (Sternberg, 2010). Human intervention in the form of dams built for water supply, irrigation, power generation and flood control have altered river systems globally (Nilsson et al., 2005). Dams have significant effects on downstream flows and sediment transport. As the regulation of river flows by dams disrupts natural patterns of flow variability (Kummu & Sarkkula, 2008), habitat heterogeneity, water temperature, nutrient cycling and channel geomorphology are altered (Poff et al., 1997). Such alterations impact the biodiversity, functions and ecosystem services provided by rivers (Nilsson et al., 2005). Dams are also effective sediment traps as they retain much of the coarse and almost all of the fine sediment carried by rivers (Kondolf et al., 2014). This reduction in sediment supply leads to sediment-starved water which erodes the river banks and bed - so-called 'hungry water' - and alters geomorphic conditions downriver (Kondolf, 1997).

Many of the recent or planned hydroelectric projects are concentrated in tropical latitudes (Winemiller et al., 2016). Growth of energy from hydropower in Malaysia, as a developing country undergoing rapid industrial expansion, is evident in the last 10 years (Energy Commission, 2020). The state of Sarawak was identified by the federal government of Malaysia as the location for the second-largest economic development corridor (Athukorala and Narayanan, 2018). The Sarawak Corridor of Renewable Energy (SCORE) aims to generate renewable energy with 12 mega-dams and fuel industrial growth. Although Sarawak already has three operational dams and plans for at least six more, very little work has been done to investigate their effects on downstream rivers and their ecosystems (Ling et al., 2019; Ling, Soo, Heng, et al., 2016; Sim et al., 2016; Wera et al., 2019). In the tropics, the impact of dams is compounded by land cover change and climate change which can also alter river conditions, so such studies are needed as a matter of priority.

A major type of landcover change observed in SE Asia is the modification of forest cover. This takes the form either of complete clearance of forest (deforestation) or its degradation, both of which have become a major cause of concern over the last few decades, not just in SE Asia but globally (Achard et al., 2002; Sodhi et al., 2004; Stibig et al., 2014). The change occurs as a result of forests being converted into different land cover types, such as agricultural or urban areas. Forest degradation is the significant biomass reduction through the removal of mature trees, though with sufficient remaining tree cover to be still classified as 'forest' (Bryan et al., 2013). Both processes are accompanied by changes in species diversity and impacts on ecosystem process and dynamics. Within Southeast Asia, Malaysia has experienced the greatest amount of forest loss in terms of land area percentage (Hansen et al., 2013). Between 1973 and 2010, 23.1% of forests in Sarawak, a state in East Malaysia, were cleared and replaced by other land use types, while an estimated 57.2% of forest cover was logged in over the same period Gaveau et al., (2014). In the same study, Sarawak was also found to have the highest density of primary logging roads in Borneo, with 0.89 km of road per km2 of forest. Large networks of logging roads, which can be seen permeating unlogged forests at lower elevations in Sarawak, are a sign that forest loss will continue to expand (Cushman et al., 2017) and contributes to issues such as fine sediment runoff (Douglas et al., 1993).

Ongoing reductions in forest cover not only pose a threat to terrestrial biodiversity and carbon emissions but alter hydrogeomorphic processes. Land use change alters components of the hydrological cycle such as infiltration, surface runoff, evapotranspiration, and groundwater recharge (Öztürk et al., 2013), and land use has a greater influence than environmental characteristics on soil erosion at the catchment scale (Valentin et al., 2008). Studies have shown that agricultural and logging practices which severely modify terrain characteristics increase soil erosion rates and vulnerability (Vijith et al., 2018). In Malaysian Borneo (the states of Sabah and Sarawak), hotspots of soil erosion created by intense logging and degradation of vegetation have experienced up to 50-fold increases in sediment yield and altered river characteristics due to increased sediment loads into the rivers (Douglas et al., 1993). Both soil erosion and sediment export to rivers are serious environmental problems because of the negative downstream effects they have on water supply, water quality, sedimentation, flooding, and river ecology (Valentin et al., 2008). The expansion of agricultural land and deforestation also contributes to an increase in surface run-off and water yield, which leads to a rise in streamflow volume, and a decrease in the groundwater component (Woldesenbet et al., 2017).

Climate change alters the water cycle and consequently affects water availability and demand (Haddeland et al., 2014) can exacerbate the effects of land cover change. Based on the greenhouse gas emission scenarios for the 21st century (Intergovernmental Panel on Climate Change (IPCC)), climate change is predicted to cause increased temperatures and changes in precipitation, which are major drivers of the temporal and spatial distribution of river flows and groundwater recharge (IPCC, 2007; Kundzewicz, 2008). The frequency and intensity of heavy precipitation events are expected to increase, particularly in tropical regions such as Southeast Asia (Kundzewicz et al., 2007). Assessment of long-term changes of rainfall distribution throughout Sarawak indicated that even though there was significant temporal variation for annual rainfall, the monsoon months of January and December experienced increases in the lower and higher quantiles of rainfall (Sa'adi, Shahid, Ismail, et al., 2017). The daily mean temperature of Sarawak between 1977-2014 was also found to be increasing (at a rate of 0.105 to 0.121^{o}C per decade). Such climate changes, compounded by the loss of protective forest cover, heighten concerns about more frequent and intense flooding. Heavy precipitation events also cause the intensification of soil erosion and increase the amount of sediment transported into rivers and lakes (Issaka & Ashraf, 2017). As heavy metals, pesticides and non-point pollutants are transported with this fine sediment, higher sediment loads result in water pollution that has negative effects on ecosystem and human health (Kundzewicz, 2008; Ouyang et al., 2010).

The complexity and severity of the individual and combined effects of damming, land cover change and climate change on rivers in the tropics, given the pressures of these factors in rapidly developing tropical countries, should warrant more research. There has been no literature published on how such damming may interact with climate and land use change to alter river flows and sediment loads in rivers in Malaysia, so work is clearly needed. A combination of first principles and work published in other climate regions would suggest some counteractive effects, along with complex longitudinal variation. For instance, higher sediment runoff from catchment areas would be expected due to forest loss, with more intense precipitation exacerbating this. However, dams are known to trap virtually all of river fine sediment loads (add a ref), so in river sections immediately downstream from the dam, even under climate and landcover change it is possible that fine sediment in the channel is reduced. Further down from the dam, as undammed tributaries whose runoff is modified by climate and landcover change

add their water and sediment to the river, suspended load will increase. How far downstream the effects of the dam remain evident will depend a lot on the number and landcover in downstream tributaries. These interactions are explored in the thesis.

The Baleh was chosen because of the opportunity to build research findings into an operational flow regime for the dam, and to influence catchment management in advance of the dam being constructed. Unfortunately most dam environmental flow regimes have been developed retrospectively, after dam completion. This is mainly because in many parts of the world dams were constructed long before awareness of their impacts, and so ecological or environmental considerations to flow management were retrofitted by redesigning patterns of flow release. However, as awareness of dam impacts increases, dam operators are coming under increasing pressure to consider river ecosystems and fluvial integrity when designing dams and operational regimes. There is an opportunity to do this with the Baleh, by modelling the potential impacts of different possible flow operational scenarios and using these simulations to help develop 'least damaging' dam release regimes before the dam beings operating. Similarly, by modelling in advance of catchment landcover change (at present it remains largely forested), it may be possible to help contribute to efforts to conserve existing forest by showing their criticality for river integrity, in terms of flow regimes and sediment loads.

1.2 Research aims and objectives

There is potential for land use change, climate change and dams to have long-lasting effects on the hydrological functioning and health of tropical river systems. There is consequently an urgent need to understand the individual and compound effects of these factors, especially in Sarawak where they pose a significant threat but where knowledge is insufficient to guide catchment or river flow management.

A new hydroelectric dam is being built on the Baleh River, one of the main headwater tributaries of the Rajang. This study aims to assess how damming, land cover and climate change interact and influence runoff of water and fine sediment in the Baleh catchment. The research objectives are:

(i) To examine the nature and extent of long term land cover change in the catchment,

(ii) To assess the influence of this change on runoff (river flow) and fine sediment loads in the Baleh, and how flows and sediment loads may be further modified by ongoing climate change,

(iii) To assess how the presence of the dam alters flow and fine sediment loads in the downstream river.

The work involved modelling different land use and climate scenarios, and incorporating the dam into these scenarios. The work is funded by Sarawak Energy Berhad (SEB), the company that will operate the dam. Results will be used by SEB to help guide the management of the catchment and the operation of the dam, especially concerning fine sediment management. The study is the first in Malaysia to combine GIS techniques and hydrological modelling to assess the interactive effects of climate, land cover and damming on fluvial processes and dynamics at the catchment scale.

CHAPTER 2. STUDY AREA AND METHODS

2. Chapter 2 Study area and methods

2.1 Baleh catchment

The Baleh catchment is located in the state of Sarawak (Figure 1). Sarawak is the largest state in Malaysia, with an area of 124,450 km^2 and a population of around 2.81 million as of 2019 (Department of Statistics Malaysia, 2021). It is one of the two Malaysian states on the island of Borneo, hence, sharing borders with Brunei and Indonesian Borneo, Kalimantan. The Baleh River is a major tributary of Rajang River, the longest river in Malaysia (total length of approximately 565km). This river has its origins in the Nieuwenhuis range on the Kalimantan-Sarawak border in the east. The catchment is within the confines of the Kapit division, the state's seventh administrative division. Kapit Town, the nearest town outside of the Baleh catchment, can only be accessed by river transportation from Sibu, which acts as the gateway town to other parts of Sarawak.

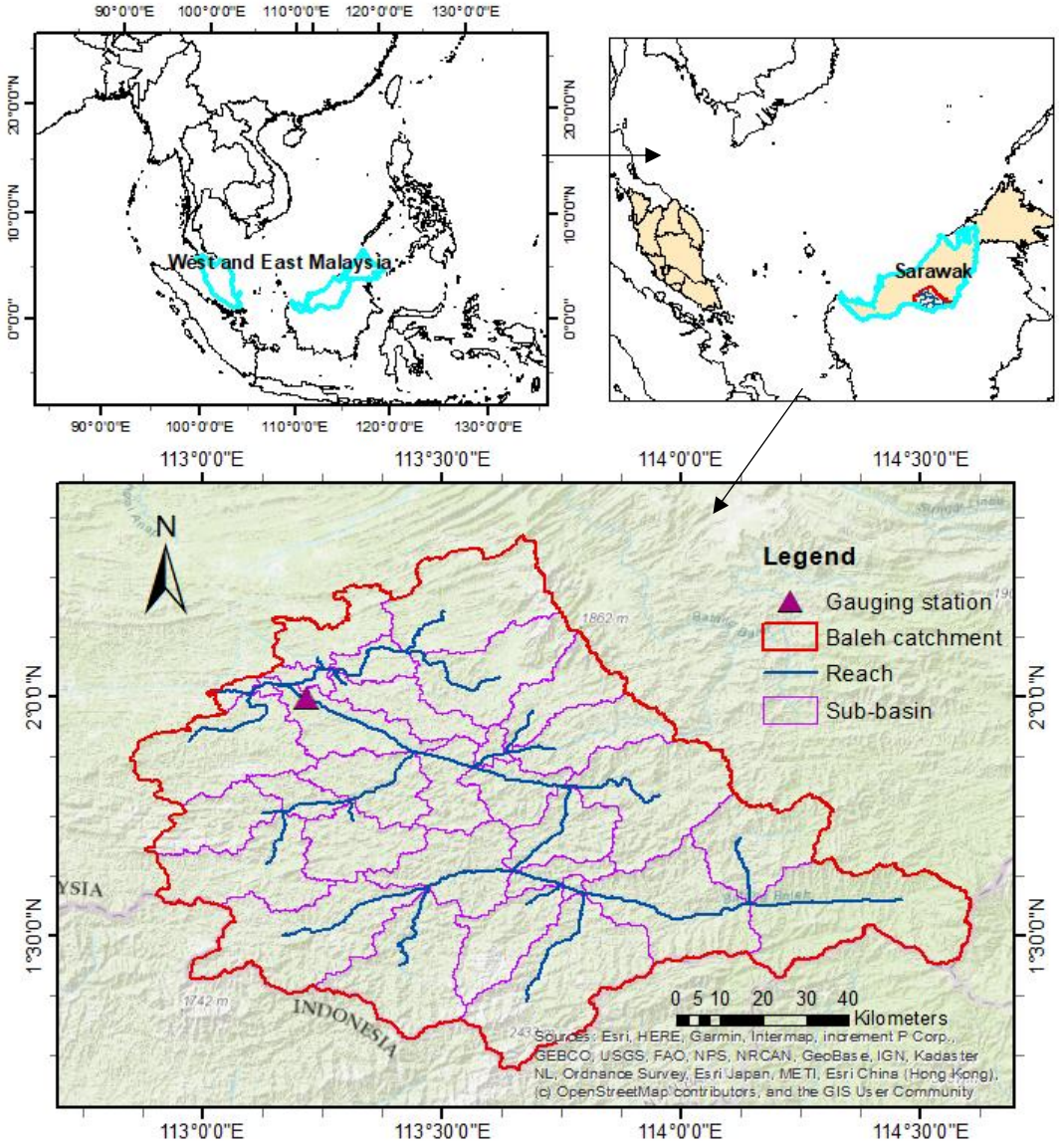

Figure 1. Clockwise from top left: location of Malaysia in Southeast Asia, location of Baleh catchment in Sarawak, boundary of Baleh catchment with reaches, sub-basins, and river gauging station. The sub-basins were defined in the SWAT analysis in Section 2.4.2.

The Baleh catchment has an area of 12,433 km^2. In 2017, the local government officially designated a portion of the Upper Baleh region, with a coverage of 66,721 hectares, as a National Park. A large proportion (>80%) of the Baleh catchment is covered by mix-dipterocarp primary forest, secondary forest, and various types of agricultural plantations. This is related to the fact that the catchment is located in the remote and not easily accessible mountainous region further away from the coast, which is where most of the urbanization and infrastructural development is concentrated. Baleh River is crucial in maintaining the hydrological and biological systems in the upstream area of Rajang (Muli et al., 2019). Most of the longhouses where the locals reside are located along Rajang and its tributaries. The local communities rely heavily on the river for transportation to Kapit for work and other business, water supply, and food (Abdullah, 2017).

2.2 Characteristics of the Rajang catchment

2.2.1 *Climate and soils*

Due to its location, the climate in Sarawak is influenced by the El Niño-Southern Oscillation (ENSO), Madden-Julian Oscillation (MJO), and Indian Ocean Dipole (IOD) (Gomyo & Koichiro, 2009; Hidayat & Kizu, 2010). Its climate is tropical, wet equatorial, with uniform temperatures and high humidity. Temperature is generally hot, varying from an average daily minimum of 23^{o}C to an average daily maximum of 32^{o}C while humidity exceeds 68% throughout the year (Sa'adi, Shahid, Chung, et al., 2017). Sarawak experiences two monsoonal seasons and is known to have high precipitation for most of the year with monthly rainfall ranging from 330 to 460 cm/month. This region has two monsoon seasons, the Northeast monsoon and the Southwest monsoon. The more prominent Northeast monsoon usually extends from November to January and is the wettest period of the year; the somewhat drier Southwest monsoon occurs from May to September (Diong et al., 2015). The majority of the Rajang catchment is covered by Red-Yellow Podzolic soils based on the Sarawak classification system (Tie, 1982). These soils comprise sandstone and shale bedrocks from the Nyalau and Belaga formations. The Belaga formation is composed simply of thick-bedded sandstone, thinly bedded heterolithic sandstone-mudstone interbeds and shale fancies (Abu Bakar et al., 2007). A study conducted in the Southwest region of the Rajang catchment discovered that the local soil texture was dominated by sand (69.9% to 83.4%), followed by clay (6.6% to 26.7%) and silt (0.2% to 14.8%) (Ling, Soo, Sivalingam, et al., 2016). The pH of the soil ranged between 4.8 to 6.11, indicating that it is slightly acidic. Measured water and organic carbon in the soil ranged between 1.25 to 1.8% and 0.15 to 0.23%.

2.2.2 *Conservation priorities*

The key threat to wildlife and the ecosystem in the Rajang Basin is commercial logging (Brander et al., 2018; Bryan et al., 2013). Logging is extremely detrimental because it reduces the area of intact forests and promotes fragmentation, both of which negatively affect species diversity and abundance (Sodhi et al., 2004). To promote sustainable development and protect biodiversity, the Malaysian, Indonesian, and Bruneian government signed an official declaration in 2006 to support the Heart of Borneo (HoB) Initiative by committing funding and resources (Persoon & Osseweijer, 2008). This transboundary project is championed by the World Wildlife Federation (WWF) with the aim of preserving charismatic megafauna, landscape connectivity, and ecosystem services in a 220,000 km^2 area in the upper to middle parts of Borneo. The HoB

Initiative covers a large part of the Rajang watershed and approximately 70% of the Baleh catchment. There have been several surveys done in the Baleh region since the launch of this initiative to acquire baseline information for the formulation of a conservation management plan. These surveys are briefly explored in the paragraphs below.

In November 2015, an avifauna survey was conducted in the logged-over forest of Upper Baleh as part of the Upper Baleh HoB Expedition to collect baseline data on the avifauna species present in the study area (Tuen et al., 2018), which is in the upper part of the Baleh catchment, on the border with Indonesia. Birds are important agents in recovery from disturbance and forest regeneration as they provide ecological services which include pollination and seed dispersal. Despite the presence of logging and shifting cultivation during the expedition, 69 species were recorded using the observation method while 36 species were recorded via mist-nets. There were four endemic species, seven 'Totally Protected', and 18 'Protected' species as listed under the Sarawak Wild Life Protection Ordinance 1998. The diverse community of birds, with the presence of charismatic species like hornbills and eagles, highlights the significance of the study area as well as its potential to support ecotourism.

Mohd-Azlan et al. (2019) carried out a camera-trapping study in the same area to identify medium to large mammal species of conservation importance. The results of this study affirmed that the Upper Baleh region is home to a variety of medium to large mammals, including Hose's civet, Bornean bay cat, and sun bear, which have conservation value. The authors expressed concern regarding the impact of the Baleh Dam construction on animal habitat and potential wildlife corridors connecting the newly designated Baleh National Park to Betung Kerihun National Park in Kalimantan, Indonesia. The validity of this concern is supported by a separate study which concluded that among the 13 planned hydroelectric dams in Sarawak, Baleh Dam will impact the largest area of core forest (~109,000 ha) and general forest (~180,000 ha) (Alamgir et al., 2020).

Nyanti et al. (2019) surveyed fish fauna composition and assessed environmental conditions in the Upper Baleh River. Surveys were conducted in April and November 2015. Fish diversity was considered moderate, with Shannon's diversity index of 2.9, while species richness is considered high with Margalef's richness index value of 6.0. Pielou's evenness index of 0.8 shows that the fish assemblages are considered evenly spread across the study area. Diversity and richness differed between the main stem and tributary sites, with higher values at the main stem. The authors also found that sedimentation, stream order, and elevation were the most significant factors affecting fish assemblages. Three of the most abundant species did not show healthy conditions based on Fulton's condition factor. Fulton's condition factor is a health index of fish calculated from the relationship between the weight of a fish and its length. It is suspected that exposure to highly turbid waters with suspended solids could have stunted their growth and reduced their feeding rate. Analysis of water samples obtained from the Upper Baleh river revealed high suspended sediment concentrations, especially after rain, with the highest recorded value being 24 mg/L (Ling, Soo, Sivalingam, et al., 2016).

The studies mentioned above clearly show that the largely forested landscape of the Baleh catchment has significant biodiversity value. Future land cover change due to commercial logging, agriculture and infrastructural developments may lead to the deterioration of the physical and ecological health of river and stream systems across the catchment. Hence, this study is valuable because it explores the interactive effects of land cover change, climate change

and the Baleh Dam on the catchment. A better understanding of how these elements affect hydrological processes can help support sustainable management of the Baleh catchment, both in terms of land use practices and flow management.

2.3 Baleh Dam

Sarawak Corridor of Renewable Energy (SCORE) is a multi-hundred-billion-dollar infrastructure development plan in Sarawak, which aims to draw an investment of US$105 billion and build 12 hydroelectric dams generating 20,000 MW along a 320 km corridor encapsulating more than 70,000 square kilometres (Sovacool & Bulan, 2012). Baleh Dam was approved by the Sarawak state cabinet in 2016 and is expected to have a total installed capacity of 1,325 MW. The dam will have a catchment area of 5,625 km^2 (Figure 2). Hydropower will be produced from five turbines, each producing 265 MW (approx. 177 m3/s; Table 1; data from Sarawak Energy Berhad, pers comm). Table 1 provides some technical details on the dam and reservoir. These data were used for the SWAT models that involved assessing the impacts of the dam on downstream flows and sediment dynamics. Precise details of the dam operational regime are currently unclear and this has rather constrained modelling of dam impacts (see further details below).

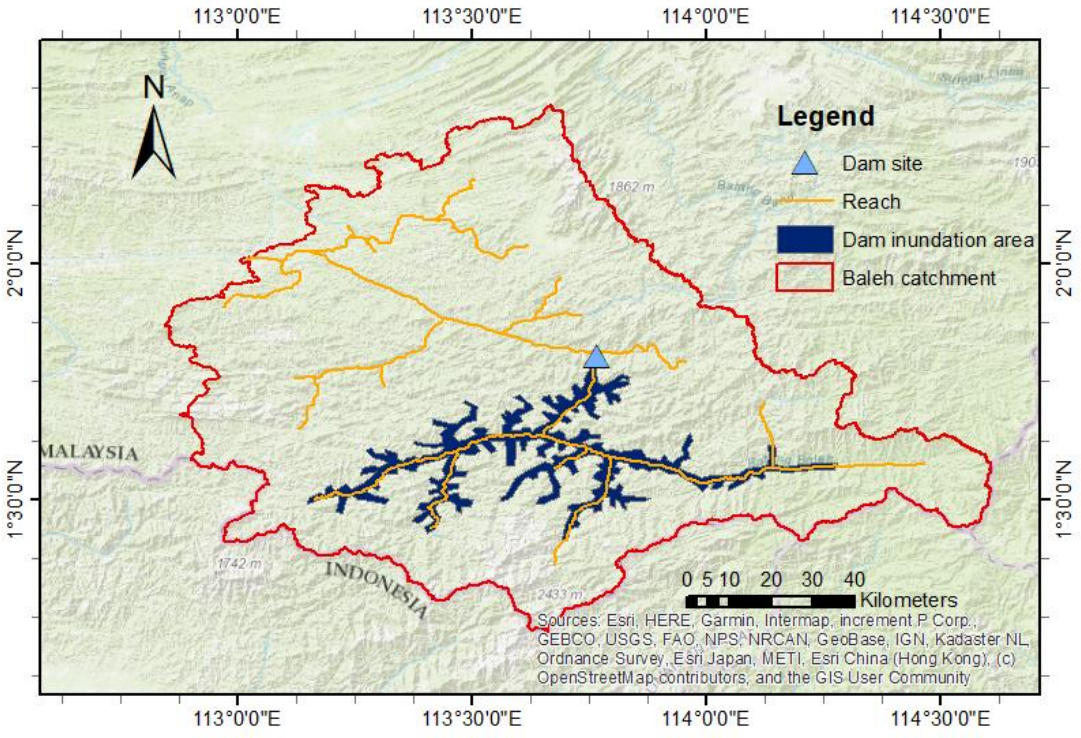

Figure 2. Map of the dam site and the reservoir area of Baleh Dam within the Baleh catchment.

Table 1. Baleh Dam technical information provided by SEB. Full supply level (FSL) is the normal maximum operating water level when not affected by floods, this water level corresponds to 100% capacity. Minimum operating level (MOL) is the water level in a reservoir below which water must not be released.

Reservoir Data and Water Levels	
Full Supply Level (FSL)	220 masl
Minimum Operating Level (MOL)	205 masl
Maximum Flood Level	225 masl
Reservoir Area at FSL	588 km²
Reservoir Area at MOL	470 km^2
Volume at FSL	29,867 x 10^6 m^3
Active Storage (intake operating range 205 to 220 masl)	7,817 x 10^6 m^3
Power Generation Data	
Nominal Plant discharge per turbine	177 m^3/s
Turbine Rated Output Per Unit	265 MW
Installed Capacity	1,325 MW

2.4 Methods

This study incorporates two main components: long-term land cover change assessment and hydrological modelling of future scenarios for the whole Baleh catchment. The land cover change assessment involves processing multi-temporal satellite images in Google Earth Engine (GEE) and carrying out supervised classification in ArcGIS. As well as providing empirical data on the magnitude and nature of land cover change, the classified image outputs from this component form input data for the second component - the catchment hydrological modelling. For the hydrological modelling, the Soil and Water Assessment Tool (SWAT) was used to simulate discharge and fine sediment loads. The model was calibrated and validated with observed data before being used to simulate future scenarios. It is the first time this method has been applied in the Rajang watershed. The two components will be explained in greater detail in the following sub-sections.

The study area was selected as being the Baleh catchment upstream from the Rajang-Baleh confluence. This meant that the effects of land cover and climate change, as well as damming, were assessed across the whole of the Baleh catchment. While effects of changes in the Baleh may also be evident further downstream in the main-stem Rajang, interpretations are likely to be confounded by the fact that flows are influenced by water coming in from the Rajang headwaters and multiple other tributaries downstream from the confluence, which will at least dampen effects of damming and potentially alter fine sediment loads. Confining the analysis to impacts within the Baleh avoids such complications, and in particular, allowed for a focus on the effects of the dam on the section likely to be most affected.

2.4.1 *Remote sensing analysis of land cover change*

The advancement of remote sensing technology has made satellite data one of the most valuable tools for assessing spatial and temporal patterns of land cover change. Remote sensing can be paired with Geographic Information Systems (GIS) techniques to process and analyse multi-temporal satellite data with image classification for the mapping and identification of land cover change. The possibility of classifying land cover change patterns over a long duration of time provides insights into interactions between humans and the natural environment in greater detail and is particularly valuable for sustainable landscape planning and management.

One of the most widely used satellite data is Landsat imagery. The Landsat satellite program started with the launch of Landsat 1 in 1972 as the first multispectral remote sensing instrument in space (Markham et al., 2004). Since then seven more successful Landsat missions have been launched, making Landsat data the longest consistent record available to document global change. The latest addition launched in 2013 is Landsat 8, which carries the Operational Land Imager and Thermal Infared Sensor. Landsat 8 provides imagery at 30-meter resolution with visible, shortwave infared, near infared bands; 100-meter resolution with thermal infared band; and 15-meter resolution with the panchromatic band ("Landsat 8", 2021).

Landsat data are suitable for land cover change detection and mapping studies because they provide high resolution (30 m) image collection at a potential frequency interval of 16 days with almost global coverage, with multiple Landsat sensors in orbit. Many studies have been conducted in Asia using Landsat. For example, most recently, Hu & Hu (2019) used Landsat imagery to derive annual land cover maps of Central Asia from 2001 to 2017 and study land cover distribution and dynamics. Hurni et al. (2017) studied the expansion of boom crops between 2000 to 2014 in mainland Southeast Asia by classifying land cover change of Landsat imagery which had been grouped into five periods of three-year time step composites.

Due to the optical nature of Landsat imagery, the presence of atmospheric contamination such as cloud and haze can be major limitations in creating accurate maps. Cloud cover is especially an issue in tropical countries, with Southeast Asia being one of the cloudiest regions in the world (Li et al., 2018). The application of advanced cloud identification and image compositing algorithms are therefore necessary to overcome this issue. Image compositing is the process of reducing large datasets of satellite imagery into single datasets with uncontaminated and "valid" data by applying a set of user-defined rules (White et al., 2014). Oliphant et al. (2019) found that 3-year composites produced the best quality gapless cloud-free images due to extremely cloudy areas found in Borneo and Sumatra when using Landsat time-series data.

The development of cloud-computing resources for geographic data analysis has enabled efficient image processing on highly computational intensive tasks involving machine learning algorithms and large volumes of imagery. Google Earth Engine (GEE) is a cloud-based platform that offers access to a vast collection of publicly available satellite data and advanced algorithms with parallel processing capabilities through the optimization of Google's computational infrastructure (Gorelick et al., 2017). It utilises a JavaScript code editor interface to enable users to test and develop algorithms, and also display results in real-time. GEE has been tested and applied successfully in Southeast Asia by Miettinen et al. (2019), Oliphant et al. (2019), and Pimple et al. (2018).

2.4.1.1 *Generation of multi-temporal cloud-free composites in Google Earth Engine*

GEE was used to access and obtain satellite images from Landsat 5, 7, and 8 processed by the United States Geological Survey (USGS). Multi-temporal land change analyses with Landsat data is more reliable and consistent when the digital number of the image bands are converted to surface reflectance values (Townshend et al., 2012). Multi-date images are more comparable through the conversion to surface reflectance which accounts for atmospheric and solar illumination effects (Hall et al., 1991). Landsat surface reflectance products are readily available to download on GEE and were used in this study. Landsat 8 images are available from April 2013, while Landsat 7 images are available from Jan 1999. Landsat 7 data acquisition is severely affected by the failure of the sensor's Scan Line Corrector (SLC), which results in a data loss of 22% for every scene (Markham et al., 2004). Hence, Landsat 5 images were incorporated into the analysis of the Baleh. A preliminary visual assessment using GEE and Google Earth Pro of the Landsat images from 2000-2019 showed that cloud cover was severe and there are insufficient daily cloud-free images of the study area for the entire period.

To overcome the cloud cover issue in the assessment of the Baleh, a cloud masking algorithm in GEE was used; this filters through a collection of images for the catchment area within a designated period, removes pixels recognized as clouds, and selects the clearest pixel in the collection to create a cloud-free composite for that period based on the summary statistic specified. The algorithm was tested with several summary statistics (mean, median, 25th percentile, 50th percentile, 75th percentile), and the one which produced the best results from visual inspection of the end product was selected. Different subsets of periods were also tested (Jan to Dec, Jan to June, July to Dec, 2 years) to find images with a lower percentage of cloud cover. The 2-year time period proved best as it yielded better chances of finding clear pixels across the study area.

The overall goal of the analysis was to assess long term changes in land cover. Three bi-annual satellite image composites representing periods in the past were chosen to assess historical patterns, commencing in 2000 (2000-2001, 2007-2008, 2011-2012) while the composite for 2018-2019 was used to create the most recent land cover map of the area (i.e. considered to be 'current' land cover). These image composites were downloaded as raster files to be further processed with ArcGIS.

2.4.1.2 *Supervised classification and accuracy assessment*

Pixel-based satellite image classification methods can be divided into two broad groups: unsupervised and supervised classification. Unsupervised classification is achieved by applying algorithms that analyse pixels within an image and produces computer-defined clusters based on spectral patterns with no direct connection to land cover types. The supervised approach requires human selection of training data for the land cover classes being considered and the application of a classification algorithm. This study utilises a supervised classification.

There are a variety of classification algorithms, including maximum likelihood classification (MLC), support vector machine (SVM), classification and regression trees (CART) and random forest (RF). The improvement of computational data processing capabilities has paved the way for non-parametric classification methods (e.g. SVM, CART and RF) to replace traditional parametric classification approaches (e.g. MLC). Non-parametric supervised classification algorithms are more efficient and accurate because they do not impose assumptions on data

distribution. Studies in Southeast Asia have shown positive results with non-parametric classification approaches (Cheng et al., 2016; Jhonnerie et al., 2015).

Using ArcGIS, training samples were created for all four of the Baleh satellite image composites to obtain the most accurate pixel signature for six land cover classes: forest, bare earth, built-up areas, disturbed vegetation, and shadow. The shadow class was included to account for remaining fuzzy or cloud shadow pixels. Supervised classification requires the training data to be completely representative of the classification problem; i.e. what is not included in the training samples will not be identified by the classifier. The shadow pixels were later replaced with 'forest' as forest proved the most abundant land cover class (>90% coverage) in the study area. This step was necessary to ensure the classified maps had no data gaps within the study area boundary as such gaps could introduce errors in the SWAT model. Due to its constantly high suspended sediment concentration, the river within the study area is a muddy-brown colour. This meant that there was difficulty differentiating the river channel from the bare earth land cover class. The decision was made to omit the river channel from the supervised classification.

RF, MLC and SVM were applied to the training dataset to produce preliminary classified images. RF was selected as the classifier for the study because it produced more visually accurate results in comparison to the others. This is consistent with a recent study by Cushman et al. (2017) who found that RF outperformed other methods in predicting and classifying forest loss in Borneo. RF is an ensemble machine algorithm with a collection of decision tree models acting as base classifiers to produce repeated multiple classifications of the same data (Breiman, 2001). An accuracy assessment was carried out for all four classified images with the generation of random sampling points. Next, a non-supervised classification was conducted to extract the main branch of the river as a separate layer. The river coverage was manually corrected and drawn where the extraction was not sufficient or accurate. This river coverage layer was then assimilated into the RF classified outputs under the new class, 'river channel' to produce the final classified land cover maps.

The post-classification comparison (PCC) method, one of the most widely-used change detection techniques, was used to investigate the land cover change in the study area (Chughtai et al., 2021). The PCC method identifies land cover changes by comparing classified images from different dates. This method not only provides information on the location but also the nature of the land cover change from one class to another (Mas, 1999). PCC was applied to each pair of classified maps (2001-2008, 2008-2012, and 2012-2009) to produce land cover change maps and the cross-tabulation matrix between every pair.

2.4.2 *Hydrological modelling with SWAT*

Hydrological models are used to predict and understand various hydrological processes by trying to simulate various characteristics of catchments such as climate, land cover and soil with a quantitative modelling framework. They have become indispensable and widely used in water and environmental resource management (Devia et al., 2015). Some examples of hydrological models include Hydrologic Engineering Centre - The Hydrologic Modelling System (HEC-HMS), Systeme Hydrologique European (MIKE SHE), Soil and Water Assessment Tool (SWAT) and TETIS. Each differs slightly in what they aim to do, and the data needed. SWAT is one of the most widely used models worldwide and has been successfully applied in watersheds with various climate and terrain characteristics. The US Agricultural Research Service developed SWAT as a

semi-distributed time-continuous physically based catchment model that can evaluate the influence of land use, climate, and agricultural activities on water quality and sediment yield (Arnold et al., 1998). The model delineates the main river catchment into smaller sub-catchments which represent hydrologic response units based on land use, vegetation, soil and slope characteristics. SWAT requires several types of input data, such as land use, temperature, topography and precipitation, to quantify the water balance of a watershed. The hydrological simulation has two components, the land phase and the routing phase. The land phase of the model controls the amount of water, sediment and nutrient loadings in each sub-basin delivered to the main channel. The routing phase involves the movement of water, sediment and nutrient through the river network of the catchment to each basin outlet (Neitsch et al., 2011).

SWAT is available in various forms of software. ArcSWAT was selected for the present study as it is a user-friendly plug-in that works within the ArcGIS suite.

2.4.2.1 *Input data*

A Digital Elevation Model (DEM) was obtained from the NASA Shuttle Radar Topography Mission (SRTM) with a resolution of 30 m per pixel, which matches the Landsat imagery. This is used in ArcSWAT for delineating the watershed and sub-watersheds. Slope values are automatically generated in ArcSWAT with the DEM. A local soil map produced by the Department of Agriculture Sarawak in 1968 was used for modelling. This was compared against the FAO-UNESCO Soil Map of the World (SMW) for the whole of Sarawak. The soil classes between both maps had broadly similar soil groups and all 3 soil classes for the Baleh region in the local soil map belonged in the same soil group. Hence, the soil classes and properties from SMW for that soil group was extracted and used for the modelling. Outputs from the supervised classification component mentioned previously were used as land use maps.

Daily rainfall data from 1998-2019 were obtained from the Department of Irrigation and Drainage (DID) for seven rainfall stations; six of them are located within Baleh catchment while one is at Kapit Town, a short distance downstream of the Baleh-Rajang confluence (Figure 3). Out of these seven rainfall datasets, several stations had long gaps in the recorded data so they could not be used for the SWAT model. The NCEP Climate Forecast System Reanalysis (CFSR) available on the SWAT's official website was used to obtain the daily minimum and maximum temperature, relative humidity, wind speed and solar radiation, all required by the model. CFSR is a high resolution, global, coupled atmosphere-ocean-land surface-sea ice system generated from meteorological model reanalysis, which is a combination of field and surface observations, a meteorological model, and remote sensing data. It has been tested and applied in tropical watershed models successfully (Duan et al., 2019; Lauri et al., 2014; Tan et al., 2017).

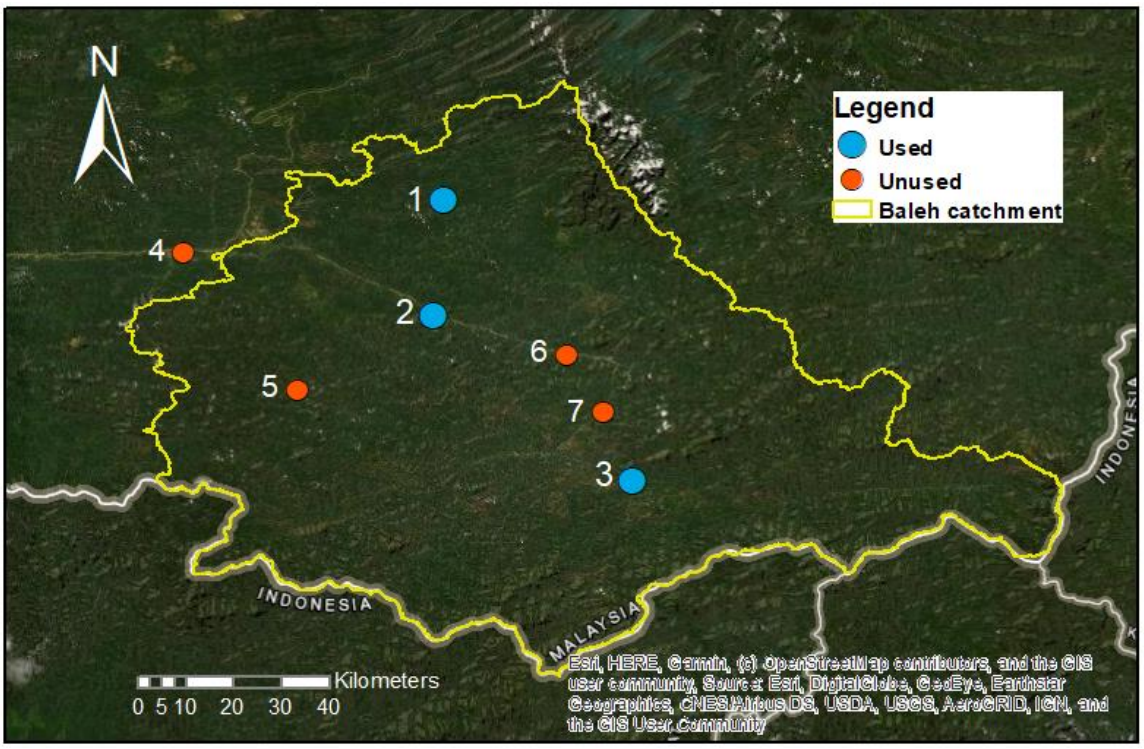

Figure 3. Map of rainfall gauges: Used – 1. Nanga Tiau, 2. Gaat Baleh, 3. Nanga Melatai; Unused – 4. Kapit Headworks, 5. Nanga Balang, 6. Nanga Entawau, 7. Nanga Merurung.

2.4.2.2 *Model calibration and validation*

Model calibration involved changing model input parameter values to produce simulated values of discharge, evapotranspiration or sediment that are as close as possible to the measured data. This step is required to ensure model parameters are optimized. SWAT-CUP (Calibration and Uncertainty Procedures) is a program developed to perform calibration of SWAT (Abbaspour et al., 2007). The program offers five calibration procedures as well as validation and sensitivity analysis tools. Several studies have indicated that the SUFI-2 (Sequential Uncertainty Fitting version 2) technique performs well in tropical areas and it is computationally efficient (Rafiei Emam et al., 2018; Shivhare et al., 2018). Hence, SUFI-2 was selected for this study.

The SUFI-2 technique is a stochastic algorithmic approach that represents all sources of uncertainties on the parameters (expressed as ranges or uniform distributions) in an interactive process and attempts to capture most of the measured data within the 95% prediction uncertainty bounds (95PPU) of the model. The 95 PPU is calculated at the 2.5% and 97.5% levels of an output variable's cumulative distribution obtained using Latin hypercube sampling. The strength of the calibration can be evaluated through the goodness of fit between the two bands, which are 95PPU for model simulation and measured data, with two statistics: P-factor and R-factor (Abbaspour, 2012). P-factor is the fraction of measured data, including its error, enveloped by the simulation result, and ranges from 0 to 1. The R-factor is the ratio of the standard thickness of the 995PU band and the standard deviation of the measured data and ranges from 0 to infinity. A P-factor of 1 and an R-factor of zero would be a simulation that precisely corresponds to the measured data. Hence, a strong calibration would have a high P-factor and a low R-factor.

For the Baleh catchment calibration, daily flow data measured at the Teluk Buing gauging station (1°59'50.0"N 113°13'20.0"E) were used. This is the only operational flow gauging station within the catchment (Figure 1). Discharge data are available from 1967 to 2012. To make an objective decision on which years to use for calibration and validation (C&V), some analyses produced by Chong (unpublished PhD thesis) were used. Modelled discharge data were included in these analyses for the years 2013-2017 to provide insight into more recent flow conditions but were not used in the final C&V. Chong calculated metrics related to discharge magnitude, duration, frequency, variability, timing, and rate of flow for the Baleh flow data set. These metrics were used to characterise the whole regime of each year using PCA (Figure 4). After examining the PCA plot (Figure 4), the period from 2004 to 2010 was selected for C&V. These years are highlighted in Figure 4; they extend across much of the PCA and so cover a good range of flows - some moderately high, some moderately low, and some close to the norm (i.e. close to the origin on the plot). These years are shown in the flow duration curve plot (Figure 5), along with the overall (long term) curve and are considered to be representative of a good range of years with different hydrological conditions to use for C&V. Key flow statistics for the C&V years are compared to respective long term values in Figure 6.

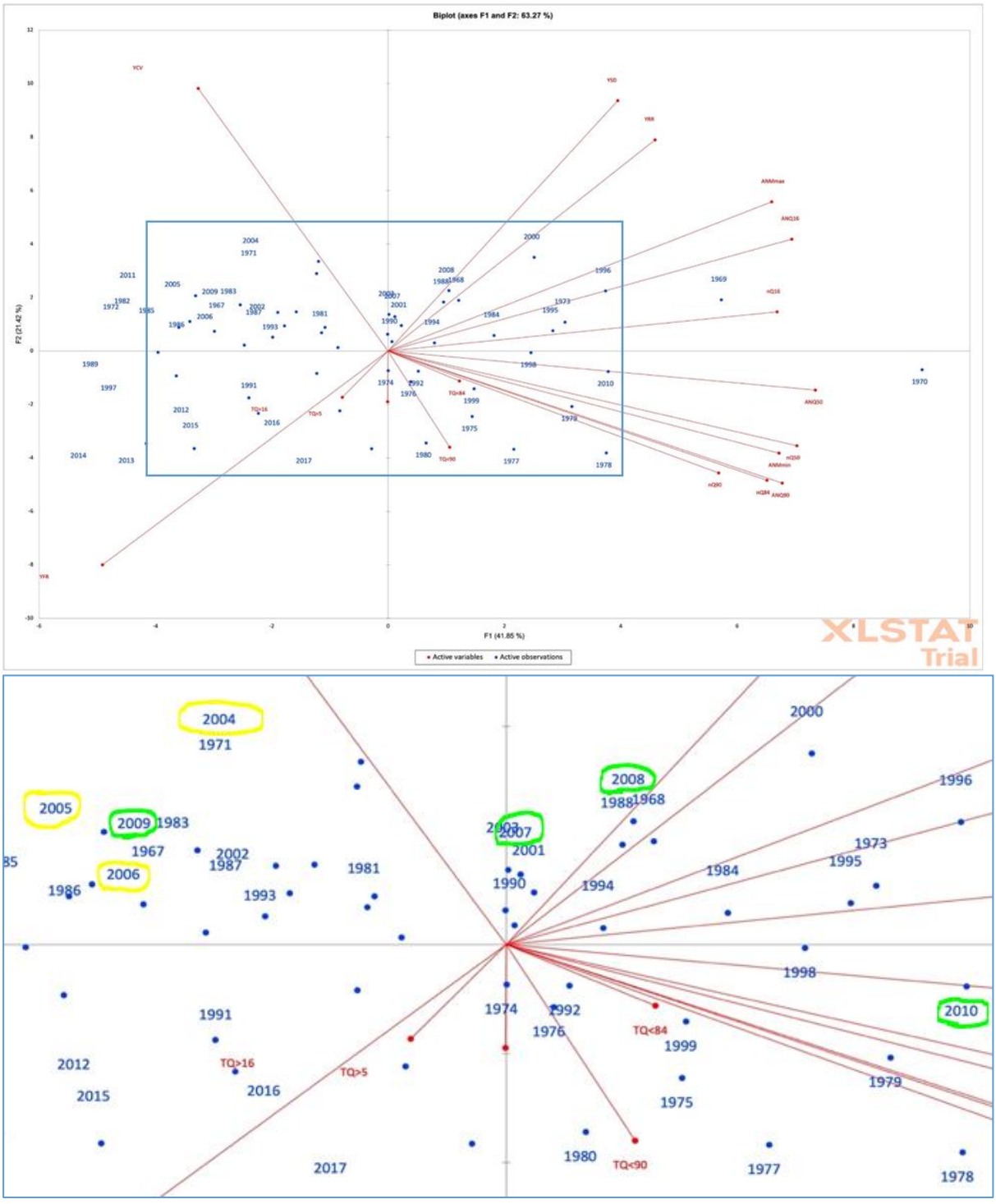

Figure 4. Top - PCA with all the flow metrics values for 1967-2012. The principal component 1 and 2 explains 41.85% and 21.42% of the variation. The variables include mean maximum monthly discharge (annual) (ANM max), mean minimum monthly discharge (annual) (ANM min), annual Q16 (ANQ16), Q50 (ANQ50) and Q90 (ANQ90), number of times exceeded Q5 (nQ5), Q50 (nQ50), Q84 (nQ84) and Q90 (nQ90), standard deviation (yearly) of Q (YSD), coefficient of variation (yearly) of Q (YCV), timing of Q5 (TQ>5), Q16 (TQ>16), Q84 (TQ>84) and Q90 (TQ>90) in a year, rise rate of each year (YRR) and fall rate for each year (YFR); Bottom: Inset of PCA with the years selected as the calibration and validation period circled in yellow and green respectively.

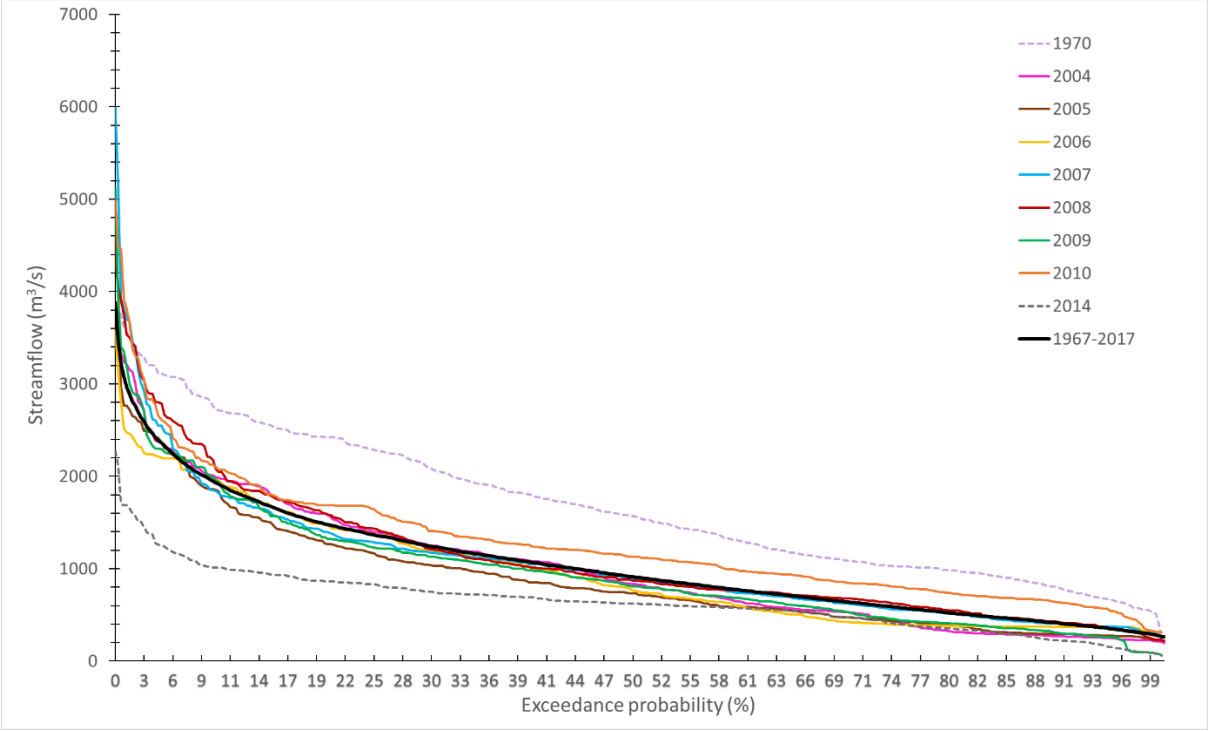

Figure 5. Flow duration curve for calibration and validation (C&V) years. The C&V years are shown along with the overall long term curve and those for the highest (1970) and lowest flow (2014) years in the long term record.

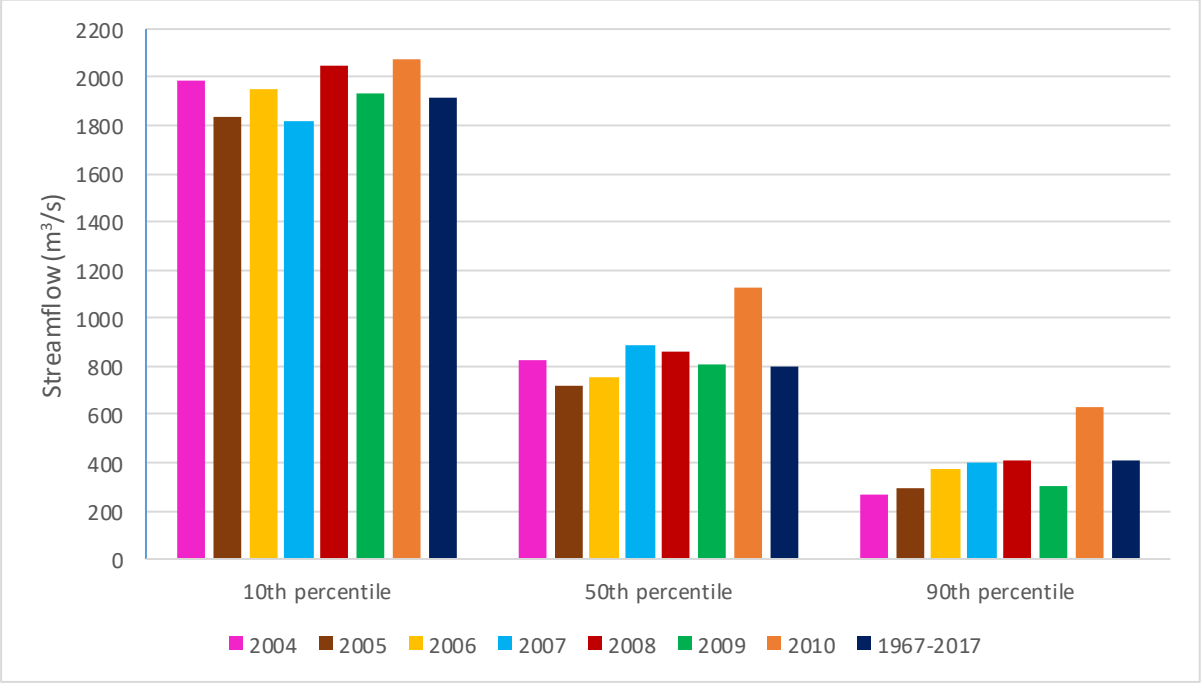

Figure 6. Streamflow at the 10th, 50th and 90th percentile for 2004-2010 as well as the average value for the whole long-term record (1967-2017).

Based on Abbaspour (2012), Amirabadizadeh et al. (2018) and Tarigan et al. (2018), 20 environmental parameters were chosen to use for calibration, with their initial minimum and maximum values used to set up the SWAT model for an initial run. Next, the sensitive parameters from the initial run were identified using SWAT-CUP's sensitivity analysis. Parameter sensitivities are determined through calculation with a multiple regression system followed by a

t-test, which produces two statistics: a t-statistic and a p-value. A parameter is more sensitive when it has a larger absolute value of t-statistic and a smaller the p-value, the more sensitive the parameter. Based on the t-stat and p-value of the 20 variables, 14 sensitive variables were incorporated into the subsequent C&V process (Table 2).

Table 2. Parameters selected for the calibration of the daily and monthly simulations after eliminating the less sensitive variables

Code	Parameter name
CN2	SCS runoff curve number, f
USLE_P	USLE equation support practice factor
CH_K2	Effective hydraulic conductivity in main channel alluvium.
CH_N2	Manning's "n" value for the main channel
GW_DELAY	Groundwater delay (days)
GW_REVAP	Groundwater "revap" coefficient
GWQMN	Threshold depth of water in the shallow aquifer required for return flow to occur (mm)
SOL_K	Saturated hydraulic conductivity
SOL_AWC	Available water capacity of the soil layer
REVAPMN	Threshold depth of water in the shallow aquifer for "revap" to occur (mm)
EPCO	Plant uptake compensation factor
ESCO	Soil evaporation compensation factor
CANMX (PAST, FRST)	Maximum canopy storage.

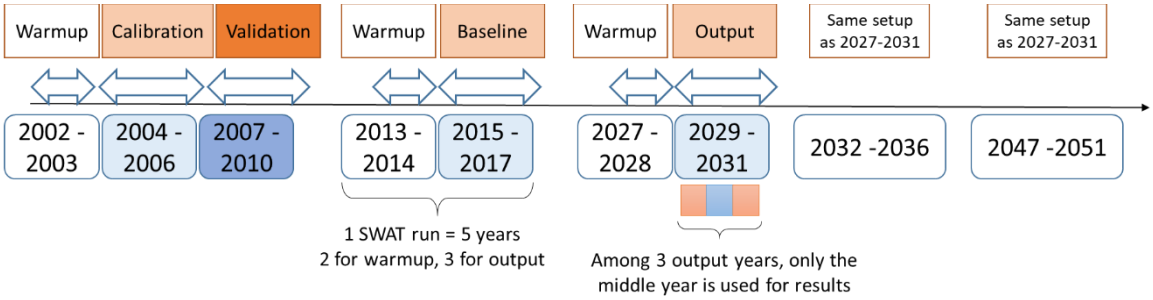

Figure 7. Conceptual diagram for the timeline of calibration and validation years, baseline years and future scenario years.

An overview of the modelling process is provided in Figure 7. This followed standard protocols involving calibration and validation, followed by model runs for periods of interest. For these periods, the convention is to run the model for at least five years, with the first two of these five used as what are timed 'warm-up' years; the remainder of the run period is then used for analysis and interpretation of patterns. For the Baleh, SWAT was calibrated and validated with two different time steps, daily and monthly, to assess and compare model performance for both. For the daily time-step, 2002-2006 was used for warm-up, 2007 for calibration and 2008 for validation. For the monthly time-step, the model was allowed to warm up from 2002-2003, then calibration was done for 2004-2006 and validation was carried out for 2007-2010. The C&V was assessed with the statistical performance measure values in terms of coefficient of determination (R^2), Nash Sutcliffe efficiency (NSE), per cent bias (PBIAS). R^2 is the square of the correlation (r) between simulated values and observed values, with a range of 0 to 1. It is interpreted as 'the proportion of variance in the dependent variable that is predictable from the independent variable' so quality of the simulation is better when it is closer to 1. NSE is a

normalized statistic that calculates the relative magnitude of the residual variance in comparison to the measured data variance (Nash & Sutcliffe, 1970). In the example of a perfect situation where the model has an estimation error variance of zero, the resulting Nash-Sutcliffe Efficiency equals 1 (NSE = 1). PBIAS determines the average tendency of the simulated values to be larger or smaller than the observed values. Its optimum value is zero and values with lower magnitude indicate better simulations. Positive values imply underestimation by the model whereas negative values are indicative of model overestimation (Gupta et al., 1999).

Table 3. Summary of reported SWAT model performance in Southeast Asia (Tan et al., 2019).

Frequency Ranges	Monthly				Daily			
	Calibration		Validation		Calibration		Validation	
	NSE	R^2	NSE	R^2	NSE	R^2	NSE	R^2
0.90–1.00	52	32	49	36	14	1	17	3
0.80–0.89	81	45	55	27	20	19	17	16
0.70–0.79	40	11	59	51	31	17	37	19
0.60–0.69	26	6	28	49	22	18	35	13
0.50–0.59	12	1	34	12	27	13	22	14
0.40–0.49	3	0	34	8	17	5	10	5
0.30–0.39	1	0	4	2	9	1	10	0
0.20–0.29	1	0	2	3	3	1	2	1
0.10–0.19	0	0	3	3	1	0	1	0
0.00–0.09	0	0	3	0	0	0	0	1
<0	1	0	4	0	1	0	4	0
Total	217	95	275	191	145	75	155	72

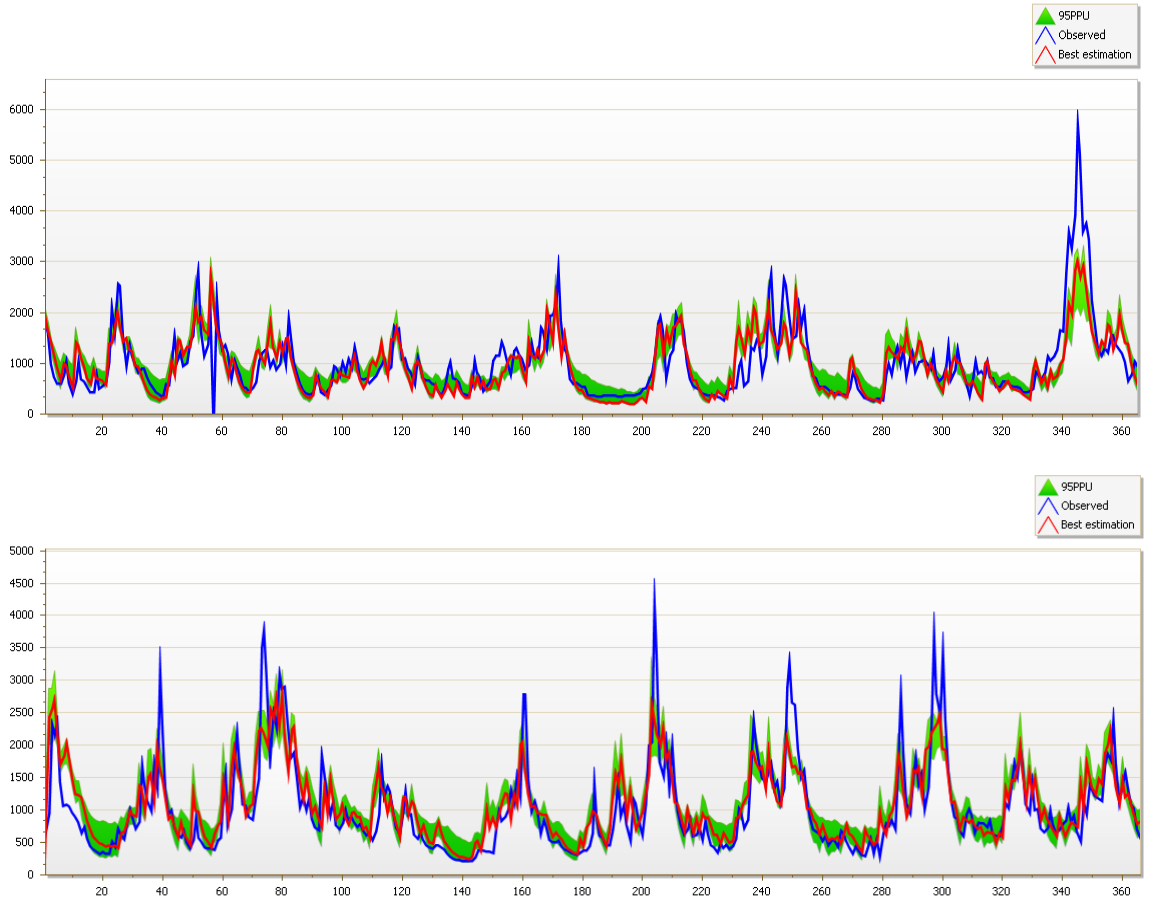

Figure 8. 95PPU plot produced in SWAT-CUP with the observed streamflow and best estimation streamflow for the calibration (top) and validation (bottom).

Table 4. Summary statistics of calibration and validation in SWAT-CUP

Time-step/C&V	p-factor	r-factor	NSE	R^2	PBIAS
Daily calibration	0.67	0.52	0.63	0.63	4.3
Daily validation	0.64	0.55	0.64	0.65	-4.2
Monthly calibration	0.69	0.38	0.78	0.78	-0.8
Monthly validation	0.65	0.29	0.62	0.63	0.5

A review of SWAT studies in Southeast Asia between 1998 and 2018 was conducted by Tan et al. (2019) and they tabulated the SWAT model performance for all the studies (Table 3). The performance of the SWAT model in this study is considered average compared to the performance of the studies in the review. Diamini et al. (2017) calibrated and validated SWAT with streamflow at the Bernam river basin and reported NSE values of 0.62 and 0.61 for C&V respectively. Examples of the predicted and measured streamflow for the Baleh catchment can be seen in Figure 8 at the calibration and validation stages. Using the criteria in (Moriasi et al., 2015), the C&V results are satisfactory (Table 4) for both the monthly and daily models. Therefore, SWAT was implemented with both time scales as they provide useful complementary insights into catchment dynamics. The calibrated values for the list of variables in Table 2 are provided in Table 5.

Table 5. Values obtained from C&V in SWAT-CUP for daily and monthly simulation. For type r, the value is used as the multiplication factor, whereas for type v, the value is used for direct replacement.

VARIABLE	TYPE	DAILY	MONTHLY
CN2	r	0.370918	0.674717
USLE_P	r	1.490173	0.465985
CH_K2	v	0.01729	-0.004457
CH_N2	v	41.022575	145.670532
GW_DELAY	v	301.411072	256.519867
GW_REVAP	v	0.137787	0.182775
GWQMN	v	902.475952	664.440125
SOL_K	r	2.737295	2.214268
SOL_AWC	r	1.997574	0.87168
REVAPMN	v	422.580017	172.589355
EPCO	v	0.399005	0.890782
ESCO	v	0.63759	0.12249
CANMX (PAST)	v	7.761296	5.371232
CANMX (FRST)	v	1.897493	7.56396

No research has estimated the amount (weight) of fine sediment running off sub-catchments of the Baleh, so it has not been possible to calibrate or validate the sediment yield estimates produced by SWAT for individual sub-catchments. Similarly, DID does not have the continuously logging turbidity sensors in the river that are needed to compute fine sediment loads, so it is not possible to check the reliability of the SWAT estimates of the loads carried by the river itself.

The only possibility of checking the SWAT sedimentary data is to use the very limited number of spot samples of suspended sediment concentration that exist. However, this exercise has limited value for a number of reasons. First, there are very few such spot samples. SEB collected SSC samples between 2008 and 2011, with 3 to 4 samples per year at 3 locations near the catchment outlet (i.e. total of less than 15 samples). The samples had no day or time stamp so they could not be compared directly with the simulated SSC values in a quantitative manner. Second, the locations do not correspond to the outlet points to which SWAT predictions apply. Depending on the degree of mixing, SSC values may differ over channel distances of a few meters, especially in instances where tributaries or eroding banks delivering new material. Without such spatial correspondence, comparing spot to modelled values of SSC has limited value. A third issue is that SWAT models were run only down to daily time steps. The estimates of SSC produced by SWAT represent sediment yield data integrated with respective daily water yield values to compute the concentration. However, as these yields are daily totals they may be too coarse to detect the variations in SSC that can happen over shorter (hourly) timescales; thus comparing spot measures of SSC to SSC calculated using total daily sediment and flow data is problematic. The spot SSC values ranged from 43 to 1520 mg/L with high inter-annual variability i.e. 231-1520 mg/L in 2008 and 43-453 mg/L in 2010. The calibrated and validated SWAT model for the Baleh catchment simulated SSC values ranging from 45 to 462 mg/L. The simulated values sit within the range of the SEB samples; 73% of spot sample were within the simulated SSC range of 45-462 mg/L, with the remainder being higher values than simulated by SWAT. It is clear that there are no major errors in the model which are leading to order of magnitude misrepresentations of sediment yield, but it is not possible to say much more than this, based on the limited samples.

2.4.2.3 *Future land use and climate scenarios*

The future scenarios modelled the influence of two factors - land cover change and climate change. The scenarios have different levels both factors:

1. Land cover change: a. Low rate of deforestation – 2% per year (termed L1), b. High deforestation – 5% per year (L2)
2. Climate change: a. No change (i.e. baseline) (R1), b. Annual increment of 0.03^{o}C in temperature and a 2.1% annual decrease in rainfall (R2)

The two factors and their levels produced a total of 4 scenarios shown in Table 6. The timeline of the SWAT models is shown in Figure 8. Future scenarios were taken for periods beyond the construction of the Baleh dam. The dam is due to be completed in (approximately) 2026 so model runs were made to include 5 years (runs 2027-31), 10 years (runs 2032-36) and 25 years (runs 2047-51) after dam opening.

Table 6. Model scenarios

Low deforestation (L1)		High deforestation (L2)	
Baseline climate (R1)	Climate change (R2)	Baseline climate (R1)	Climate change (R2)
L1:R1:N	L1:R2:N	L2:R1:N	L2:R2:N

For land cover scenarios, Cushman et al. (2017) estimated the total forest loss for Malaysian Borneo to be 23.3% from 2000-2010 and 23.2% from 2010 to 2020 (i.e. around 2.3 pa). Hence,

the modelling for Baleh used a 2% annual decrease in forest cover for the 'constant low deforestation' scenario and a 5% annual forest loss for the 'high deforestation' scenario, applied incrementally (i.e. % per year). The deforestation was applied manually in ArcGIS by converting the pixel classified as 'forest' to 'disturbed vegetation' and 'bare earth' based on the relevant deforestation percentage. As with the historical land cover maps, the assumption was made that there would be more forest degradation (represented by disturbed vegetation) than deforestation (represented by bare earth). Future land use maps were created for the final years in each future SWAT simulation and an external software, SWAT- Landuse Update Tool, was used to incorporate the land cover changes gradually on an annual basis in every SWAT model run.

Sa'adi et al. (2017) applied statistical downscaling of General Circulation Model (GCM) projections to assess changes in rainfall patterns of Sarawak due to climate change. They predicted that some regions in Sarawak will be experiencing localized decreases rainfall under all scenarios from 2010-2039, which includes the Lower Rajang basin (0.0% to −3.2%) and Upper Rajang basin (−0.4% to −2.1%). Based on these findings, the SWAT models in this study used a 'no change' scenario and a 'decreased rainfall' scenario, using 0 % and 2.1 % decrease in rainfall respectively. Changes in rainfall were manually implemented on the historical observed daily rainfall data collected at rainfall gauges in Figure 3. Loh et al. (2016) conducted a study to predict changes in temperature and rainfall over Malaysia by the end of the 21st century based on the Intergovernmental Panel on Climate Change (IPCC) Special Report on Emission Scenarios (SRES) A2, A1B and B2 emission scenarios using the Providing Regional Climates for Impacts Studies (PRECIS). Their projections predict a general warming over the entire country by the end of the 21st century. The projected temperature increment for A2, A1B and B2 scenarios ranges from 2.5 to 3.9^{o}C, 2.7 to 4.2^{o}C and 1.7 to 3.1^{o}C respectively. Based on these values, the current study used an annual increment of 0.03^{o}C to the minimum and maximum daily temperature obtained at Kapit station for the climate change scenario. The 'no change' scenario used the daily baseline temperature values. It should be noted that the goal of the climate change modelling was not to simulate the effects of occasional extreme weather events on flows or sediment yield. In fact, such events have happened in the past, so it is possible to look at the empirical historical data to see, e.g., what instantaneous river discharge levels were reached during times of extreme rainfall (4000-6000 m^3/s; Figure 8). Instead, the goal of the modelling was to integrate over longer time intervals, to look at how a progressive climate change might affect annual water and sediment yields. Such events are considered by virtue of being included in the calculations of annual yield, but are not detailed explicitly. Some discussion of these events is provided in Chapter 5.

Each of the 4 scenarios in Table 6 was applied to climate and land cover data to establish conditions at the various points in the future with the five-year model runs then used to extract flow and sediment data for the focal years (2030, 2035 and 2050; as shown in Figure 8). The most recent 5 years on record for rainfall data, 2013-2017, were used to run the present-day scenario (baseline conditions).

2.4.2.4 *Dam simulation scenarios*

Baleh dam is expected to start operating by 2026. SEB was unable to give precise details of the dam operational regime, largely because it will be driven by electricity demand which is currently not clear. Two plausible operational scenarios were therefore devised (ratified by SEB) and used for the dam simulations in SWAT (Figure 9). These runs were on a daily time-step. The scenarios were applied to conditions (rainfall, land cover and corresponding inputs to the dam and all downstream sub-basins) in the most recent baseline year (2017). The first dam operational scenario is a simulated controlled outflow built into SWAT where dam releases are programmed to balance water inflows and outflows within a designated range in a way that prevents dam overspill. It involves opening and closing turbines to match inflows which are themselves a function of the climate and land cover over the simulation period (Figure 9, top plot). The second scenario is a hydropower (HEP) generation one; it assumes that the dam will rarely operate at maximum or minimum capacity (based on number of turbines) but instead, most frequently using 3 of its fine turbines. The scenario involves releasing from 3 of the 5 turbines (60% capacity) for 50% of the time, and frequency of other numbers of turbines as shown in Figure 9 (bottom plot). Thus, these simulations show flow and sediment loads under two different operational regimes, and are compared to the 'real' no-dam baseline.

The implementation of the HEP scenario involved randomly allocating a number of turbines (= flow release) to each day within the one-year period, such that over the 365 days the frequency curve plotted in Figure 9 was retained. 50 unique randomisations of the flow allocation (randomly allocating a flow to each day) were generated and used to run 50 SWAT model variations of the HEP scenario. This allowed assessment of whether variation in the day of release magnitude altered over flow and sediment impacts and created an 'envelope' of estimated yield values. The non-HEP scenario was only run once as SWAT uses the measured baseline conditions as inputs to simulate the dam release. The impact of the dam on flow and sediment loads under these two scenarios were assessed at two key points in the catchment - the dam site and the catchment outlet. Thus, impacts in the likely most affected section of the river were assessed, as well as one further downstream where tributary inputs may dampen the dam effects.

It was initially planned to run a continuous SWAT model for 25-years post dam. However, the measured daily rainfall and temperature data, which are compulsory input data for SWAT, from the government only had useable continuous data for 5 years (2013 – 2017) closest to the present year. Running the dam simulations with a climate model in addition to two hypothetical dam operational regimes would introduce more uncertainty in the SWAT model. Any change in flow or sediment load could then be a result of the uncertainty from the rainfall and temperature data, making it difficult to determine the specific effect of the dam. Therefore, assessment of the dam impacts on downstream flows and sediment loads, the decision was made to run SWAT for only the first 5 years after the dam.

A final scenario involved combining the dam with climate and land cover change. To limit the number of possible combinations, this was run only with the low deforestation rate (2% pa) and climate change scenario (annual increment of 0.03°C in temperature and a 2.1% annual decrease in rainfall). The decision was made to use the 5-year measured daily rainfall and temperature data similar to the future scenarios without the dam in Table 6 for the 2030, 2035 and 2050 simulations.

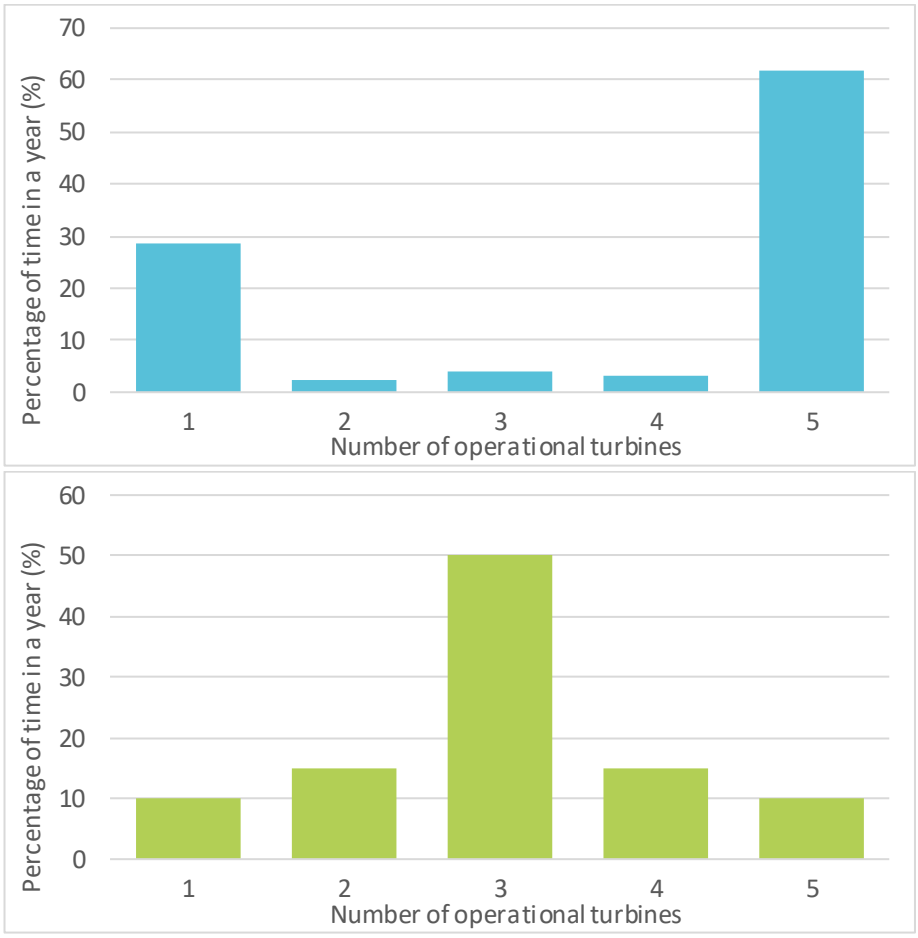

Figure 9. Number of operational turbines within a one-year period for the two dam operational scenarios. Top – Non-hydropower regime (Non-HEP); Bottom – Hydropower regime (HEP).

CHAPTER 3. LAND COVER CHANGE IN THE BALEH CATCHMENT

3. Chapter 3 Land cover change in the Baleh Catchment

3.1 Land cover maps and land use trend from 2000 to 2019

Figures 10 and 11 show the land cover maps for all four periods. From a visual comparison of the classified maps, the logging road network was observed to expand with time, so much so that most of the study area is made accessible to vehicles. The construction of the access road from Kapit Town to the Baleh Dam construction site was fully completed by 2019 and it can be observed as a continuous line of bare earth class pixels. There was no sign of construction of the road in the 2012 classified map. Most of the built-up areas along the river remain unchanged from 2001-2019 and there were no new structural developments observed.

After tabulating the distribution of land cover classes from the land cover maps (Table 7), the changes of each land cover class between each time step were compared in terms of the percentage of total study area covered. It was observed that the forest and bare earth classes experienced an overall decrease of 2.72% and 1.26% respectively while the disturbed vegetation class experienced an overall increase of 3.65% between 2001 to 2019. The forest and disturbed vegetation classes experienced the most change between 2001 to 2008 with a decrease of 4.3% and an increase of 4.33%. The bare earth class decreased by a drastic 0.68% between 2012 to 2019. The built-up areas and river channel classes experienced no overall change in area coverage between 2001 to 2019.

Table 7. Land cover class distribution for all four periods as a percentage of the total study area covered.

Land cover class	Area covered in 2001 (%)	Area covered in 2008 (%)	Area covered in 2012 (%)	Area covered in 2019 (%)
Forest	93.6	89.3	91.23	90.88
Bare earth	1.66	1.63	1.41	0.73
Built up areas	0.03	0.03	0.02	0.03
Disturbed vegetation	4.13	8.46	6.77	7.78
River channel	0.57	0.57	0.57	0.57

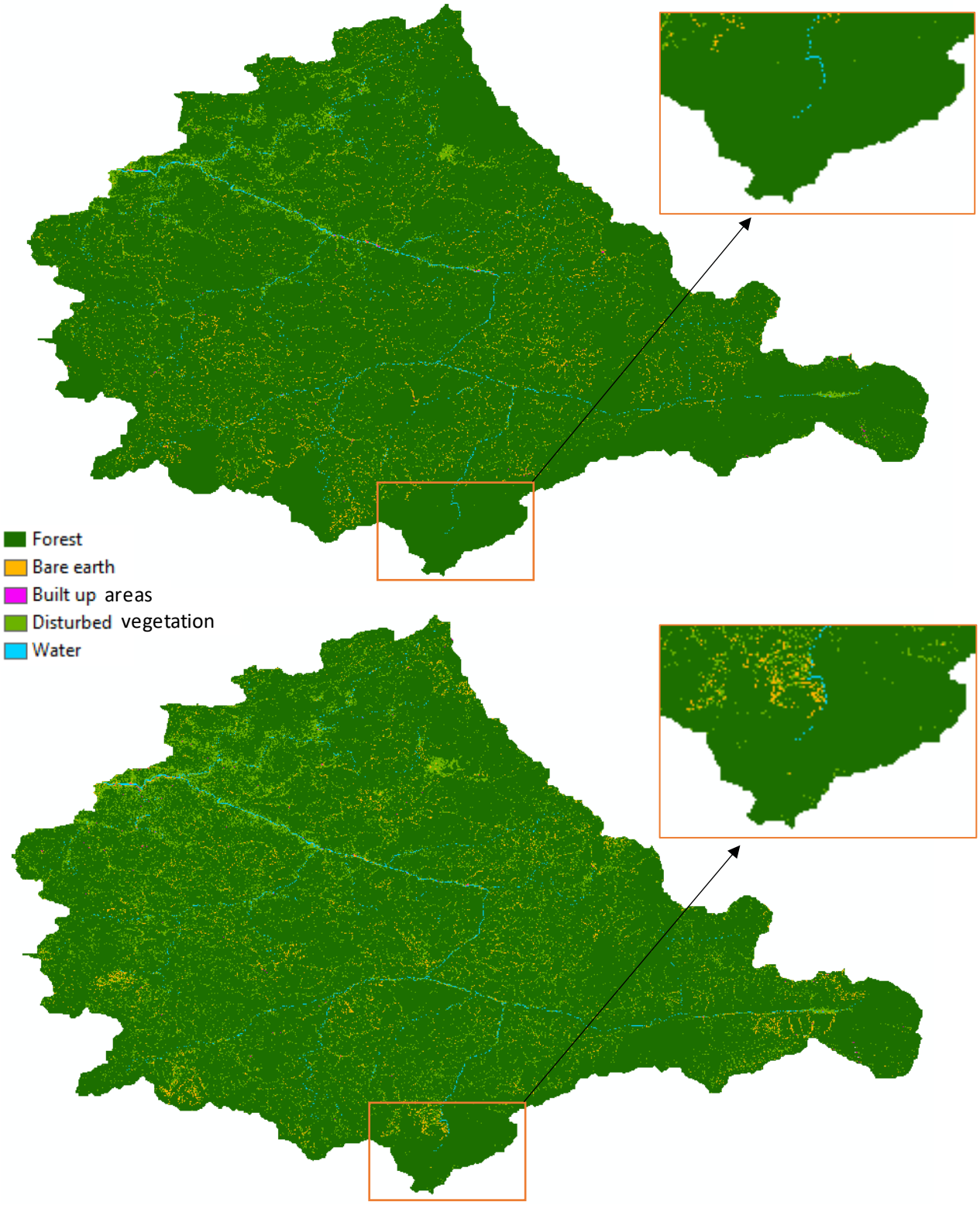

Figure 10. Top - 2001 land cover map, Bottom - 2008 land cover map. The difference in land cover between 2001 and 2008 can be seen in the zoomed-in section of Baleh catchment's southern region.

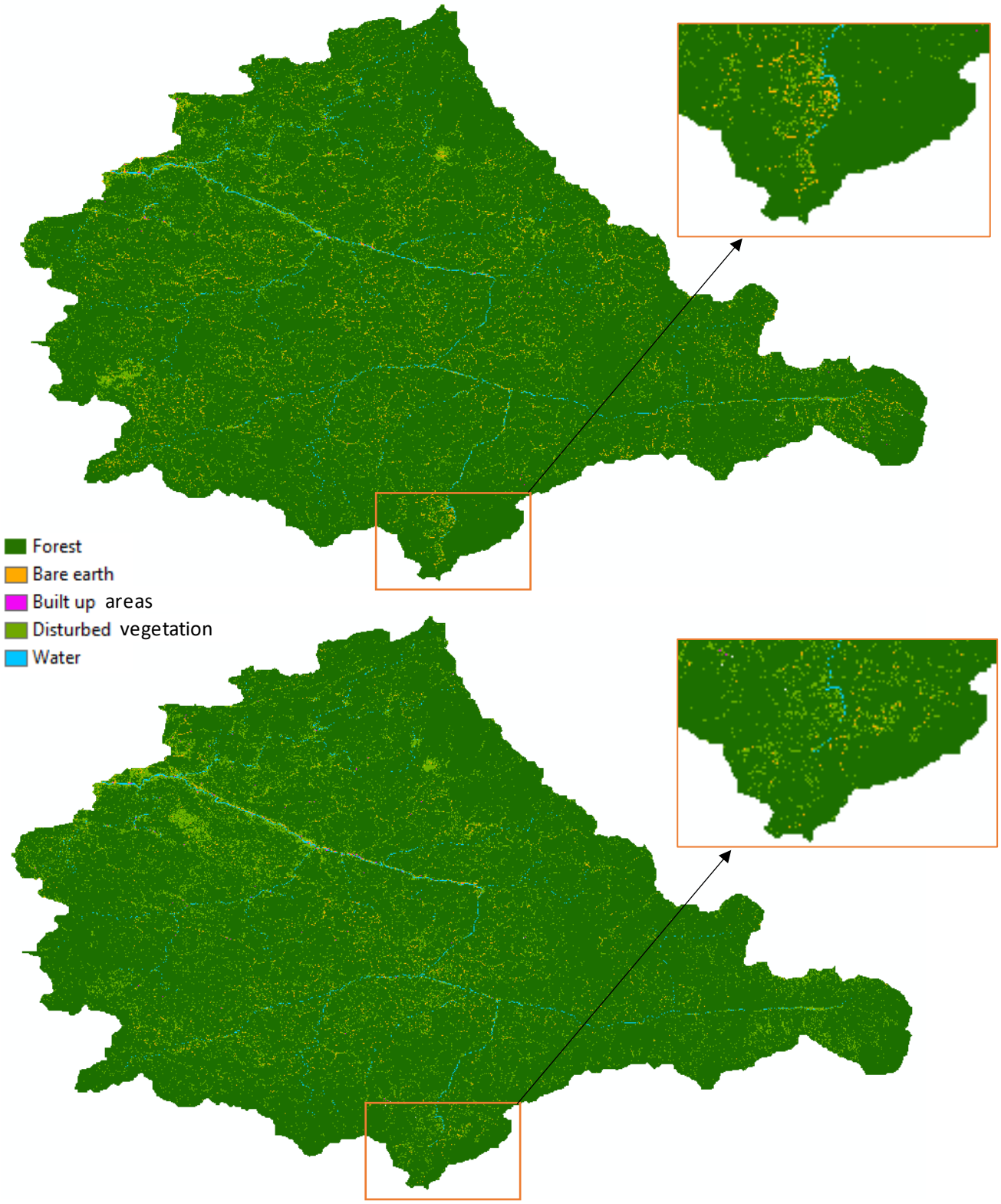

Figure 11. Top - 2012 land cover map, Bottom - 2019 land cover map. The difference in land cover between 2012 and 2019 can be seen in the zoomed-in section of Baleh catchment's southern region.

Table 8. Land cover change matrix for the period 2001 to 2008.

		Land cover class 2008				
		Bare earth	**Built-up area**	**Disturbed vegetation**	**Forest**	**Total**
Land cover class 2001	**Bare earth**	58.41	0.52	116.52	27.57	203.01
	Built up area	2.41	0.89	0.68	0.58	4.55
	Disturbed vegetation	31.14	0.86	334.40	148.36	514.76
	Forest	108.75	2.21	594.39	10901.40	11606.75
	Total	200.71	4.48	1045.99	11077.91	

Table 9. Land cover change matrix for the period 2008 to 2012.

		Land cover class 2012				
		Bare earth	**Built-up area**	**Disturbed vegetation**	**Forest**	**Total**
Land cover class 2008	**Bare earth**	67.29	0.91	65.65	66.82	200.67
	Built up area	0.97	0.87	0.66	1.97	4.47
	Disturbed vegetation	68.10	0.31	451.03	526.50	1045.93
	Forest	35.67	0.93	319.80	10720.70	11077.10
	Total	172.03	3.03	837.13	11315.98	

Table 10. Land cover change matrix for the period 2012 to 2019.

		Land cover class 2019				
		Bare earth	**Built-up area**	**Disturbed vegetation**	**Forest**	**Total**
Land cover class 2012	**Bare earth**	40.46	1.38	108.67	21.51	172.03
	Built up area	0.94	0.78	0.63	0.67	3.03
	Disturbed vegetation	21.59	0.62	402.65	412.23	837.09
	Forest	25.86	1.35	445.89	10842.80	11315.90
	Total	88.86	4.13	957.85	11277.20	

The cross-tabulation matrices (Table 8, 9 and 10) show that the major changes observed were from the two classes with the most area coverage, which are forest and disturbed vegetation. Although the bare earth class only covered less than 2% of the study area, it experienced significant variability (66-77% change). From 2001 to 2008, ~100 km^2 (0.94%) of forest was deforested and converted into bare earth while another ~600 km^2 (5.08%) was degraded into disturbed vegetation causing the total area of disturbed vegetation to increase by 100%. ~144 km^2 (71%) of bare earth experienced revegetation. From 2008 to 2012, ~320 km^2 (2.89%) of forest was degraded to disturbed vegetation while ~530 km^2 (50%) of disturbed vegetation was restored to forest. Meanwhile, ~130 km^2 (66%) of bare earth was converted back to either disturbed vegetation or forest. From 2012 to 2019, ~130 km^2 (75%) of bare earth experienced

revegetation. ~450 km^2 (3.94%) of forest was degraded to disturbed vegetation while ~410 km^2 (49.25%) of disturbed vegetation recovered to become forest.

An analysis of the percentage of land cover change type for each time step compared to the total area covered by each land cover change type from 2001 to 2019 was done (see Figure 12). The forest class experienced the most degradation (Forest to Disturbed vegetation- 43%) and deforestation (Forest to Bare earth- 63%) between 2001 to 2008. On the other hand, the disturbed vegetation class was mostly changed to forest (~50%) and bare earth (~60%) from 2008-2012. More than half of the afforestation from bare earth to forest occurred between 2008-2012. Conversion of forest and disturbed vegetation to bare earth was the lowest between 2012-2019 at 15% and 18% respectively.

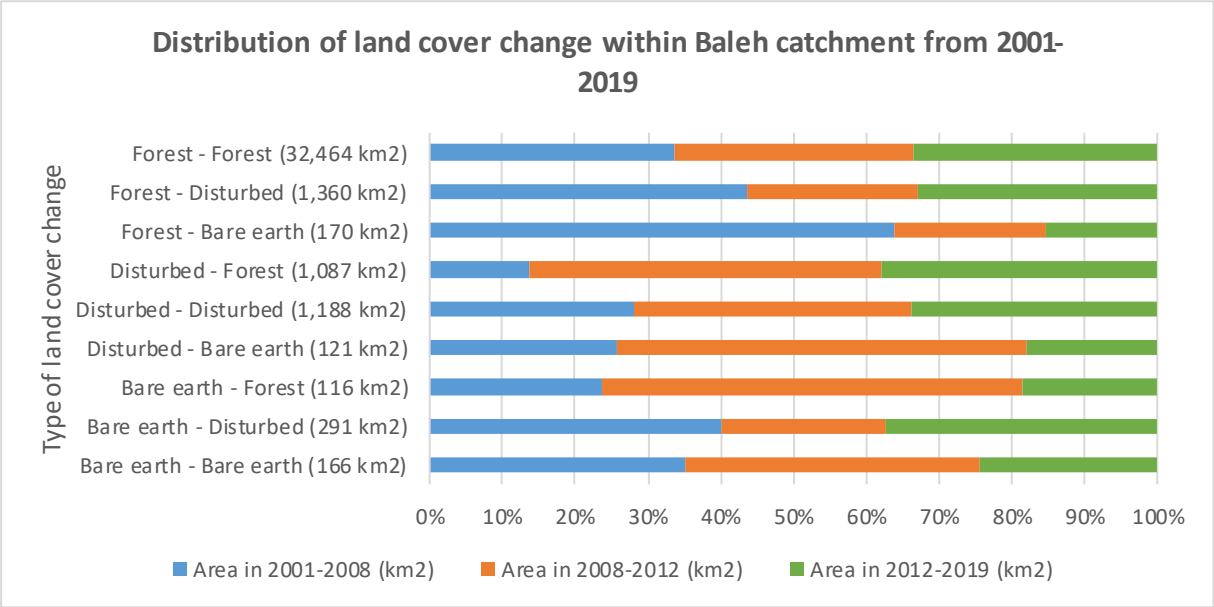

Figure 12. Percentage of land cover change type contributed by the years 2001 to 2008, 2008 to 2012 and 2012 to 2019 in terms of the overall area percentage. The total area covered by each type of land cover change is also labelled on the y-axis.

3.2 Accuracy assessment of land cover classification

From this point onwards, the four periods 2000-2001, 2007-2008, 2011-2012, 2018-2019 will be referred to by the ending years: 2001, 2008, 2012 and 2019. The accuracy assessment confusion matrices for 2001, 2008, 2012, 2019 are shown in Tables 11 to 14. The overall accuracy for the 4 classified maps ranged between 83% to 85.8%. The built-up areas class was the least accurate class in all the maps with values between 46-50% except for 2007-2008 which was only 31%. This class was mostly confused with bare earth and shadows. The other classes had accuracies above 90% for three or four maps. The accuracy assessment also showed that the shadows class was able to be identified well (88-98%). The pixels in this class were later combined with the forest class. The river channel class was not included in the assessment as it was overlaid onto the classified images after being manually extracted and corrected.

Table 11. Accuracy assessment confusion matrix for 2001. Overall accuracy is 85%.

Class	Forest	Bare earth	Built-up areas	Disturbed vegetation	Shadows	Total	User Accuracy
Forest	74	0	0	4	2	80	0.925
Bare earth	0	72	0	8	0	80	0.9
Built up areas	1	34	40	2	3	80	0.5
Disturbed vegetation	2	0	1	77	0	80	0.9625
Shadows	3	0	0	0	77	80	0.9625
Total	80	106	41	91	82	400	0
Producer Accuracy	0.925	0.679	0.976	0.846	0.939	0	0.85

Table 12. Accuracy assessment confusion matrix for 2008. Overall accuracy is 83%.

Class	Forest	Bare earth	Built-up areas	Disturbed vegetation	Shadows	Total	User Accuracy
Forest	78	0	0	0	2	80	0.975
Bare earth	1	72	0	7	0	80	0.9
Built up areas	2	7	25	24	22	80	0.3125
Disturbed vegetation	1	0	0	79	0	80	0.9875
Shadows	2	0	0	0	78	80	0.975
Total	84	79	25	110	102	400	0
Producer Accuracy	0.929	0.911	1	0.718	0.765	0	0.83

Table 13. Accuracy assessment confusion matrix for 2012. Overall accuracy is 83.5%.

Class	Forest	Bare earth	Built-up areas	Disturbed vegetation	Shadows	Total	User Accuracy
Forest	78	0	0	2	0	80	0.975
Bare earth	0	75	0	4	1	80	0.9375
Built up areas	0	19	37	4	20	80	0.4625
Disturbed vegetation	5	0	0	74	1	80	0.925
Shadows	3	2	0	5	70	80	0.875
Total	86	96	37	89	92	400	0
Producer Accuracy	0.907	0.781	1	0.831	0.761	0	0.835

Table 14. Accuracy assessment confusion matrix for 2019. Overall accuracy is 85.8%.

Class	Forest	Bare earth	Built-up areas	Disturbed vegetation	Shadows	Total	User Accuracy
Forest	79	0	0	0	1	80	0.9875
Bare earth	0	79	0	1	0	80	0.9875
Built up areas	1	33	38	5	3	80	0.475
Disturbed vegetation	10	1	0	69	0	80	0.8625
Shadows	2	0	0	0	78	80	0.975
Total	92	113	38	75	82	400	0
Producer Accuracy	0.859	0.699	1	0.92	0.951	0	0.858

CHAPTER 4. HYDROLOGY AND SEDIMENT LOADS IN THE BALEH: CURRENT CONDITIONS AND FUTURE SCENARIOS

4. Chapter 4. Hydrology and sediment loads in the Baleh: current conditions and future scenarios

4.1 Baseline patterns of flow and sediment yield in the Baleh

The SWAT model for the Baleh catchment was calibrated and validated for the years 2002-2010 (as detailed in Methods). The length of a typical SWAT run can range between 5 and 15 years. It is recommended that at least the first 2 years in a model run are used as 'warmup' years (Abbaspour, 2012), and thus for a 10-year run, interpretations are based on the final 8 years of the simulation. In the Baleh, simulations for various future scenarios are compared to a recent 'baseline' period. The most recent 5-year period for which empirical rainfall, temperature and flow data are available for the Baleh was 2013-17 inclusive, so this was used for baseline model runs. The SWAT run to establish baseline conditions was therefore 5 years, with the first 2 years (2013 and 2014) considered as a warmup and output for 2015-2017 used for analysis (Figure 8).

In the baseline years, the sub-basins had annual runoff values ranging from 3 up to a maximum of 598 mm/km^2/year (Figure 13). The magnitude of difference in runoff between sub-basins was around 520 mm in 2015 and 2016 while for 2017 it was 590 mm. Overall, 2017 was a wetter year, with 600 mm more rainfall than the others. The sub-basins in the western part of the catchment contributed more sediment in 2015 and 2017 compared to the other sub-basins; in 2016, sediment yield was greater in the eastern region (upstream) where the values were 2-3 times higher than the rest of the catchment. The estimated total sediment yield at the basin outlet was in the order of 100-150 million tonnes per year (Table 15) for the three baseline simulation years. This represents the gross export of sediment from the Baleh to the Rajang.

Table 15. Minimum, maximum and mean of annual water and sediment yield from the whole catchment in the baseline years.

	MINIMUM	MAXIMUM	MEAN
ANNUAL WATER YIELD (MM)	87,252	94,799	90,601
ANNUAL SEDIMENT YIELD (METRIC TON)	102,663,629	149,233,451	119,837,766

Figure 14 shows the simulated cumulative water and sediment yields for the baseline years. The patterns for water and sediment yield differed greatly. Cumulative water yield increased continuously throughout the year (i.e. similar slope) whereas for sediment it was stepped, with some months contributing relative little and some large amounts of sediment. Although magnitudes differed, temporal patterns for each year were broadly similar. Water yield was more or less continuous within each year, while for sediment yield the months from March to approximately October contribute very little sediment. 2016 was the most distinct year because of the significantly large sediment contribution (~80% of annual sediment yield) from the first two months. In 2015, the starting and ending months of the year contributed more water while in 2016 February and March contributed sudden increases in cumulative yield. August, September and November contributed the most volume of water in 2017. 2015 and 2017 both experienced two distinct periods of high sediment contribution: for 2015, this was from February to March and November to December while for 2017, it was in August to September and November. The high sediment yield months in 2015 and 2017 were months with high water

yield as well. The cumulative water yield was strongly correlated with rainfall, with months with high rainfall having in high water yield (Figure 14).

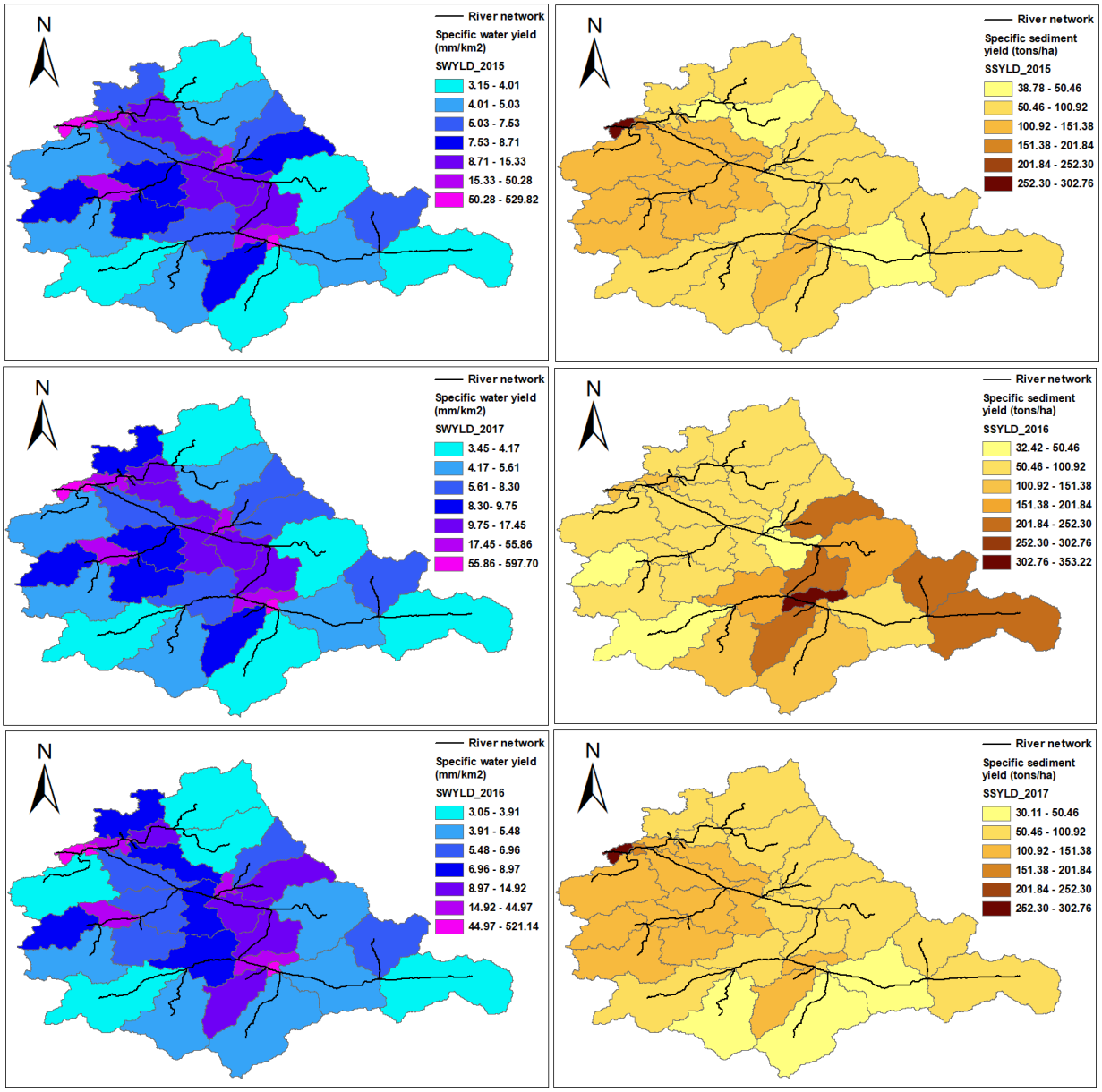

Figure 13. Left column (top to bottom) - Annual specific water yield (mm per km^2) from each sub-basin in 2015, 2016, 2017; Right column (top to bottom) - Annual specific sediment yield (metric ton per ha) from each sub-basin in 2015, 2016, 2017.

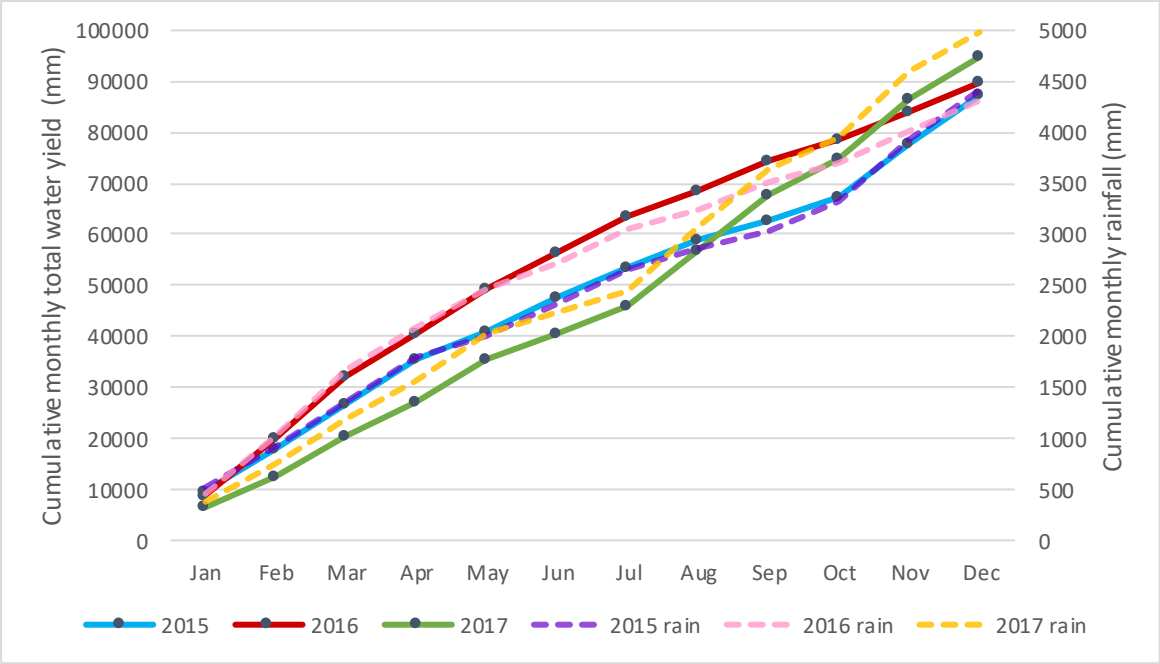

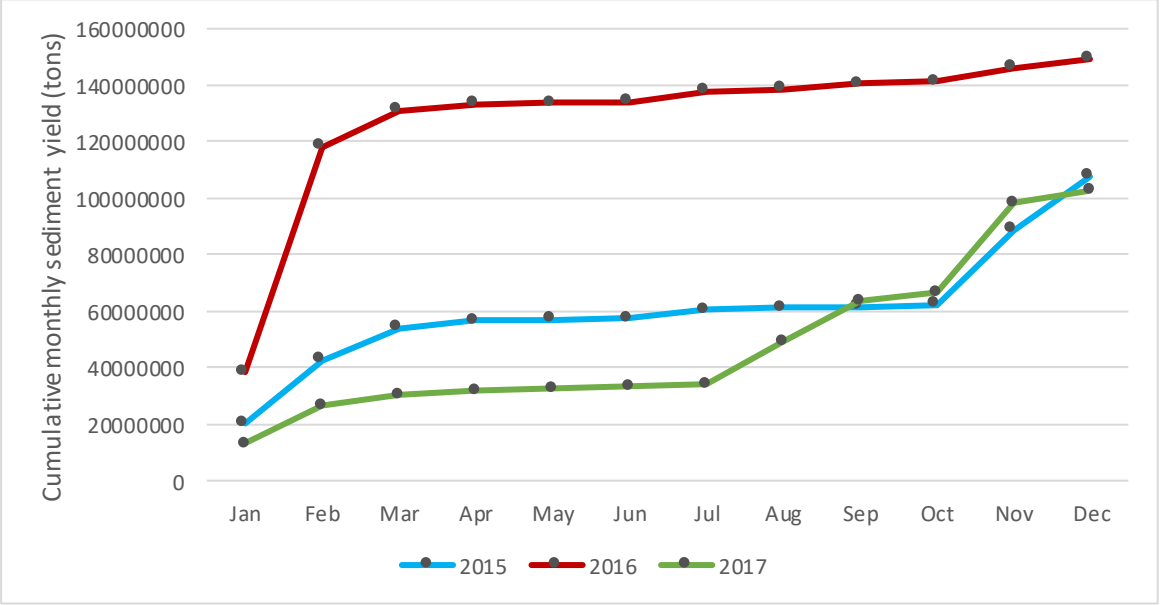

Figure 14. Cumulative total water (top) and sediment (bottom) yield on a monthly time-step from all the sub-basins in the Baleh catchment for the baseline years with cumulative monthly rainfall data from the weather stations in the catchment.

Example flow and sediment accretion curves for points along the Baleh are shown in Figure 16. The points used are the confluences of each tributary and the main stem (Figure 15), with values shown for the month with the highest water yield for each of the baseline years. While flow accumulated fairly continuously downstream, as a result of inputs of water from tributaries, there is a notable drop in annual sediment load between the dam and the point 23 km downstream. This suggests a reduction downstream conveyance, due to some combination of deposition in the first section downstream from the dam site (=reduced competence to transport its load), and/or a limited supply of new material from the catchment or channel.

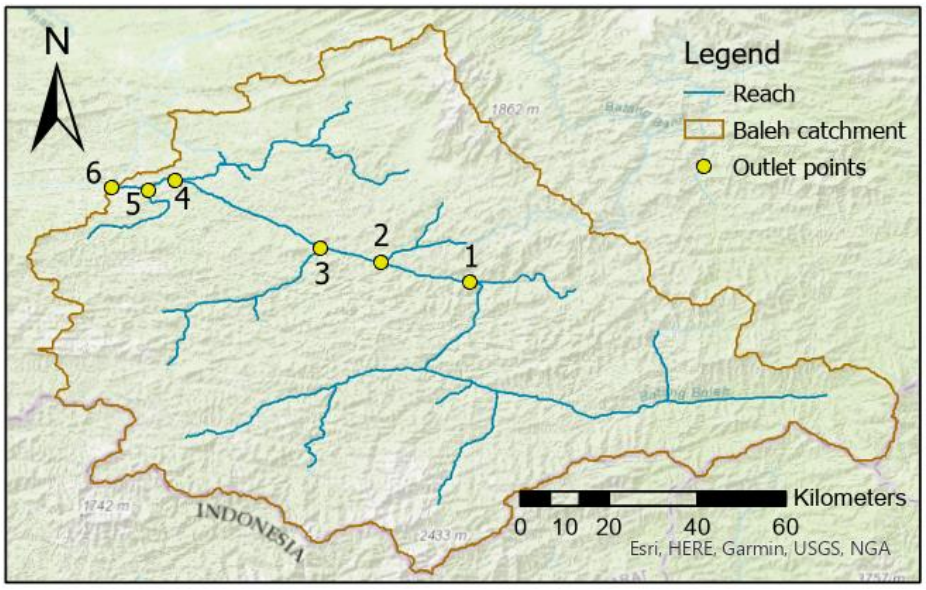

Figure 15. Map of outlet points used to show sediment and flow accretion. Point 1 is the outlet for the dam site and the reference point of distance measured from the other points: Point 2 (23 km), Point 3 (38 km), Point 4 (77 km), Point 5 (85 km), Point 6 (94 km).

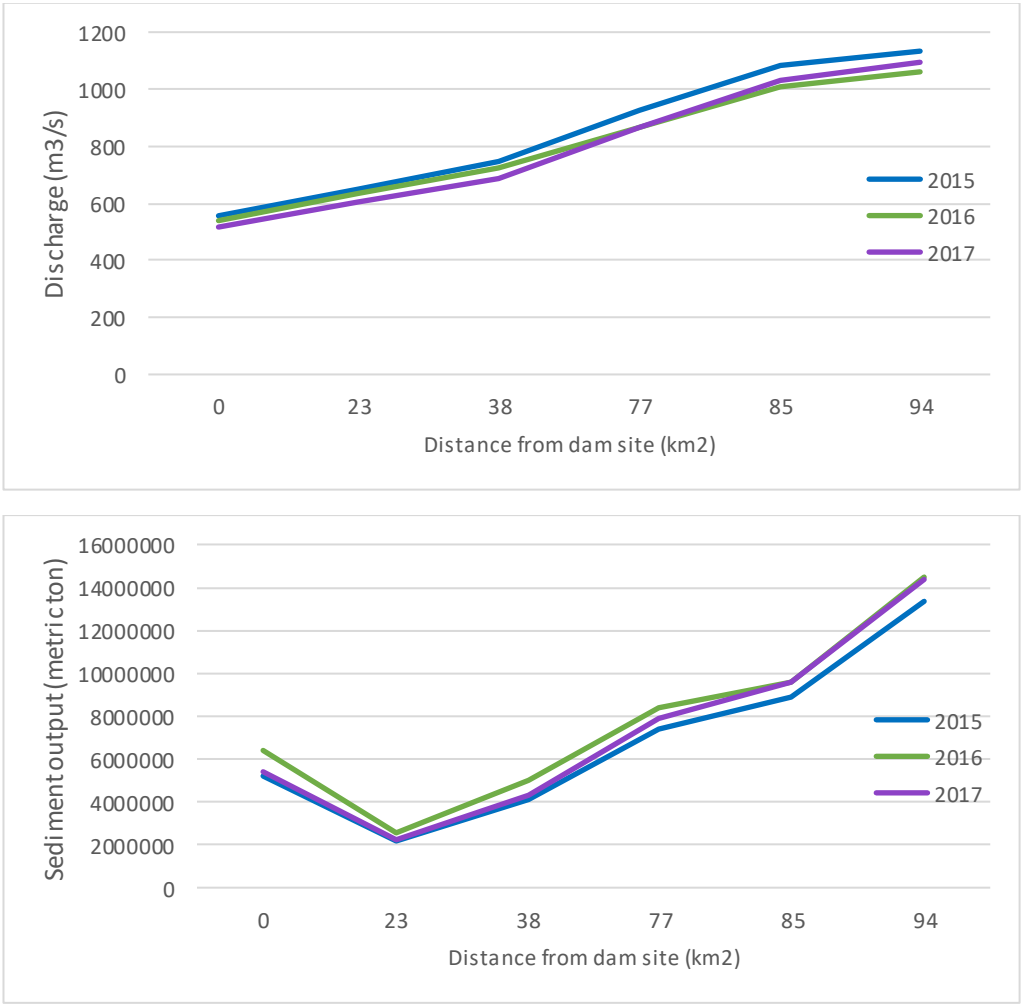

Figure 16. Top – Flow accretion curve (with the median monthly flow) from the dam site to catchment outlet with distance from dam site as the x-axis; Bottom - Sediment output accretion curve (with annual sediment load) from the dam site to catchment outlet.

Figure 17 shows the daily simulated SSC and flow values for each of the baseline years. For 2015, flow fluctuated between 157-2300 m^3/s while SSC ranges between 40-120 mg/L except for a singular peak flow event (2921 m^3/s) and a peak SSC event (160 mg/L). High flow events were concentrated at the start and end of the year. For 2016, flow fluctuated between 181-3180 m^3/s while SSC ranges between 46-160 mg/L except for a singular peak flow event (3802 m^3/s) and a peak SSC event (305 mg/L). High flow events were concentrated in February and March. For 2017, flow fluctuated between 166-3341 m^3/s while SSC ranged between 40-150 mg/L except for a singular peak flow event (3972 m^3/s) and a peak SSC event (250 mg/L). High flow events were concentrated in the months of September to November. Of the baseline years, 2017 had the largest range of flows and the highest daily flow value while 2016 had the largest range of SSC and the highest daily SSC value (Table 16). The median value for flow increased from 2015 to 2017, with values of 708.6 m^3/s, 776.4 m^3/s and 907.5 m^3/s. A scatterplot of the SSC and flow values for all the baseline years indicates that there is a moderate correlation (Figure 18), with much scatter at high discharges. The correlation is statistically significant.

Table 16. Summary statistics for daily suspended sediment concentration (SSC) and flow for all the baseline years.

	Suspended sediment conc. (mg/L)			**Flow (m^3/s)**		
	2015	**2016**	**2017**	**2015**	**2016**	**2017**
Median	79.01	77.275	72.09	708.6	776.4	907.5
Maximum	160.5	304.7	250.2	2921	3802	3972
Minimum	43.77	46.4	34.07	157.1	180.6	166.1

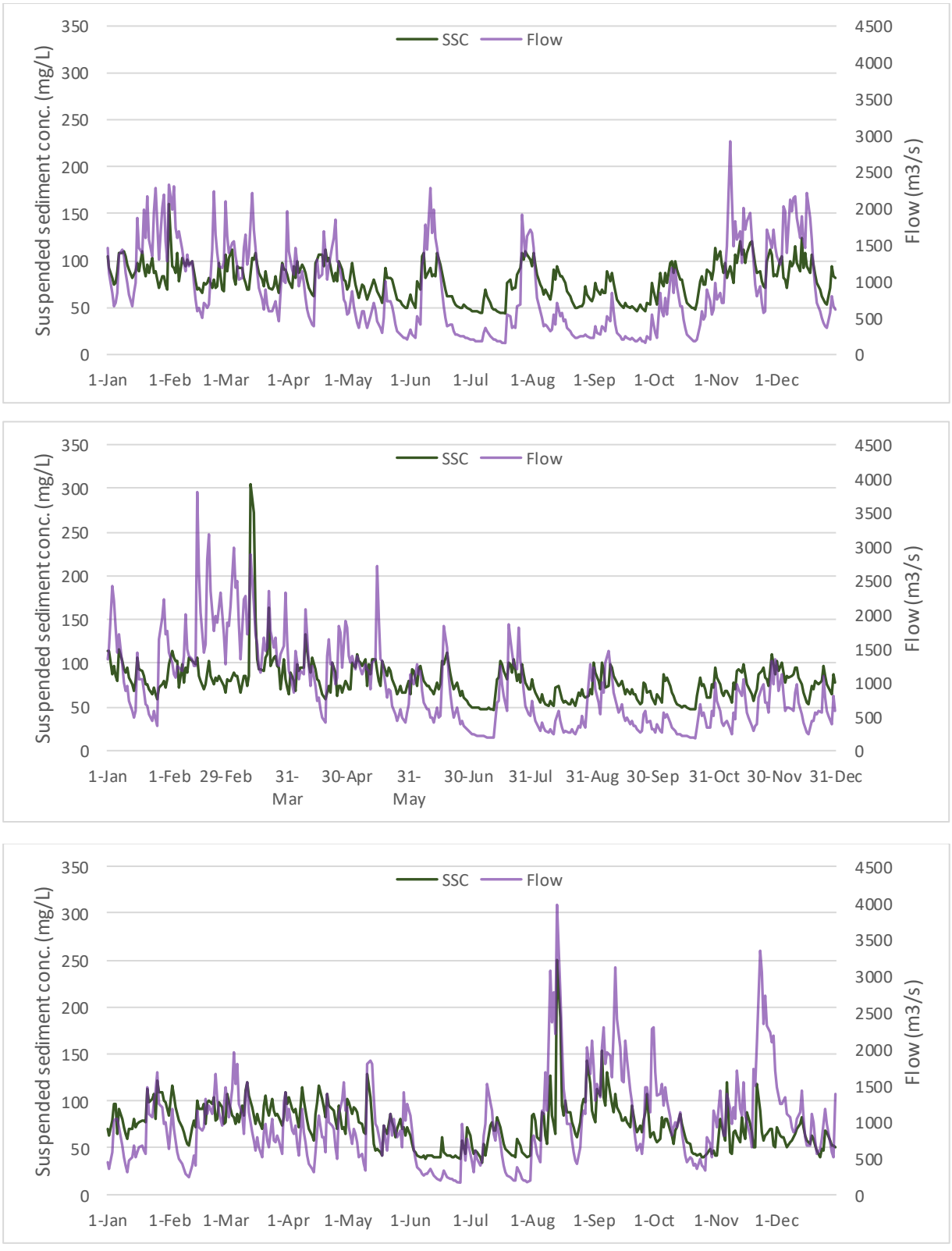

Figure 17. Daily simulated SSC and flow values in 2015 (Top), 2016 (Middle) and 2017 (Bottom).

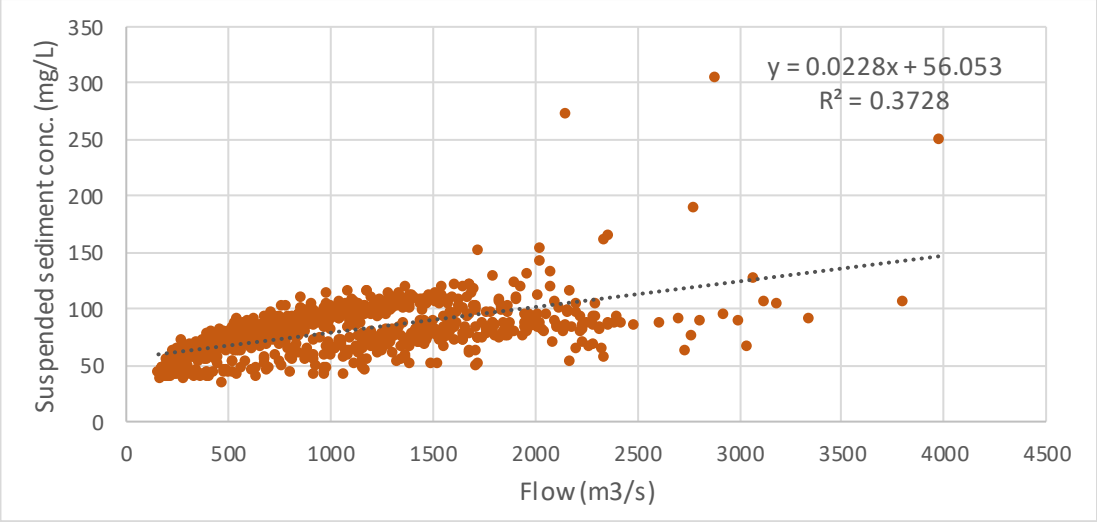

Figure 18. Flow-SSC plot at gauging station from 2015-2017. The p-value for R^2 is 6.21×10^{-113}, which indicates that the correlation is statistically significant.

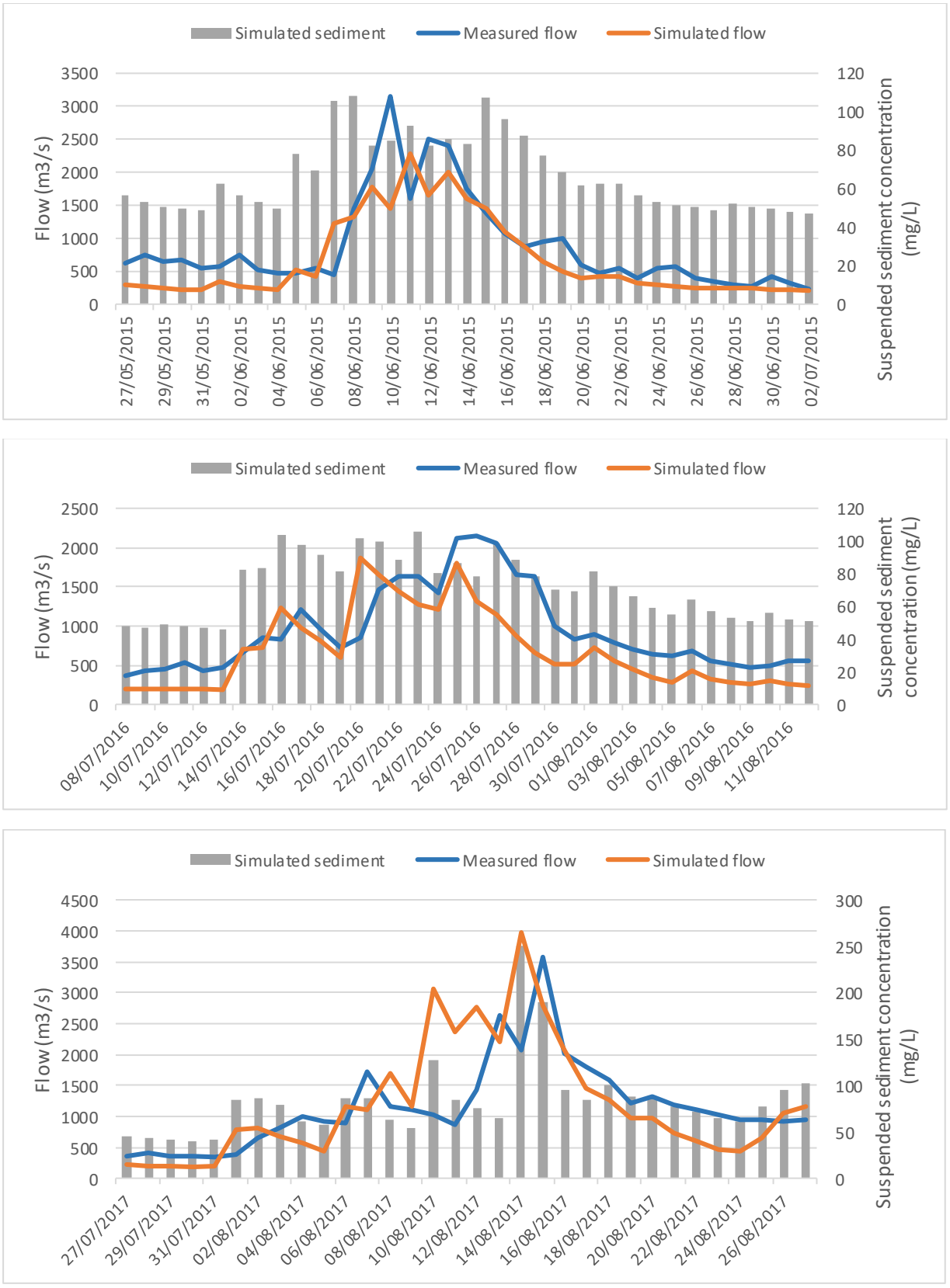

Figure 19. Hydrograph of a high flow event in 2015 (Top), 2016 (Middle), and 2017 (Bottom) on a daily time-step.

To understand the flow and sediment dynamics over shorter timescales, an example high flow event was chosen for each of the baseline years (Figure 19). Events chosen were all Q10 or higher and are illustrated at sub-basin 13 where the flow gauging station is located. The values of simulated flow and suspended sediment concentration were extracted from SWAT on a daily time-step for each event. All the plots illustrate a general correspondence between flow and SSC, with the latter increasing in response to the former. In the 2015 event, flow increased from approximately 280 to 2280 m^3/s and sediment from 50 to 108 mg/L; for 2016 flow increased from 200 to 1868 m^3/sec and sediment from 50 to 105 mg/L, and for the 2017 event flow increased from 220 to 3972 m^3/s and sediment from 40 to 250 mg/L. The rise and reduction in the simulated discharge and SSC match up well in these events. Notably, there was little evidence of any lag between flow and sediment increases. Despite the generally high SSC in the river (always above around 50 mg/L), concentrations increase further during floods and high flows (~4000m^3/s) can reach 250 mg/L. The figure also shows that at the scale of individual events, the model matched gauged flows quite well even though some differences in magnitude and timing were observed (full statistical details on calibration and validation were given in Chapter 2 and will not be repeated here).

Using the daily recorded rainfall along with the daily simulated runoff, a scatter diagram was drawn for the basin outlet and the dam site (Figure 20). The R^2 values indicate that there is only a moderate correlation between these two variables and that flow is not highly coupled to rainfall. This correlation is statistically significant. This is a sign of the influence of factors such as temperature, soil type and land cover influence runoff generation at both sites. These values are discussed further in relation to other catchments in Borneo in Chapter 5. After conducting an analysis of covariance (ANCOVA) on the daily rainfall and runoff values at the catchment outlet and dam site, the regression line slope for the dam site (See Figure 20) was significantly greater than the slope at the catchment outlet (ANCOVA, $p < 0.05$). The greater slope indicates that headwater areas respond more markedly to rainfall than downstream areas.

Figure 21 shows the percentage of time taken to transport different fractions of the Baleh's annual fine sediment load. For comparison, included on the plot are examples of a Mediterranean (Robera Salada) and temperate (Ganga) river. In the two other rivers, most of the sediment load is transported in a small percentage of the time - short periods when SSC is high. For example, in these rivers, 65-70% of all fine sediment is transported during events that together make up around 4% of the time (=14 days per years). In the Baleh the gradient of the line indicates that fine sediment transport is a more or less continuous process, with therefore a large % of the time being needed to convey most of the (relatively) fine sediment load; e.g. it takes around 40 % of the year (146 days) to transport the same per cent of the annual fine sediment load that in the other rivers is transported in just 4% of the time. The patterns in the Baleh were broadly similar for each of the three years.

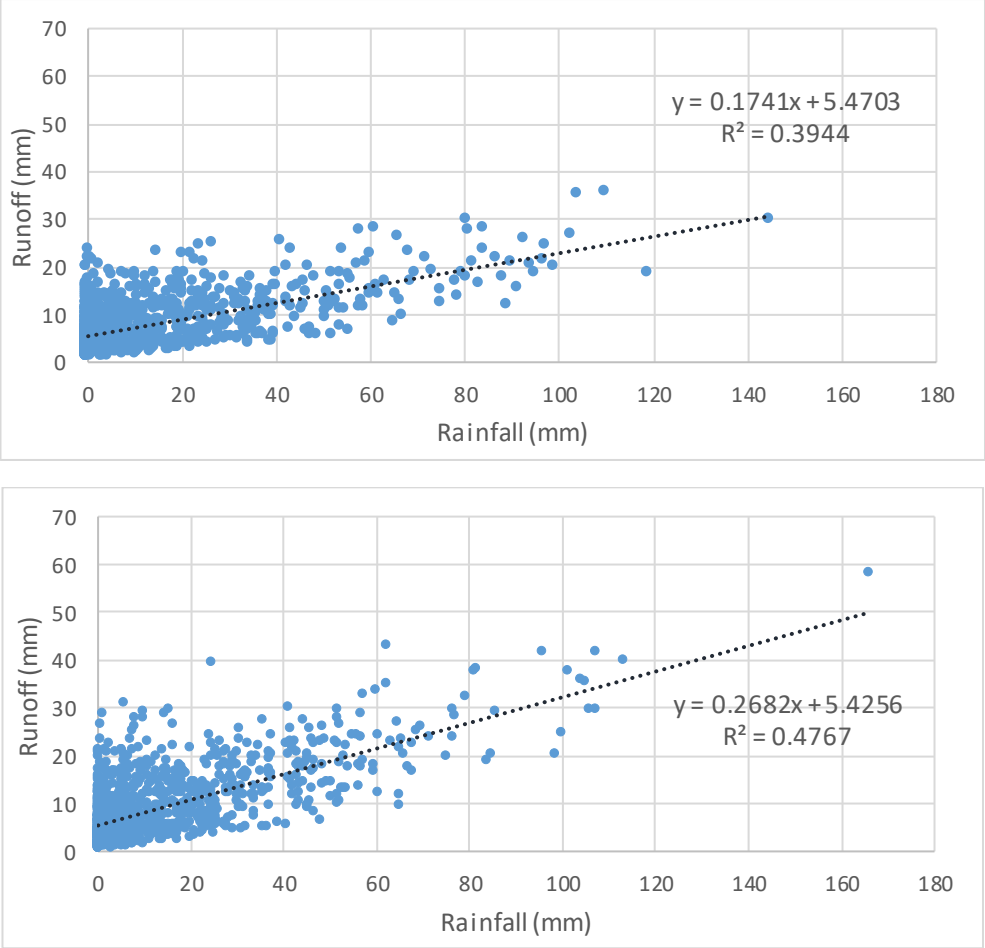

Figure 20. Rainfall-runoff plot using daily simulated runoff and measured rainfall for the baseline years at catchment outlet (Top, p-value = 2.74 x 10 $^{-121}$) and dam site (Bottom, p-value = 3.16 x 10 $^{-126}$).

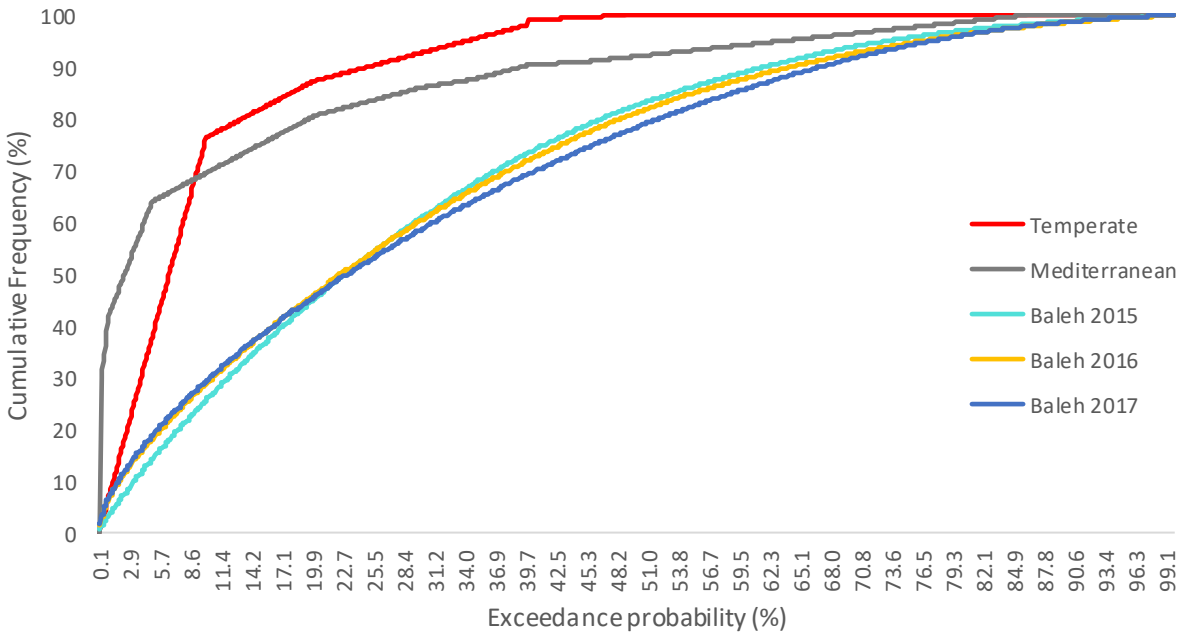

Figure 21. Comparison between tropical, temperate and Mediterranean streams in terms of the percentage of cumulative sediment transported in a percentage of the time.

4.2 Impact of land cover change on sediment yield

Figures 22 to 27 show the land cover maps used as land use inputs for the low and high deforestation future scenarios for the 2027-2031, 2032-2036 and 2027-2051 SWAT runs as well as the difference in specific sediment yield (SSYLD) for each of the sub-basins in each scenario. To ease the assessment of change, each scenario is shown in terms of difference from baseline (2015-2017). The 2027-2031, 2032-2036 and 2047-2051 SWAT runs will henceforth be referred to as the 2030, 2035 and 2050 simulations respectively. The land cover scenarios were described in detail in Methods (Chapter 2). Note that spatial patterns of land clearance followed historic ones, rather than being assigned randomly or evenly; hence clearance occurs in particular areas/sub-basins.

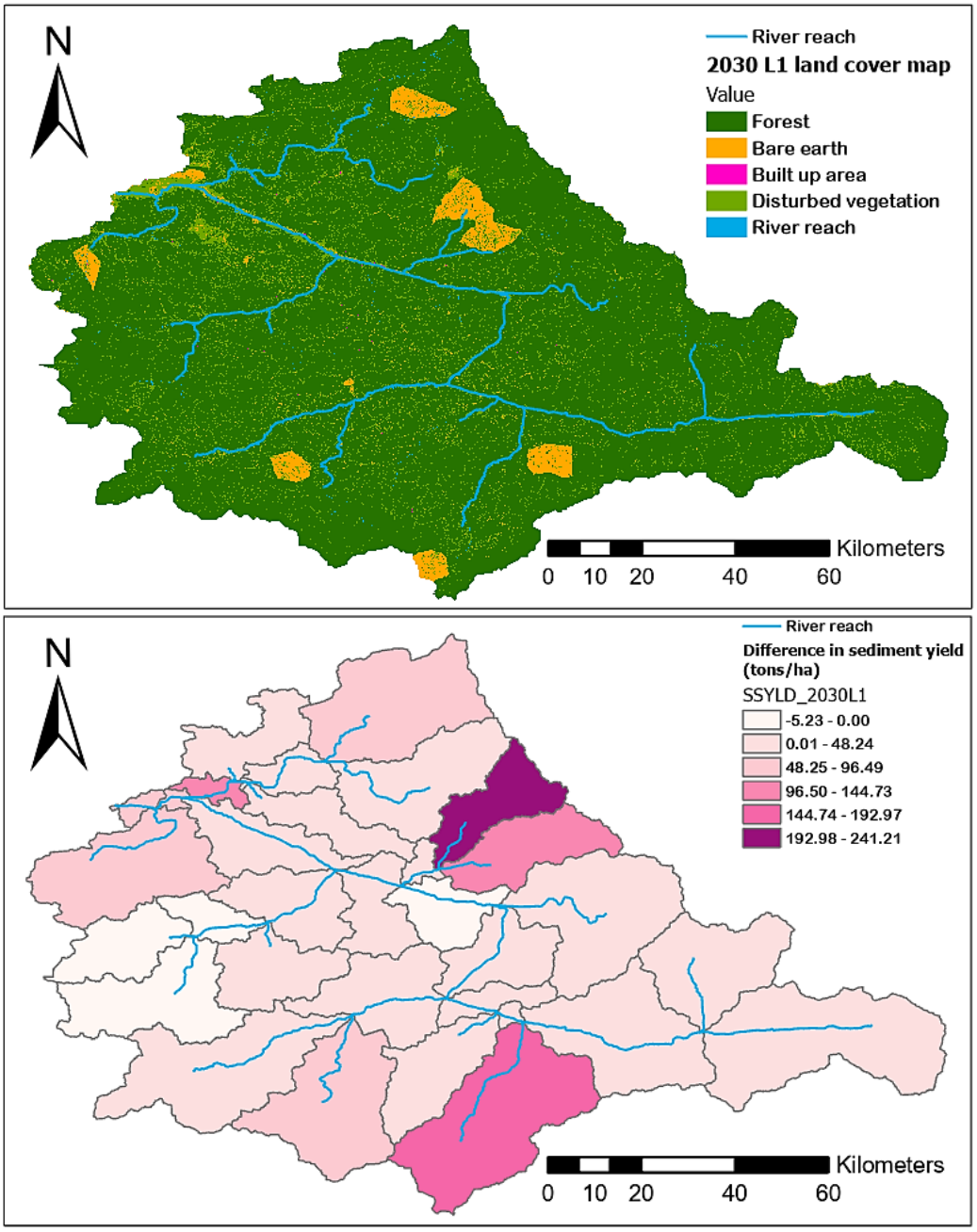

Figure 22. Top- Low deforestation (L1) land cover map for 2031 used as land-use input; Bottom- Percentage difference in specific sediment yield (SSYLD) of each sub-basin (averaged across 2029-2031) under low deforestation land cover change compared to the baseline scenario.

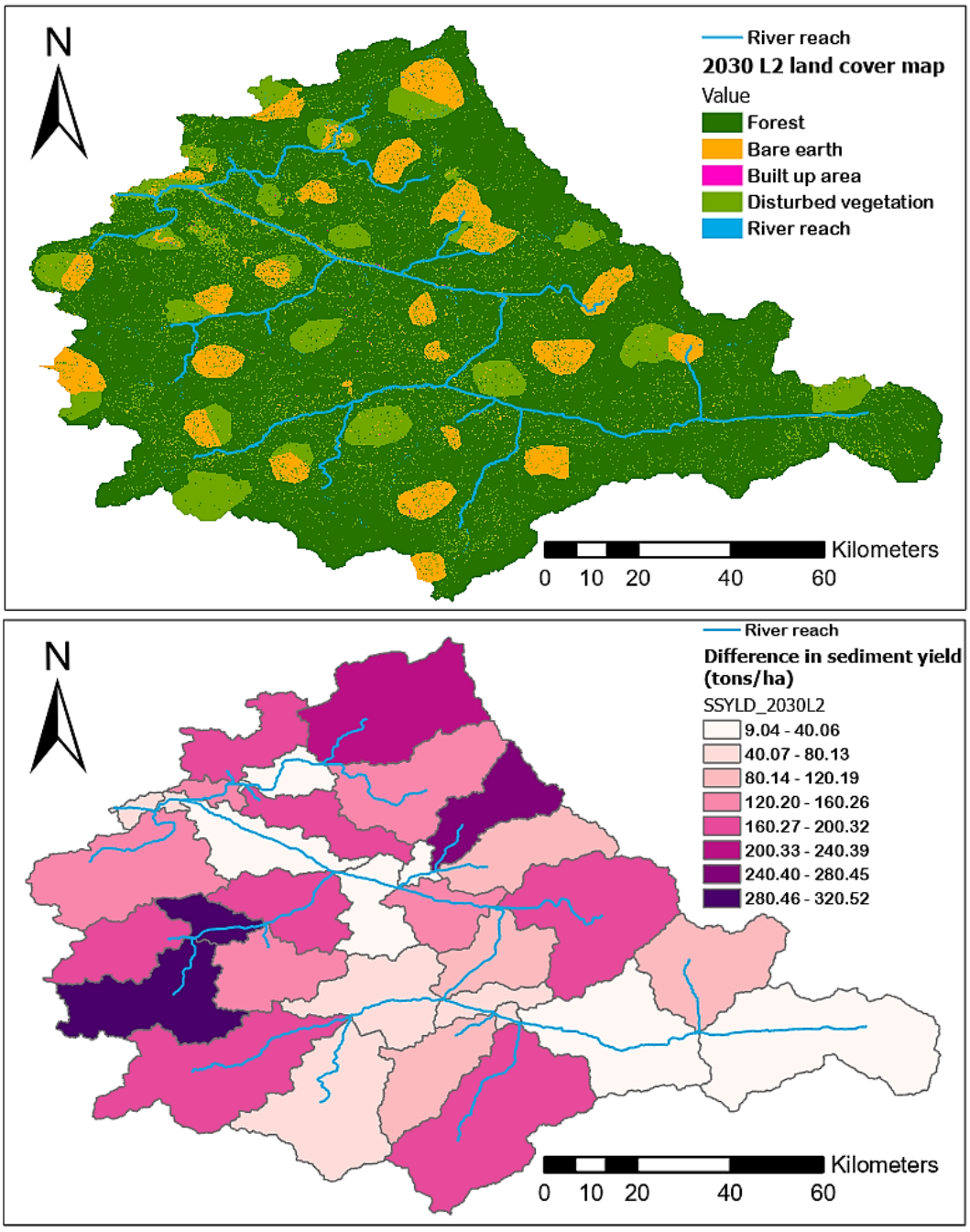

Figure 23. Top- High deforestation (L2) land cover map for 2031 used as land-use input; Bottom- Percentage difference in SSYLD of each sub-basin (averaged across 2029-2031) under high deforestation land cover change compared to the baseline scenario.

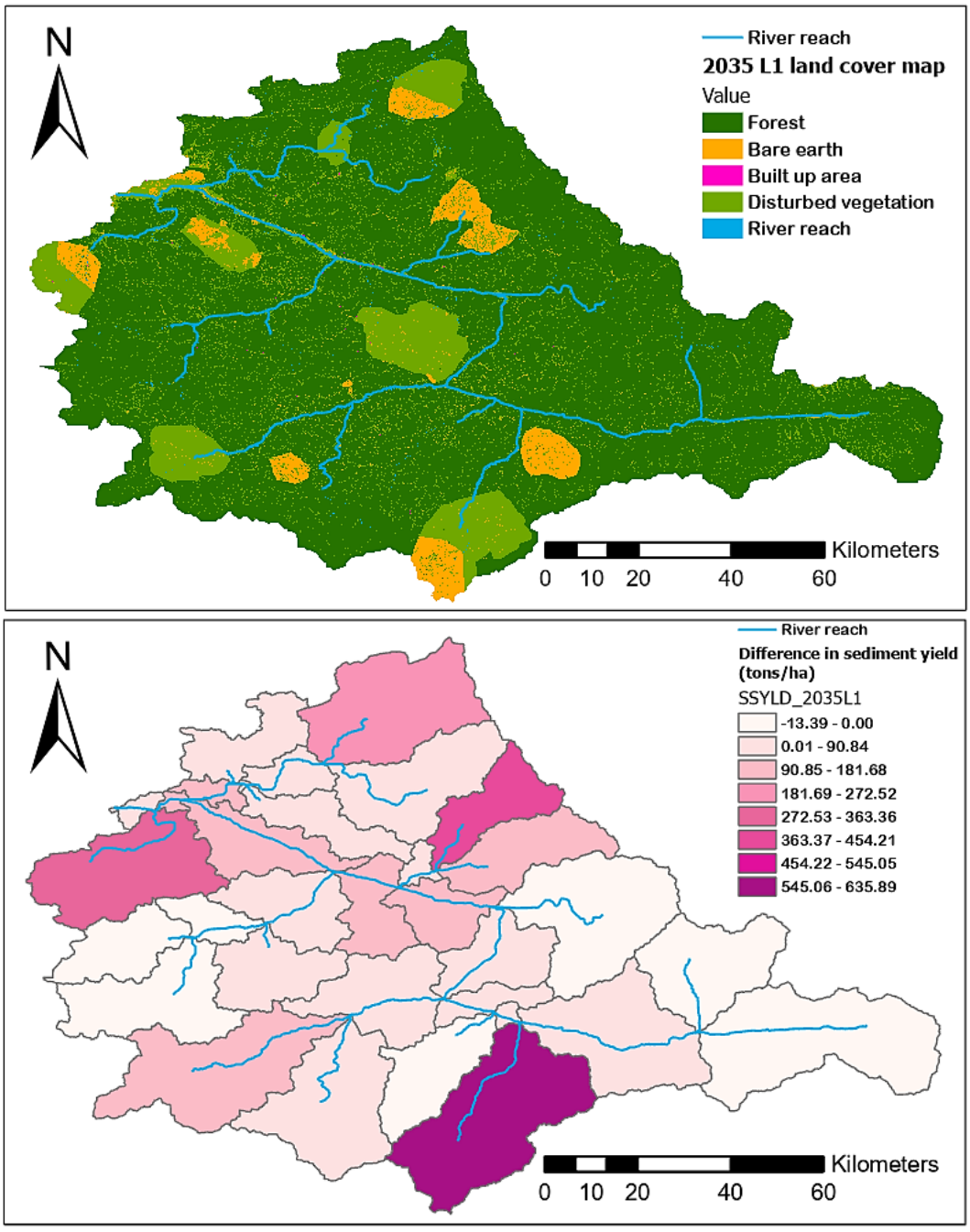

Figure 24. Top- Low deforestation (L1) land cover map for 2036 used as land-use input; Bottom- Percentage difference in SSYLD of each sub-basin (averaged across 2034-2036) under low deforestation land cover change compared to the baseline scenario.

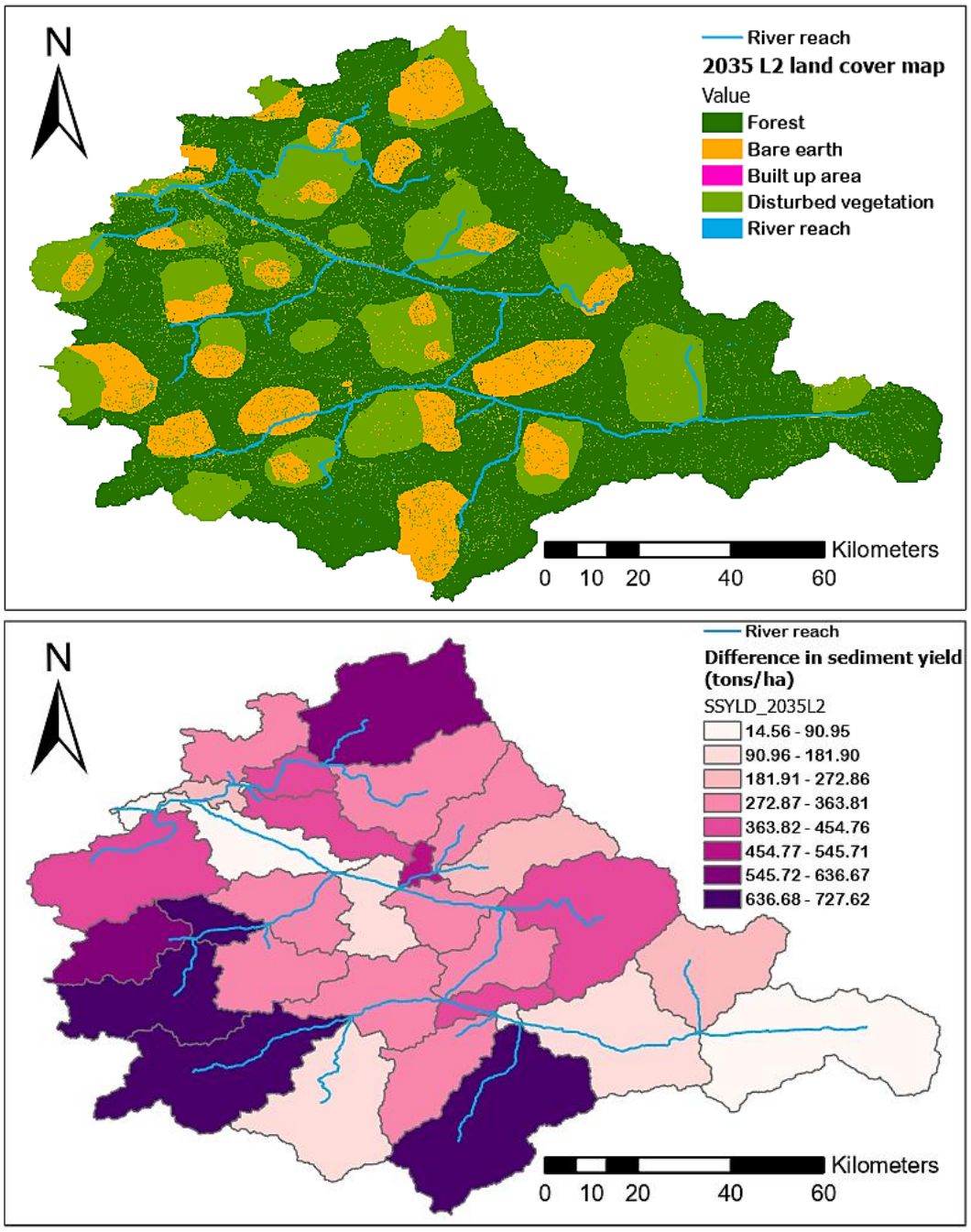

Figure 25. Top- High deforestation (L2) land cover map for 2036 used as land-use input; Bottom- Percentage difference in SSYLD of each sub-basin (averaged across 2034-2036) under high deforestation land cover change compared to the baseline scenario.

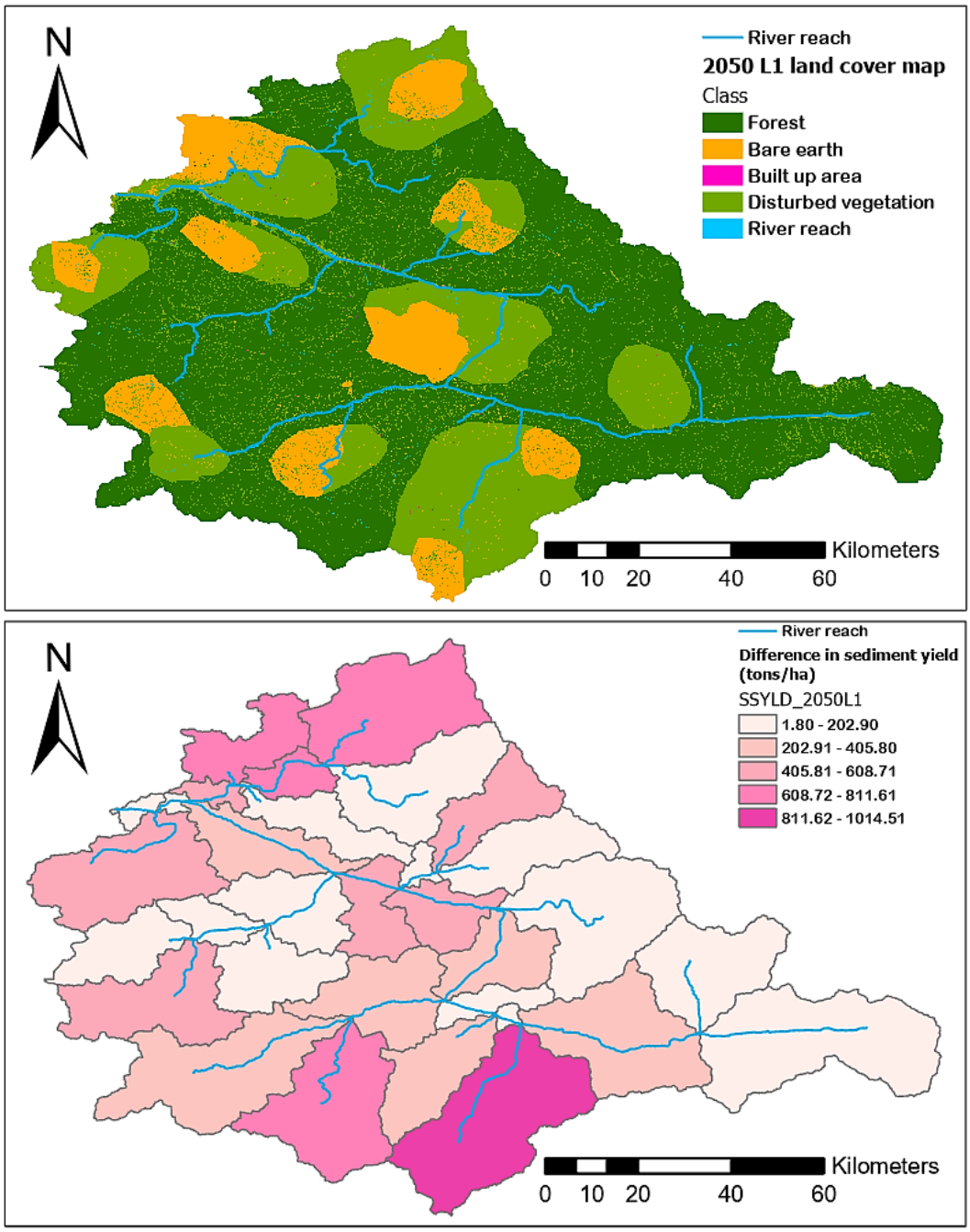

Figure 26. Top- Low deforestation (L1) land cover map for 2051 used as land-use input; Bottom- Percentage difference in SSYLD of each sub-basin (averaged across 2049-2051) under low deforestation land cover change compared to the baseline scenario.

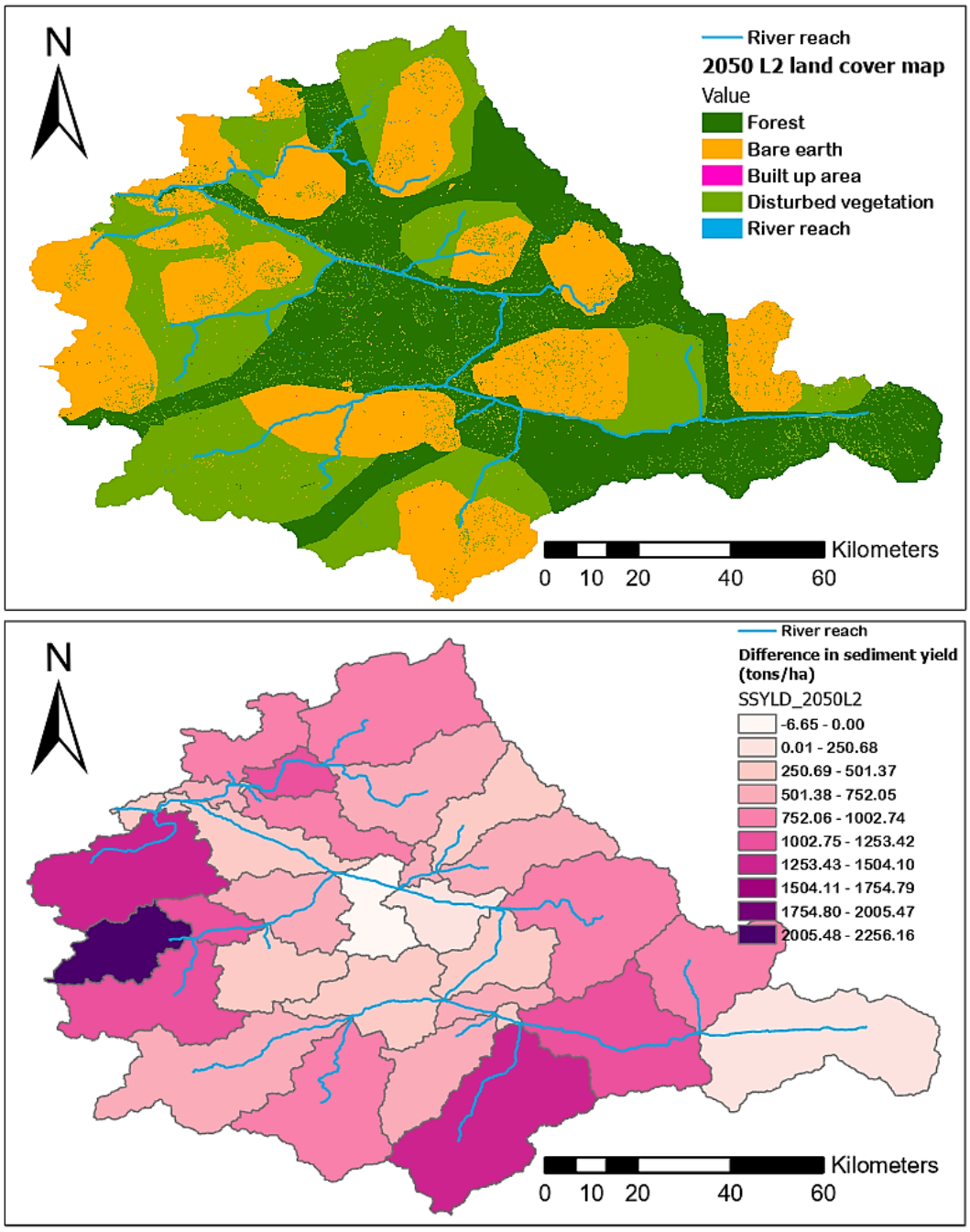

Figure 27. Top- High deforestation (L2) land cover map for 2051 used as land-use input; Bottom- Percentage difference in SSYLD of each sub-basin (averaged across 2049-2051) under high deforestation land cover change compared to the baseline scenario.

Low deforestation land cover change in the 2030 simulation caused an increase in the specific sediment yield (SSYLD) from the sub-basins of up to 240%, while high deforestation land cover change in the same period caused an increase of up to 320%. For the 2035 simulations, low deforestation and high deforestation increased SSYLD from the sub-basins by up to 625% and 15 to 728% respectively. SSYLD from the sub-basins in the 2050 simulations increased up to 1015% under low deforestation while high deforestation caused an increase of 2256%.

The magnitude of increase in SSYLD was proportional to the amount of bare earth and disturbed vegetation in the sub-basins for all the simulations. The bare earth class caused a greater

increase in specific sediment yield compared to the disturbed vegetation. There was some between sub-basin variation in the degree of change for each land cover scenario, reflecting spatial patterns in the degree of forest loss and disturbance; e.g sub-basins in the south and southwest had consistently higher yields while those in the central region of the catchment generally had lower yields.

The average annual sediment yield from the Baleh catchment for each monthly-time step simulation (2030, 2035 and 2050) under low (L1) and high (L2) deforestation scenarios is shown in Table 17. For the L1 scenarios, the annual sediment yield in 2030, 2035 and 2050 increased by 47%, 97% and 322% respectively from the baseline. For the L2 scenarios, the annual sediment yield in 2030, 2035 and 2050 increased by 127%, 338% and 736% respectively from the baseline.

Table 17. Annual sediment yield for low deforestation (L1) and high deforestation (L2) scenarios for 2030, 2035 and 2050 simulations with the percentage difference compared to the baseline value. The values in the brackets are the percentage difference between L2 and L1 within the same period.

Land cover change scenarios	***Baseline***	***2030 L1***	***2030 L2***	***2035 L1***	***2035 L2***	***2050 L1***	***2050 L2***
Average annual sediment yield (tonnes)	1.20E+08	1.76E+08	2.72E+08	2.36E+08	5.25E+08	5.06E+08	1.00E+09
Percentage difference compared to baseline (and L1)	NA	47%	127% (+54%)	97%	338% (+122%)	322%	736% (+98%)

4.3 Impact of climate change and low deforestation rates on flow and sediment dynamics

The average annual sediment yield from the Baleh catchment was tabulated for each monthly-time step for the focal years (2030, 2035 and 2050) under no climate change (R1) and climate change (R2) scenarios (Table 18). All the simulations had a low level of annual deforestation of 2% (L1), rather than the less likely high value of 4%. R1 uses the baseline rainfall and temperature values whereas R2 experiences reduced rainfall and increased temperature. All the scenarios experienced higher sediment yield compared to the baseline. For the R1 scenarios, the annual sediment yield in 2030, 2035 and 2050 increased by 47%, 97% and 322% respectively from the baseline. For the R2 scenarios, the annual sediment yield in 2030, 2035 and 2050 increased by 17%, 70% and 178% respectively from the baseline. Climate change was predicted to reduce the annual sediment yield of the Baleh catchment for each SWAT simulation by 14 to 34% compared to R1.

Table 18. Annual sediment yield for no-climate change (R1) and climate change (R2) scenarios for 2030, 2035 and 2050 simulations with the percentage difference compared to the baseline value. The values in the brackets are the percentage difference between R2 and R1 within the same period.

Climate change scenarios	***Baseline***	***2030 L1R1***	***2030 L1R2***	***2035 L1R1***	***2035 L1R2***	***2050 L1R1***	***2050 L1R2***
Average annual sediment yield (tonnes)	1.20E+08	1.76E+08	1.41E+08	2.36E+08	2.04E+08	5.06E+08	3.33E+08
Percentage difference compared to baseline (and L1)	NA	47%	17% (-20%)	97%	70% (-14%)	322%	178% (-34%)

The predicted effects of climate and land cover change on suspended sediment concentration (SSC) are illustrated in Figure 28. The climate change scenario has a smaller SSC range for most of the year due to lower maximum SSC values with the greatest effect between June to August. On the other hand, climate change affected flow dynamics by lowering the maximum and minimum daily flow values for the monsoon months of January to March and November to December (Figure 29). The no-climate change scenario had nearly an identical daily flow value range to the baseline scenario.

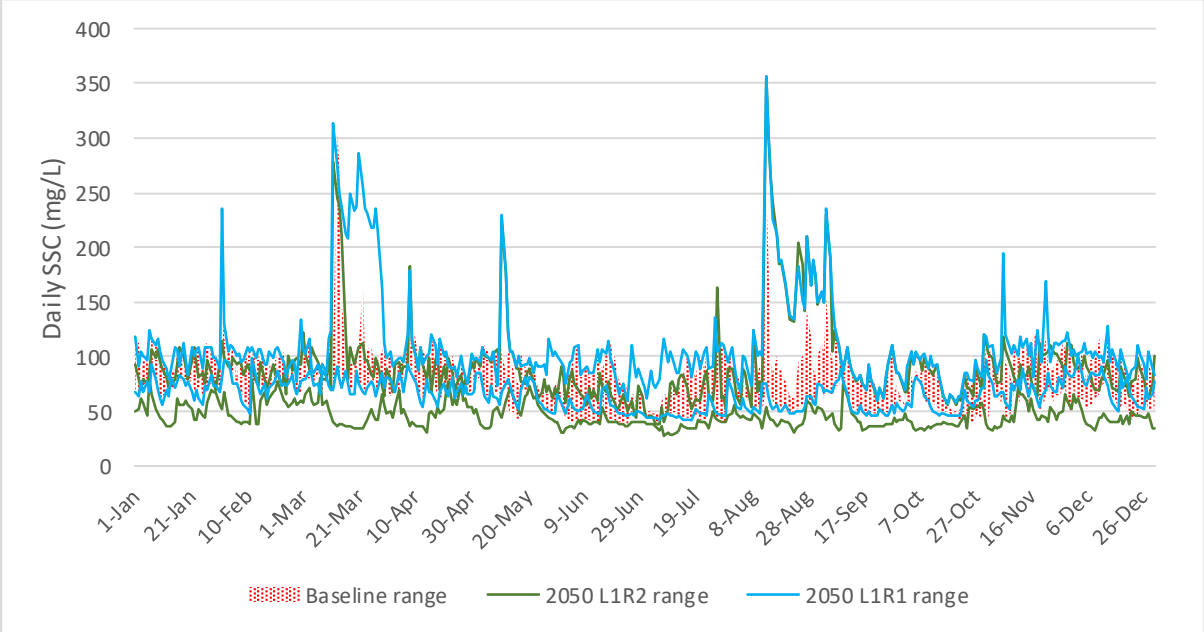

Figure 28. Range of values for the baseline, 2050 low deforestation + climate change (L1R2) scenario and 2050 low deforestation + no climate change (L1R1) scenario.

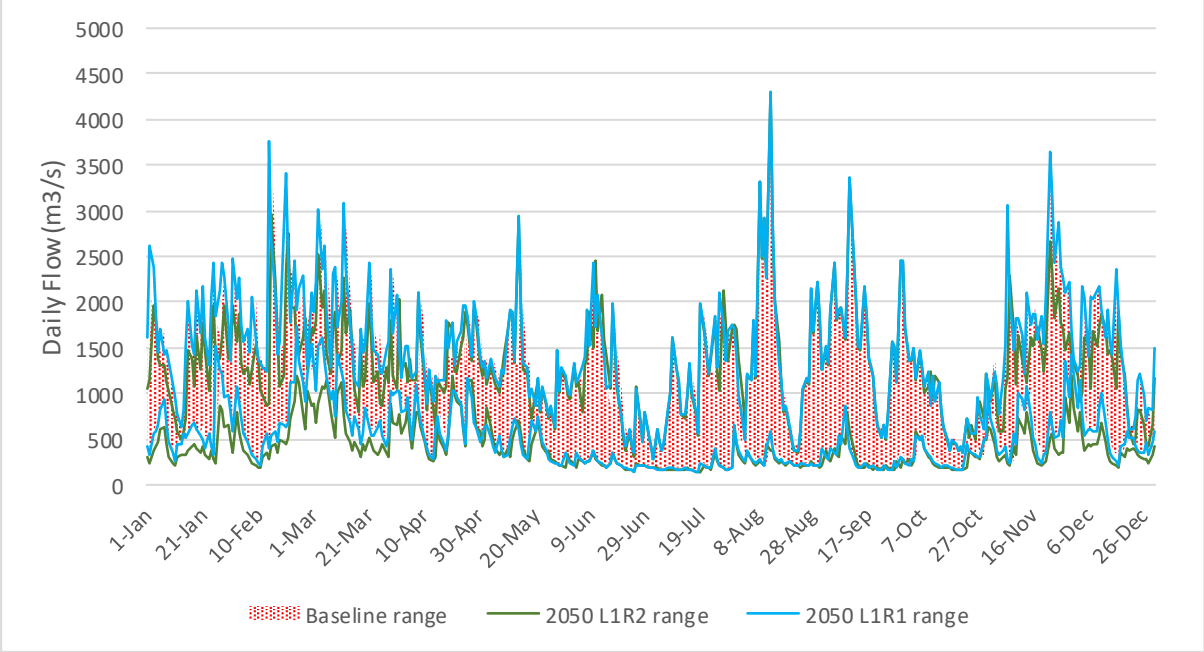

Figure 29. Range of daily flow values for the baseline, 2050 low deforestation + climate change (L1R2) scenario and 2050 low deforestation + no climate change (L1R1) scenario.

4.4 Impact of climate change and high deforestation rates on flow and sediment dynamics

Table 19 gives model results for the interactive effects of climate change and high rates of deforestation. It appears that climate change significantly reduced the increased annual sediment yield caused by high deforestation rates - the percentage difference between L2R2 and L2R1 for the 2030, 2035 and 2050 simulations are 40%, 94% and 41% respectively as compared to the difference between L2 and L1 scenarios with no-climate change of 54%, 122%, 98%. The possible causes for these patterns are discussed in Chapter 5, along with a discussion of the predicted SSC values and what they mean for river conditions (turbidity).

Table 19. Annual sediment yield for low deforestation + no climate change (L1R1), high deforestation + climate change (L2R2) and high deforestation + no climate change (L2R1) scenarios for 2030, 2035 and 2050 simulations with the percentage difference compared to the baseline value. The values in the brackets are the percentage difference between the L2R2 and L2R1 scenarios and L1R1 within the same period.

Land cover + climate change scenarios	***Baseline***	***2030 L1R1***	***2030 L2R2***	***2030 L2R1***	***2035 L1R1***	***2035 L2R2***	***2035 L2R1***	***2050 L1R1***	***2050 L2R2***	***2050 L2R1***
Average annual sediment yield (tonnes)	1.20E+08	1.76E+08	2.46E+08	2.72E+08	2.36E+08	4.59E+08	5.25E+08	5.06E+08	7.15E+08	1.00E+09
Percentage difference compared to baseline (and L1)	NA	47%	106% (+40%)	127% (+54%)	97%	283% (+94%)	338% (+122%)	322%	497% (+41%)	736% (+98%)

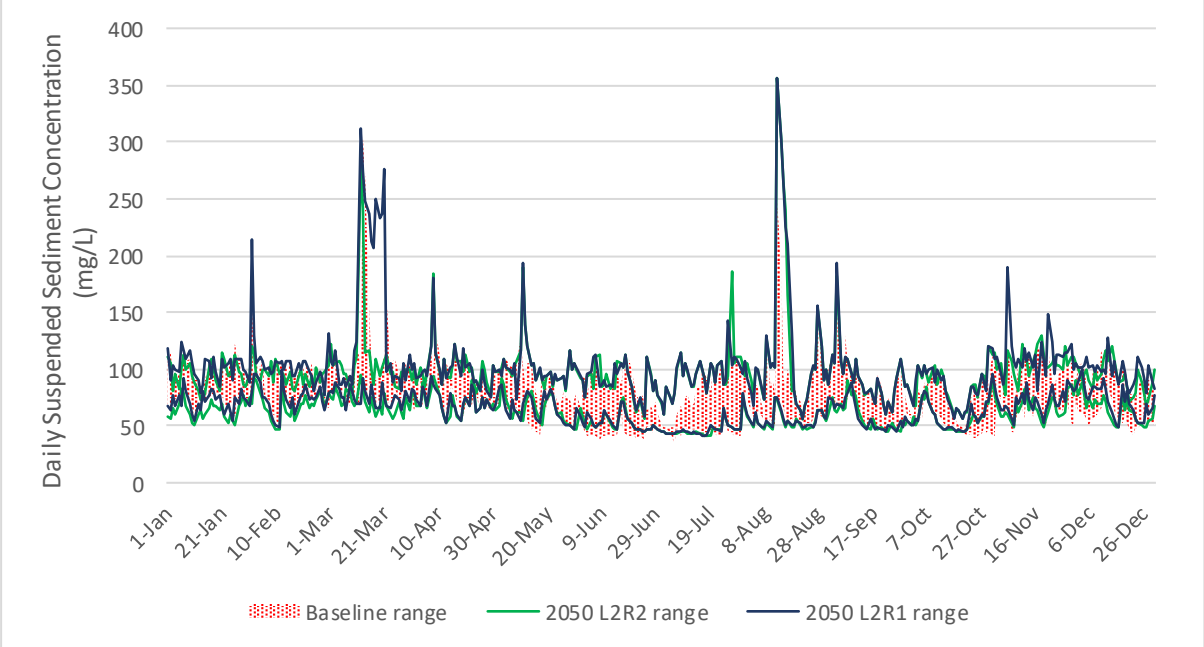

Figure 30. Range of daily suspended sediment concentration (SSC) values for the baseline, 2050 high deforestation + climate change (L2R2) scenario and 2050 high deforestation + no climate change (L2R1) scenario.

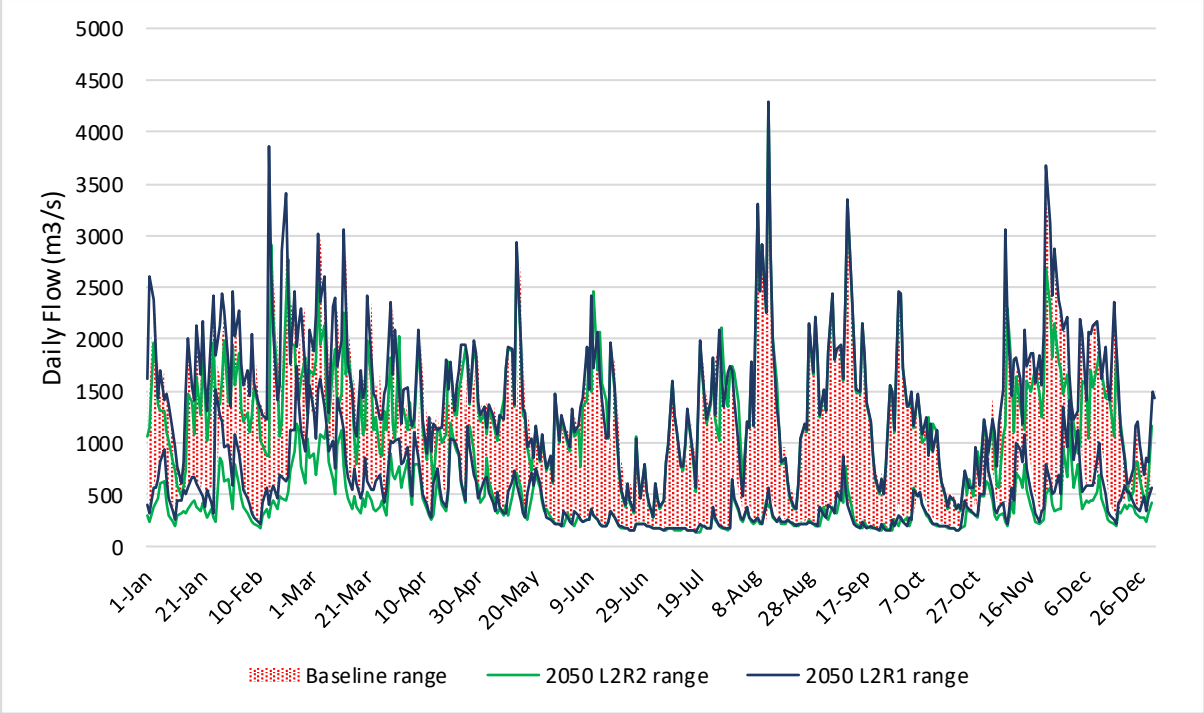

Figure 31. Range of daily flow values for the baseline, 2050 high deforestation + climate change (L2R2) scenario and 2050 high deforestation + no climate change (L2R1) scenario.

The effects of climate change on suspended sediment concentration (SSC) is illustrated in Figure 30 with a comparison between the high deforestation scenarios of 2050 with climate change and without climate change. The climate change scenario has a slightly smaller range during the first 100 days of the year and the last 60 days when compared to the no-climate change scenario. On the other hand, climate change affected flow dynamics by lowering the maximum and minimum daily flow during the monsoon months (Figure 31). The no-climate change scenario had nearly an identical daily flow value range to the baseline scenario. The combined effects of high deforestation land cover change and climate change had similar effects as climate change with low deforestation land cover change on flow but affected SSC to a lesser degree.

4.5 Comparing effects of climate change and land cover change at sub-basin level

Figure 32 (a-c) shows the variation between sub-basins in the impacts of climate and land cover change on sediment yield. To aid comparison, data are expressed as change relative to baseline, and used modelled values of sediment yield for one future time period (2050); to simplify, only selected scenarios are depicted - the low deforestation + no climate change (L1R1) scenario, the low deforestation + climate change scenario (L1R2) and high deforestation + no climate change (L2R1) scenarios. The main goal is to assess whether some basins appear more sensitive than others, and to see whether climate change or landcover contributes most to changes in yield. The same data are plotted in different ways in a-c.

In most of the sub-basins, climate change caused sediment yield to decrease while land cover change caused it to increase. This is expected as the climate change scenario of reduced rainfall would result in less runoff which reduces the erosion of soil into the rivers whereas the land cover change scenario with a higher deforestation rate would increase the surface area of bare earth and result in greater amounts of soil being washed away by precipitation. The magnitude of the impact of land cover change is greater.

Responses vary greatly between sub-basins. For example, as evident in Fig 32 b, basin 20 is very responsive to both landcover and climate change, showing the greatest reduction in yield as result of climate and the highest increase in response to landcover change. Conversely, a sub-set of the basins behave in a similar way – those clustered at the top left of Fig 32 b. These differences have implications for directing forest protection.

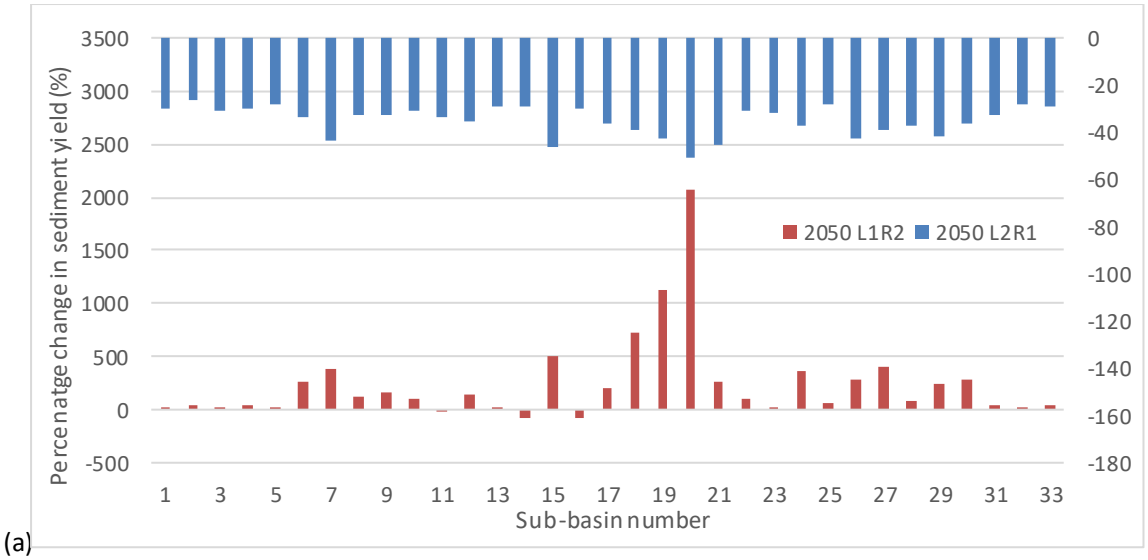

(a)

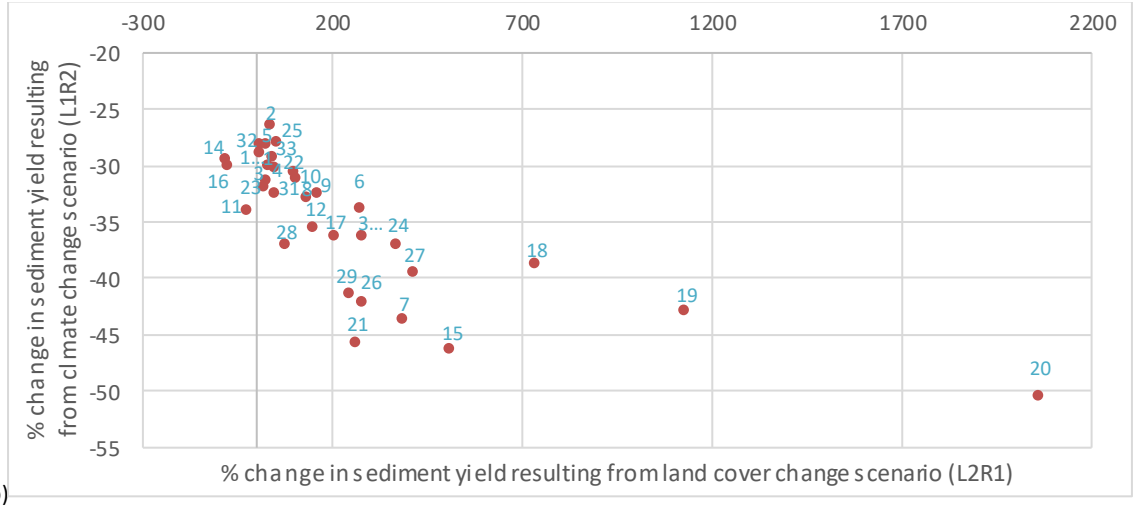

(b)

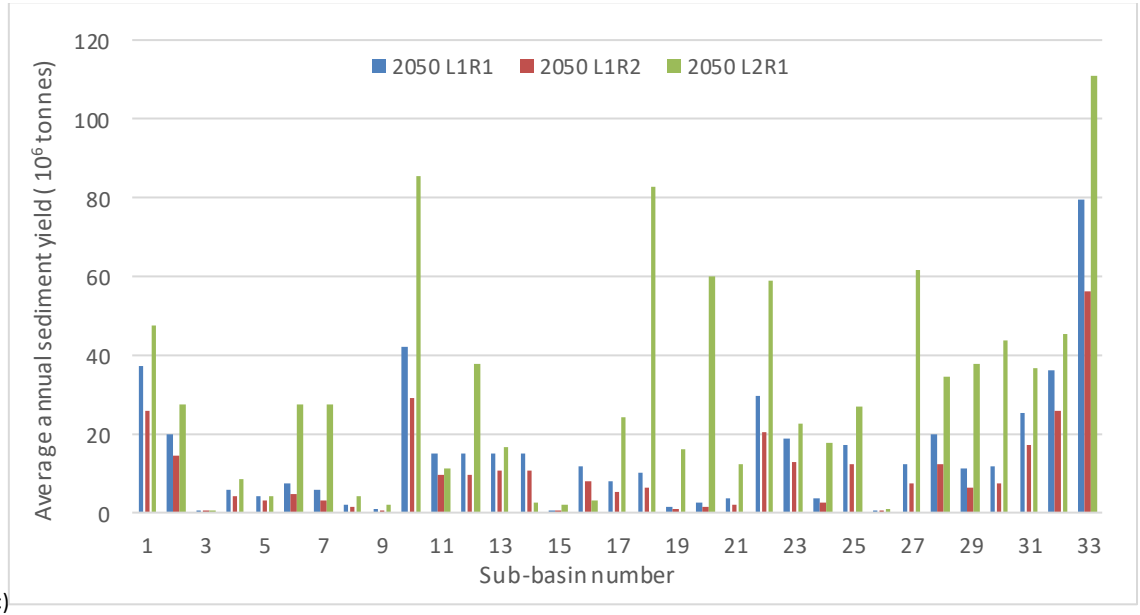

(c)

Figure 32. Top and middle (a & b) - Percentage change in sediment yield resulting from the climate change (L1R2) and land cover change scenarios respectively (L2R1); Bottom (c) - Average annual sediment yield for all the sub-basins.

4.6 Impact of Baleh dam with different operational scenarios on flow and sediment loads

Figure 33 show an example of the hydrographs at the dam site and the catchment outlet resulting from the two dam operational scenarios. Note that (as described above) 50 randomisations were run for the HEP regime and only one run was made for the non-HEP one, but to make a direct comparison of the two scenarios, the figure shows them applied to the same year (same rainfall and temperature) and only one of the HEP randomisations is shown (rather than all 50). The Figure shows that the non-HEP scenario results in some seasonal patterns of flow; this is because the volume of water released from the dam balances inflows which differ between the wet and dry period. During the May to September period one turbine is needed to balance the low inflows during these non-monsoon months) while for the wetter months of the year, more water is released. In contrast, the HEP scenario does not have seasonality in its release patterns because of the randomised allocation of flow to days. Overall it fluctuates around a modal flow which is set by the use of three turbines.

The two scenarios have impacts on flows that remain visible in the hydrograph as far downstream as the catchment outlet, with a more seasonal stepped pattern resulting from the non-HEP scenario (lower in May to Sept, and higher the rest of the year).

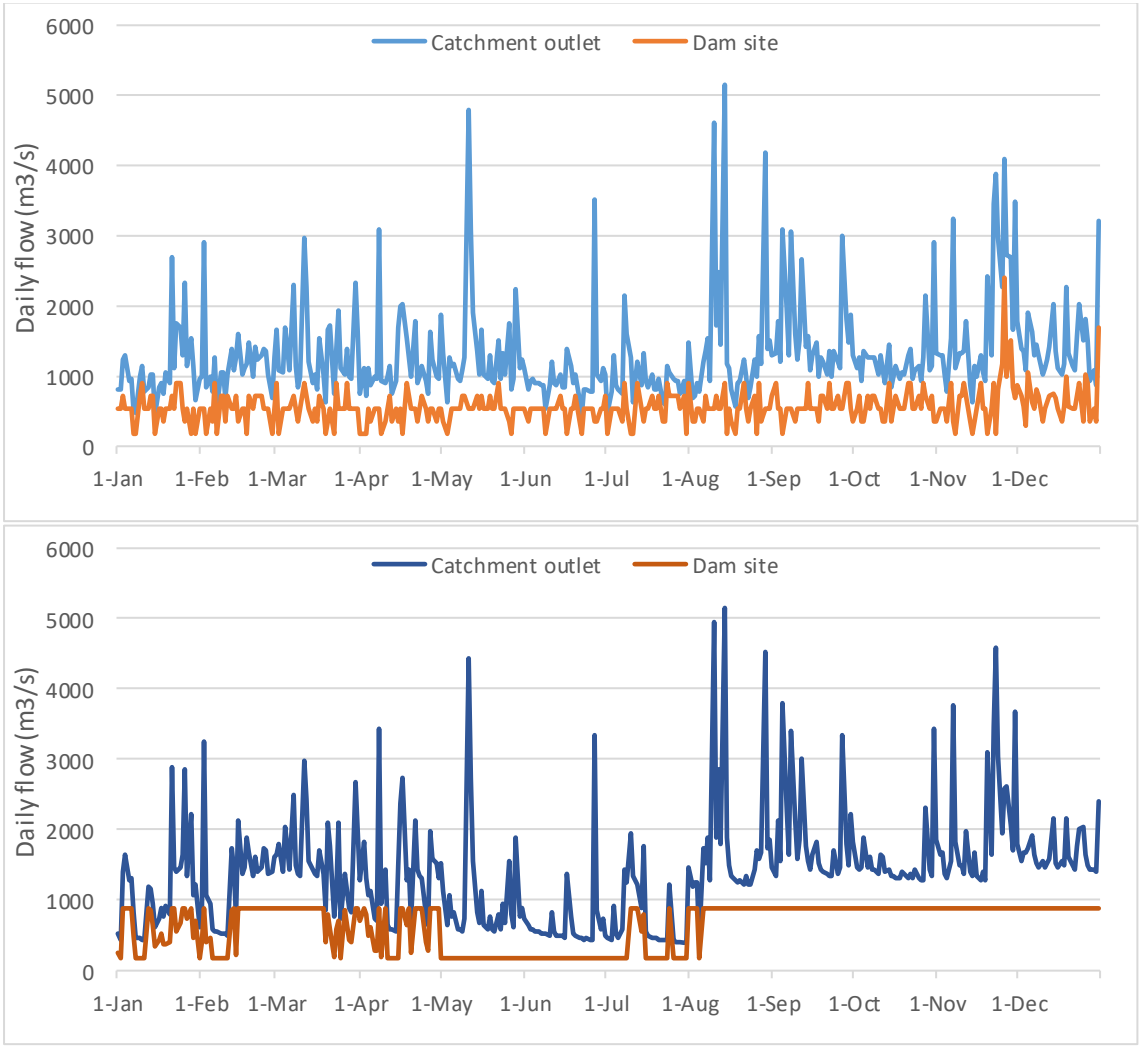

Figure 33. Impacts of the HEP scenario (Top) and the non-HEP scenario (Bottom) on flows at the dam site and the catchment outlet.

Flow duration curves were created for the baseline, HEP and non-HEP scenarios at the dam site and the catchment outlet (Figure 34). Relative to baseline, at the dam site the HEP scenario markedly reduced discharges in the high flow range (percentiles 5-15) and increased slightly the moderate and lower flows (approx. 45-90 percentiles). At the catchment outlet, HEP increased the discharge magnitude of the low flow percentiles and had very little impact on high flows. The non-HEP scenario resulted in a very flat duration curve at the dam site, with markedly reduced discharge in the high flow range and increased discharge magnitude for the percentiles 20-60; impacts on low flows were hardly evident. At the outlet, its relative effects across the flow range were similar to the dam site but much less marked.

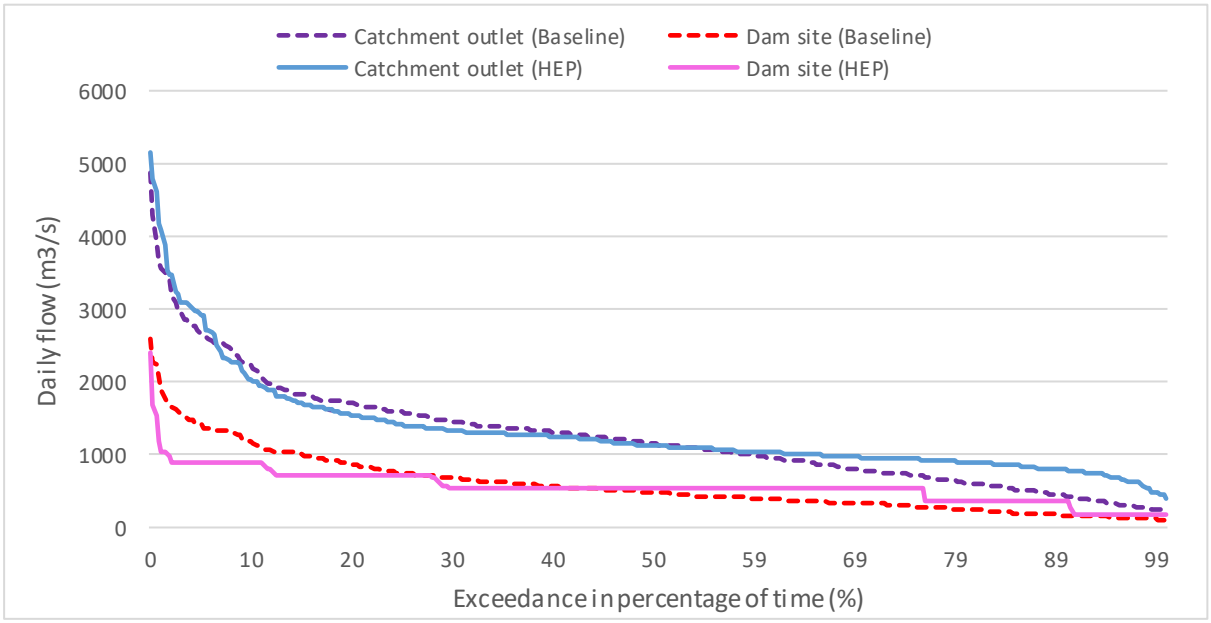

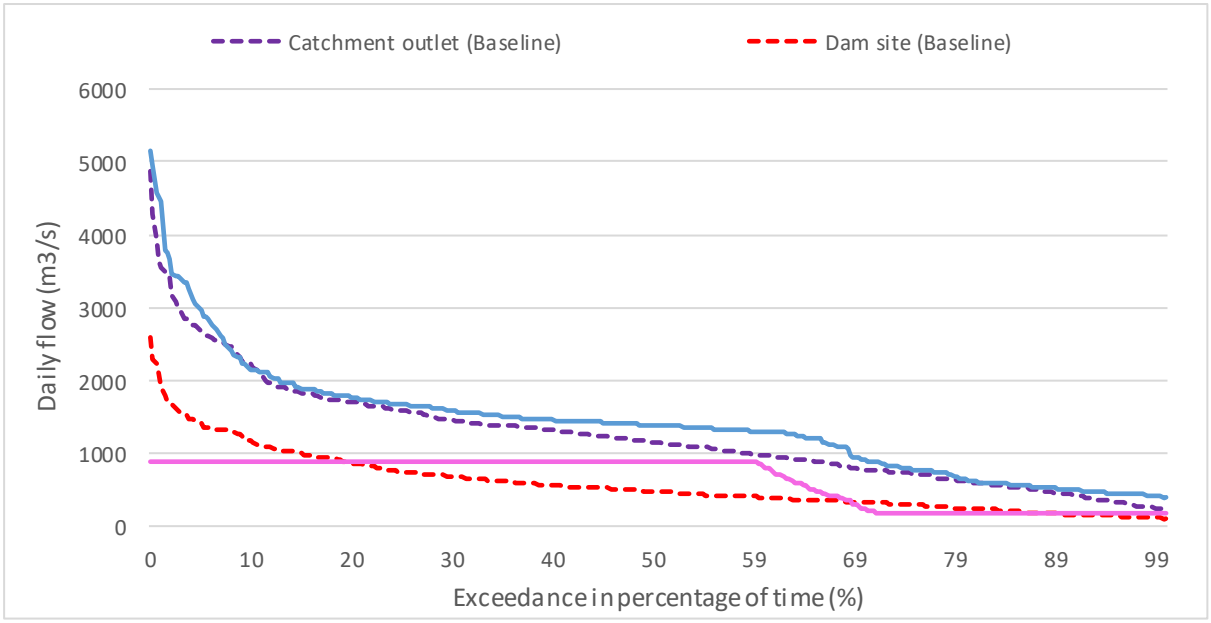

Figure 34. Top - Flow duration curves (FDC) comparing the baseline with the HEP scenario (Top) and the non-HEP scenario (Bottom) at the dam site and catchment outlet. Only one of the randomisations of HEP was used as the representative.

The dam under the HEP and non-HEP scenarios are predicted to have higher release rates than the baseline average flow (Figure 35). The non-HEP scenario starts off having about 100 m^3/s higher flows at the dam site and experiences a steeper accretion pattern than the baseline. On the other hand, the HEP scenario only has slightly higher flows at the baseline but achieves a significantly higher flow (200 m^3/s higher) at the catchment outlet.

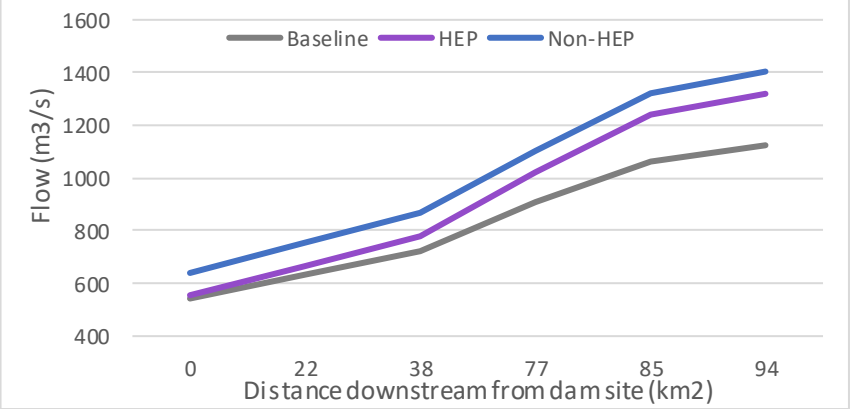

Figure 35. Flow accretion curves of the monthly average flow for the HEP and the non-HEP scenario from the dam site and catchment outlet compared to the baseline. Only one of the randomisations of HEP was used as the representative.

The scenarios had different predicted effects on sediment loads. To illustrate relative loads at the dam site, predicted daily sediment loads were divided into 4 classes based on their values: low (0 to 391.3 tonnes), medium (391.4 to 645.6 tonnes), high (645.7 to 1154.1 tonnes) and very high (1154.2 to 2171 tonnes). High sediment loads were dominant in the non-HEP scenario with an occurrence of approximately 60% of the time while the HEP scenario had medium sediment load levels for 55% of the time (Figure 36). The HEP scenario experienced a few days with very high sediment loads whereas the non-HEP scenario did not have any.

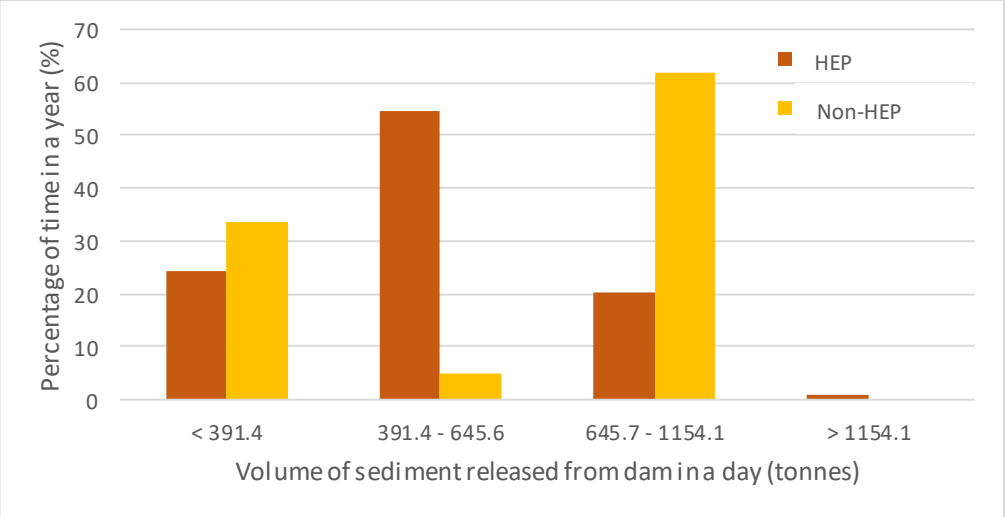

Figure 36. Frequencies of different sediment loads under the HEP and non-HEP scenario.

At the dam site, both scenarios are predicted to reduce sediment loads markedly (Figure 37). However, unexpectedly they predict that loads at the outlet will increase. Possible explanations for this increase are discussed in Chapter 5.

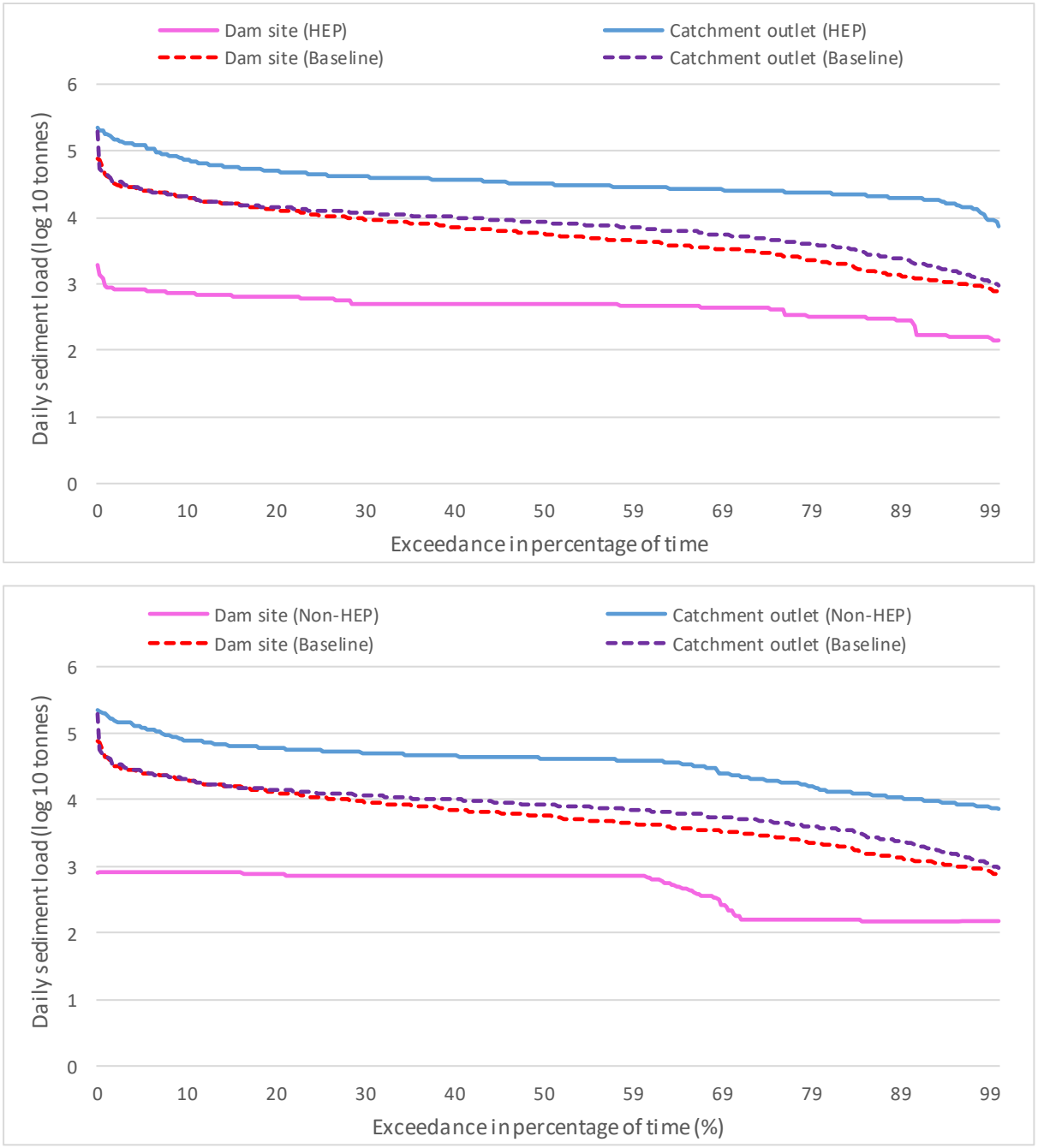

Figure 37. Sediment duration curves comparing the baseline with the HEP scenario (Top) and the non-HEP scenario (Bottom) at the dam site and the catchment outlet. Only one of the randomisations of HEP was used as the representative.

The results of the 50 simulations indicated that varying the day of HEP releases has no major effect on the overall (annual) patterns of sediment transport (Figure 38), with the lines representing each of the 50 simulations all sitting very close together. There was, however, a clear difference between HEP and non-HEP scenarios, notably across the 30-90 % time

exceedance values. The sediment load frequency curve at the catchment outlet was different than the dam site for both scenarios. This is discussed in Chapter 5.

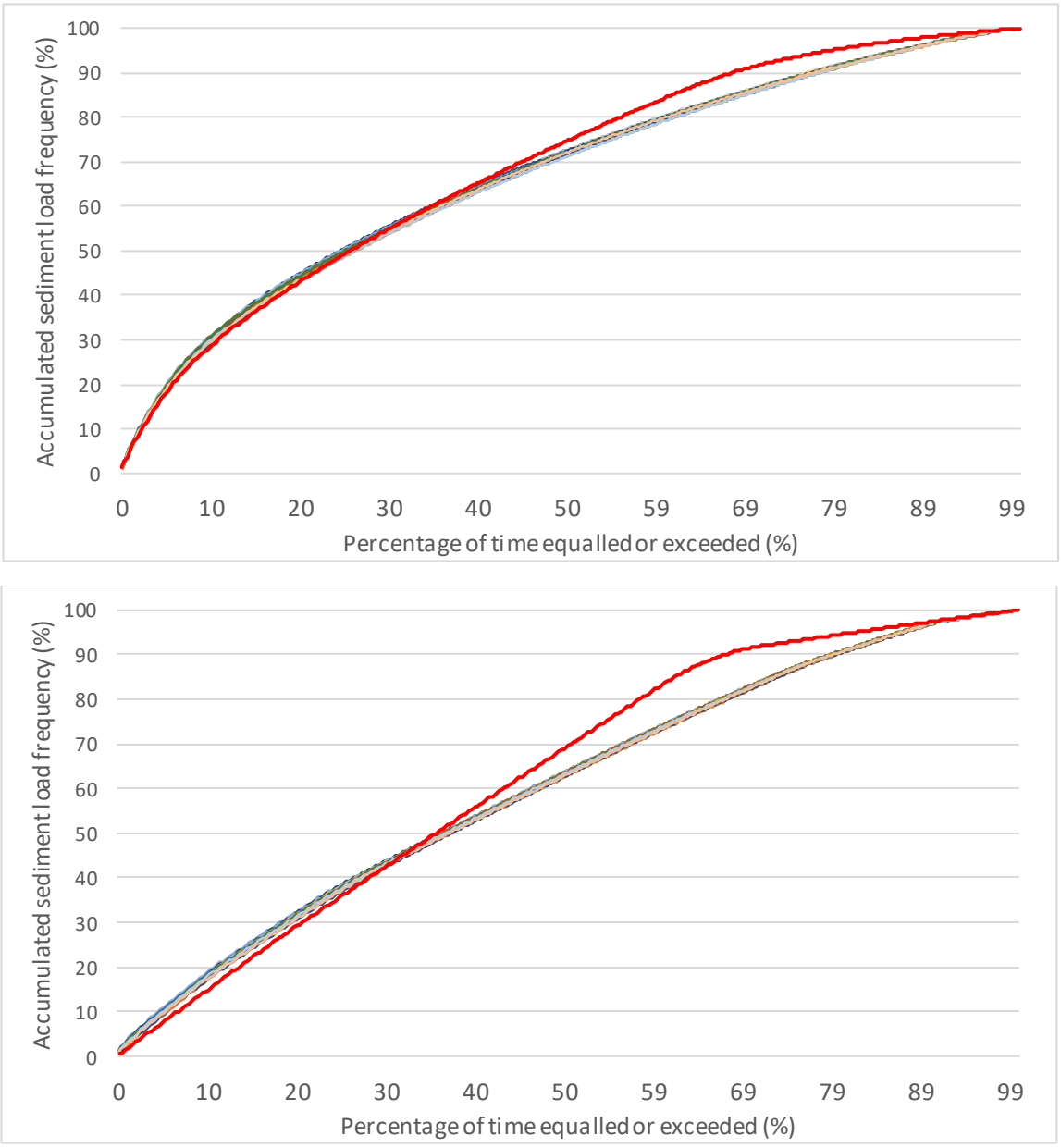

Figure 38. Sediment load frequency curve at the dam site (Top) and the catchment outlet (Bottom). The multi-coloured lines are the observations from the 50 HEP simulations while the red line is the observation for the non-HEP scenario.

A reduction in sediment load is predicted in the first 22 km downstream from the dam (Figure 39). When the dam is incorporated in the SWAT model, the sediment starts close to 0 but recovers on the way downstream and eventually exceeds the baseline sediment loads at the catchment outlet for both the HEP and non-HEP scenarios. The non-HEP scenario makes a quicker recovery immediately after the first 22 km downstream from the dam while the HEP scenario recovers later at the 77 km downstream point. The distances measured downstream from the dam mark the confluences of tributaries and the main stem.

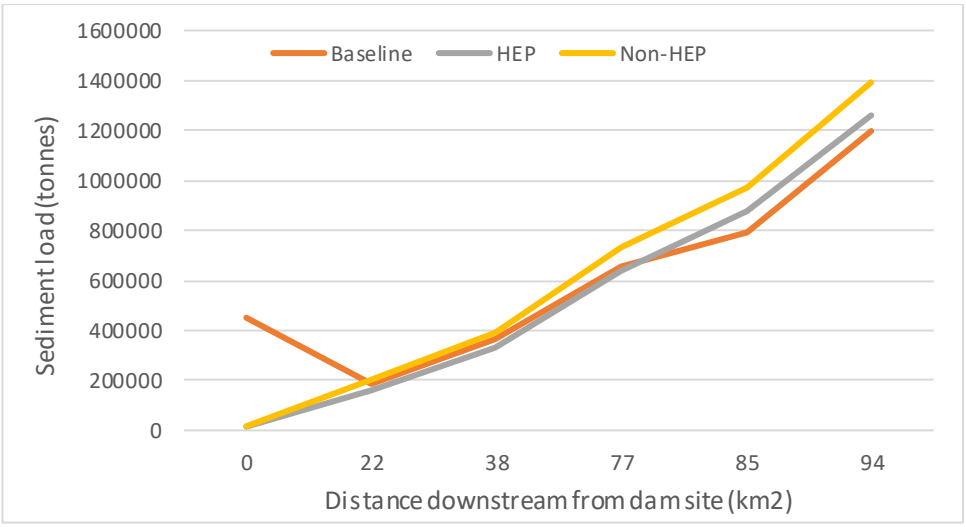

Figure 39. Sediment accretion curves of the HEP and the non-HEP scenario from the dam site and catchment outlet compared to the baseline. Only one of the randomisations of HEP was used as the representative.

4.7 Combined impact of the dam and climate change on flow regime and sediment loads

The dam did not significantly affect the peak flow at the catchment outlet under the HEP and non-HEP scenarios under baseline climate (Figure 34). However, with the incorporation of climate change, the very high flows at the catchment outlet from 0 to 10% exceedance are drastically reduced (by 300 - 1400 m^3/s; Figure 40). Similar to the previous HEP scenario simulations, the low flows from 60-100% exceedance are predicted to experience a slight increase. Hence, it is likely that this effect was not the result of climate change.

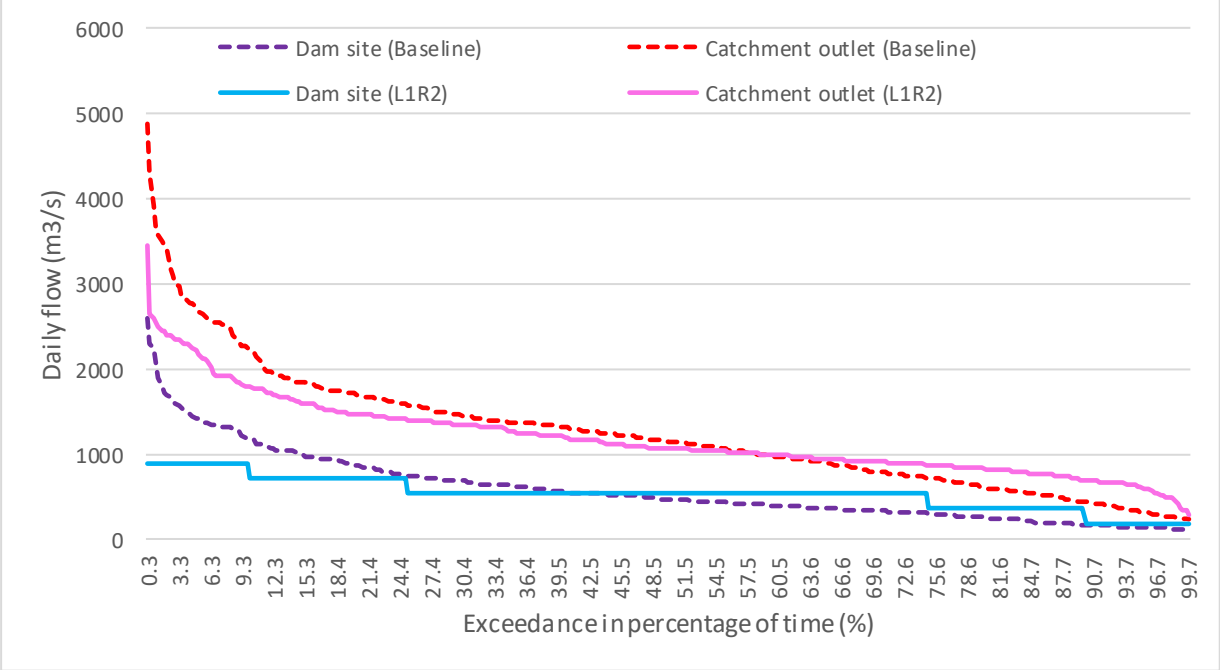

Figure 40. Flow duration curves (FDC) comparing the baseline with the low deforestation + climate change (L1R2) scenario in 2031 at the dam site and catchment outlet.

The annual sediment load at the dam site is solely determined by the release regime of the HEP scenario and the percentage of sediment input being trapped by the dam. From Table 20, it appears that the dam traps 94.5% of the sediment arriving from the upstream sub-basins at the start of dam operation. It is interesting to note that despite this effect, the annual sediment load at the catchment outlet is only 3.8% less than the baseline. This indicates a steady recovery of sediment supply from the various tributaries between the dam site and the catchment outlet. This pattern may, however, be partly a function of how the models run. This issue is discussed in Chapter 5.

With the increasing effect of land cover and climate change by 2051, the sediment load at the catchment outlet and the dam site are expected to decrease and increase respectively. The 2050 simulation only provides a 'snapshot' of how flow and sediment would change with the land cover and climate data for 2047-2051.

Table 20. Annual sediment load at the dam site and catchment outlet for the L1R2 scenario (2031 & 2051) and the baseline (2017).

	L1R2 (HEP) CATCHMENT OUTLET	BASELINE CATCHMENT OUTLET	L1R2 (HEP) DAM SITE	BASELINE DAM SITE
ANNUAL SEDIMENT LOAD IN 2031 (TONNES)	13,825,500	14,370,100	297,140	5,402,100
ANNUAL SEDIMENT LOAD IN 2051 (TONNES)	12,535,300		653,820	
PERCENTAGE DIFFERENCE OF 2031 TO THE BASELINE (%)	-3.8	N/A	-94.5	N/A
PERCENTAGE DIFFERENCE OF 2051 TO THE BASELINE (%)	-13.0		-87.9	

CHAPTER 5. DISCUSSION

5. Chapter 5 Discussion

5.1 Context

The research objectives and main findings of this study are:

(i) *To examine the nature and extent of long-term land cover change in the catchment*. There has been very minimal land cover change in the Baleh catchment from 2001 to 2019 (<2% change in forest cover) but a significant expansion of logging roads which may promote future deforestation.

(ii) *To assess the influence of land cover change on runoff (river flow) and fine sediment loads in the Baleh, and how flows and sediment loads may be further modified by ongoing climate change*. The high deforestation land cover change did not have any significant effects on flow and water yield but is predicted to increase suspended sediment concentration (SSC) levels and sediment load; climate change in the form of lower rainfall and high temperature is predicted to decrease flow and sediment loads significantly.

(iii) *To assess how the presence of the dam alters flow and fine sediment loads in the downstream river*. The impacts of the dam in reducing sediment loads, reducing discharge in the high flow range and increasing discharge in the low flow range are predicted to be greatest at the site immediately downstream. However, impacts of different operational scenarios on flow can still be observed much further downstream at the catchment outlet.

The following sections discuss the main findings for each objective in more detail.

5.2 Nature and extent of long-term land cover change in the Baleh catchment

There were no significant large scale forest clearances in the catchment and > 89% of the study area was classified as forest for all four of the time-steps (2001, 2008, 2012 and 2019). A study investigating logging in Borneo between 1973 and 2010 found that more than 97% of the deforestation occurred in the coastal lowlands (Gaveau et al., 2014). This is consistent with the finding of very limited deforestation in the Baleh (low average annual deforestation rate of 0.15%), which is an inland, headwater sub-catchment of the Rajang. The loss rate estimated for the Baleh is less than the approximately 0.7% annual forest loss rate in Southeast Asia from 1990 to 1997 determined by Achard et al. (2002). The results from the cross-tabulation matrices indicate that forest degradation (from 'Forest' to 'Disturbed vegetation') was more common in the Baleh than forest clearance (Forest to Bare earth). The selective harvesting production system used in Sarawak's legal commercial logging applies a minimum diameter cutting limit (Bryan et al., 2013). According to Gaveau et al. (2014), logging practices in Sarawak are effective in penetrating the uneven forest terrain to harvest natural timber and rarely results in mass forest clearance. Therefore, change in forest canopies and structure due to selective logging might not be reflected as change in land cover (Stibig et al., 2014). The 30 m resolution of the Landsat images used for land cover classification is unable to detect small scale forest clearances and hence, could cause under-estimation of the bare earth class area coverage. This is significant within the context of fine sediment in the river, where even with most of the forest cover remaining, fine sediment is continuously high and the river is always highly turbid.

The land cover maps indicated that logging activity shifted across the catchment from one section to another as different areas are cleared and become barren land or disturbed vegetation. The extensive coverage of the logging road network was consistent with findings by

Bryan et al. (2013) that Sarawak had the highest density of logging roads in Borneo. Hon & Shibata (2013) recorded the presence of logging camps within the Baleh catchment as networks of bare earth. The most common land cover change (66-75%) experienced by the bare earth class is being converted to disturbed vegetation or forest. This suggests that much of the bare earth class is cleared for logging roads or small scale agricultural plantations. The built-up land, likely to be settlements, present along the river and construction of the dam access road, is consistent with observations by Liew et al. (2020). The absence of new structural developments can be explained by the remoteness and inaccessibility of the Kapit district, which is in the central part of the Baleh catchment (Abdullah, 2017).

Over the 19-year period of the current study, the intensity of deforestation and forest degradation was the highest at the start and showed a decreasing trend as the years passed. The highest proportion of forest loss was observed between 2001-2008 while there was more land cover change from disturbed vegetation to forest observed in 2008-2019. Logging activity has been reported by others to have decreased in intensity since 2000 as unlogged forests which are accessible became less available after the initial logging boom in the 1970s (Gaveau et al., 2014). A study by Gaveau et al. (2016) found a shift in Malaysian Borneo's logging trend; The role of industrial plantations (oil palm and pulpwood) in total deforestation increased rapidly between 2005-2010 in Malaysian Borneo and by 2015, the contribution was 20% higher than 2005. The clearing of forests for industrial plantations could explain the forest recovery observed in the latter years as those crops are fast growing and are indistinguishable from natural forest without very high-resolution satellite images.

Based on the nature and extent of historic land cover change in the Baleh catchment, the construction of the Baleh dam and the associated flooding of a large area of forest will present the most significant change in land cover in the catchment. Among the 13 dams in SCORE, Baleh dam will impact the largest forest area (~180,000 ha) and it is located in the second largest remaining blocks of core forest in Sarawak (Alamgir et al., 2020). Forest within the Baleh catchment will also be vulnerable to future land cover change from the associated infrastructure and industrial developments related to the Baleh dam. Such changes - greater than observed historically - were in incorporated into the SWAT modelling to assess their impacts on flow and sediment in the river.

5.3 Flow and sediment loads in the Baleh river under current conditions

The simulated flow and sediment load values from the SWAT model are compared to other major tropical rivers in Figure 41. There is a significant log-linear relationship between mean discharge and upstream catchment area across 5 orders of magnitude. Long term sediment loads of the tropical rivers also scale with mean discharge although there is rather more scatter as physical and human factors may exert some influence. Based on Figure 41 (Top), the Baleh has a higher discharge than expected for a catchment of its size. Conversely, it has a lower suspended sediment load for its discharge volume and a much lower suspended sediment concentration for its sediment yield (Figure 41; middle and bottom). The lower sediment load may reflect the fact that much of the catchment remains forested. The lower concentration, relative to sediment yield, suggests a role of somewhat higher specific discharges in diluting the fine sediment in the channel. These relations provide a useful baseline for assessing future changes in the catchment.

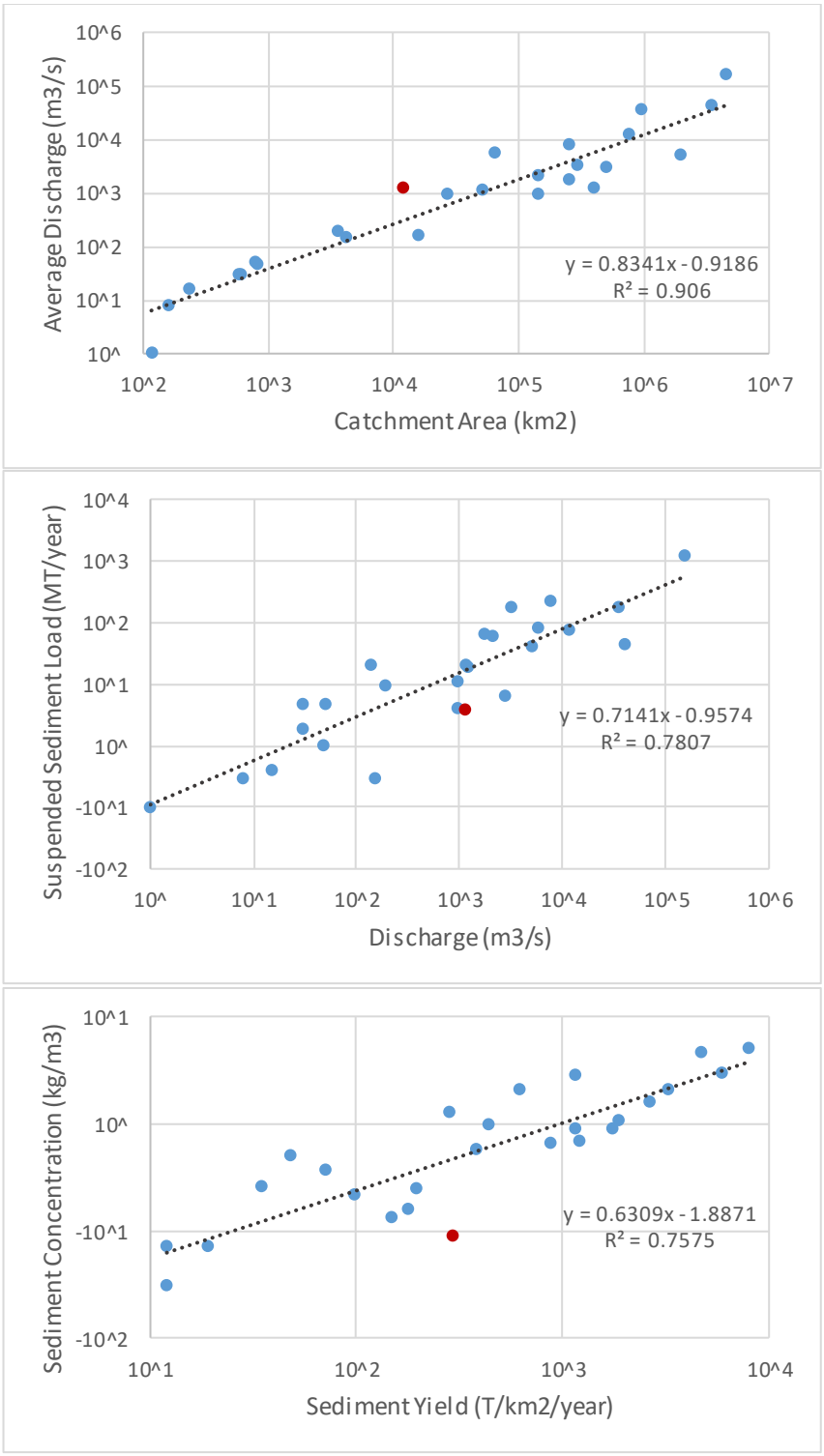

Figure 41. Scatter plots of observational data collected from 35 Tropical river basins with the red dot identifying Baleh catchment (Syvitski et al., 2014). The trend lines and the equation were added by the author, to aid comparison with the Baleh data.

Figure 20 showed the rainfall-runoff plot for the Baleh, using daily simulated runoff and measured rainfall for the baseline years (2015-2017) at the catchment outlet and dam site. The R^2 values obtained for the two locations are 0.3944 and 0.4767. A study conducted in Danum Valley, Sabah, obtained an R^2 value of 0.3028 from a selectively-logged plot, R^2 = 0.4633 from a logging road plot and R^2 = 0.0302 from a pristine forest plot (Cleophas et al., 2017). In

comparison, the R^2 values at the Baleh catchment outlet and dam site are closer to the logged plot and logging road R^2 values. The gradients of the rainfall-runoff regressions for the Baleh catchment outlet (0.174) and dam site (0.268) are much higher than those of all the plots in Danum Valley (selectively logged = 0.062, logging road = 0.089, pristine forest = 0.024). These higher slopes indicate higher relative runoff generation in the Baleh catchment. Runoff generation is influenced by forest canopy density and soil characteristics among other factors. The density of the forest canopy affects the amount of rainfall reaching forest soils while soil texture and bulk density control the infiltration rate of water into the soil. Lower vegetation density and infiltration rates generally result in more surface runoff (Jadczyszyn & Niedzwiecki, 2005; Li et al., 2016). Soil type impacts runoff because different soils have different properties that influence water movement through them. The sandy loam texture of the Baleh soils has high saturated hydraulic conductivity which allows for more infiltration of water and less runoff (Askari et al., 2008).

5.4 Impact of land cover change and climate change on flow and fine sediment loads

The land cover change scenarios of 2% and 5% annual deforestation were not predicted by SWAT to have any significant effect on flow and water yield even in 2050 when approximately 40% and 60% of the forest area is converted to disturbed vegetation and bare earth. On the other hand, an incremental 2.1% rainfall reduction and 0.03°C temperature increment, resulting in a cumulative 18% less rainfall and 0.15°C hotter temperatures by 2050, were predicted to have a significant effect on flow, decreasing daily values by 20-50%. The combined effect of land cover and climate change did not show any major difference compared to the climate change-only scenario. Thus, SWAT suggests that for water runoff the catchment is more sensitive to climate change, at least for the land cover change extents modelled. Conversely, sediment yield in the Baleh catchment is predicted to be highly sensitive to land cover change, with annual sediment yield predicted to increase by 322% and 736% in 2050 under low (2% annually) and high (5% annually) deforestation rates. Increased fine sediment loads have major detrimental effects on aquatic habitats (Dudgeon, 1992) so such changes are a cause of concern. Increased sediment yields from upper sub-catchments also have potentially serious implications for the operation of the Baleh dam as sedimentation leads to loss of storage volume and reduces long-term hydropower generation potential (Walling, 2011). This is discussed further below.

Notably, there were apparently counteracting pressures imposed by climate and land cover change. Compared to baseline conditions, climate change was predicted to decrease the annual sediment yield by 34% by 2050 in the scenario with limited land cover change. The same effect was observed in the daily suspended sediment concentration (SSC) values, with a 30-50% decrease. However, when high deforestation land cover change was applied along with the climate change scenario, annual sediment yield experienced a decrease as compared to without climate change - the combined effect of land cover and climate change only decreased SSC values by 10-20%.

The result from the land cover change scenario is similar to the findings in Tan et al. (2015), where the conversion of 35% forest area to disturbed vegetation and bare earth in the Johor River catchment only resulted in a minor increase in annual streamflow (0.1%). Khoi & Suetsugi (2014) investigated the impact of climate and land use changes on hydrological processes and sediment yield in the Be River catchment using SWAT. Under the climate change scenario of 0.4°C increased annual temperature and 12.8% higher precipitation, annual streamflow and

sediment load increased by 26.3% and 31.7% respectively. Their land use change scenario incorporated 30% deforestation and agricultural expansion which also resulted in annual streamflow and sediment load increases of 1.2% and 11.3%. Climate change was observed to have a stronger effect on flow and sediment load compared to land-use change in Be River. The same inference can be drawn from the outputs for the Baleh. Note though that the effect of climate change was in the opposite direction, where there was a decrease in flow and sediment load. These comparisons suggest that it is hard to generalise about the implications of climate and land cover change in tropical Malaysian catchments, with effects being catchment-specific.

The climate change scenario applied in this study is different to that of Amin et al. (2016) who used climate projections from downscaled GCMs under the SRES A1B emission scenario to assess water resources in Sabah and Sarawak. Their climate projection resulted in an increase in mean monthly temperature and rainfall of approximately 0.5^{o}C and 7% respectively by 2050. With this climate projection, the mean monthly river flow of the Rajang catchment was projected to be similar to that of their baseline of 1980-2000. An increase in temperature generally increases evapotranspiration which then reduces river flow, while an increase in rainfall generally increases surface runoff which consequently increases flow. Due to the specific details in the climate projection applied by Amin et al. (2016), it is likely that the opposing effects of increased temperature and rainfall cancelled each other out to result in a no-change effect on river flows. In contrast, the reduced rainfall and increased temperature applied in the current study can be expected to result in lower flow levels, as indeed predicted by SWAT. It is notable that if the climate projections used by Amin et al hold true, then they represent a marked change from what has happened historically in the Baleh, since Chong (in press) found that over the last 50 years there was no clear trend in rainfall at any of the monitoring stations in the catchment.

The climate change simulations in this study were focussed on understanding their overall effects, scaled up to total annual flow and sediment load values (e.g. Table 18). Thus, they show the gross effects of particular climate change scenarios. Nevertheless, there are other changes not considered by this approach which are worth mentioning, since they may affect river processes and dynamics and hence the river's ecosystems. Climate change may increase the frequency, timing or severity of extreme events (e.g. high rainfall, drought) and indeed some such changes are anticipated for Malaysia. Chang et al. (2015) reported that the global temperature increase has caused stronger and more frequent Madden-Julian oscillation (MJO) in the tropics while Lim et al. (2017) observed a larger number of cold surge (CS) events in Southeast Asia between 1998-2012. The interaction of MJO and CS results in the increase in frequency and intensity of extreme rainfall events. The SWAT model for the Baleh can provide an insight into the consequences of such extreme events, especially since the model was deliberately calibrated using years with some of the most extreme conditions on record (wet and dry years) so we can be confident about the resulting predictions. For example, 2014 was a very dry year in the Baleh (low rainfall), with the lowest flows on record (median discharge for 2014 was approximately 800 m^3/s compared to a long-term value of around 1200 m^3/s). The low rainfall resulted in extended periods of very low flow; e.g. between 13th June and 6th Aug when flows dropped to around 150 m^3/s (Figure 42). During this period, SWAT predicted that SSC was between 36 and 63 mg/L. Such low values most likely reflect reduced sediment yields from the basins, in the absence of any marked precipitation. Thus, under future climate scenarios where extended low rainfall is expected, such periods of low flow and altered river SSC and turbidity can be anticipated. Conversely, SWAT can be used to simulate flow and SSC magnitude during periods of high rainfall (e.g. Figure 43 and 44). For example, sustained rainfall of 45-75 mm/day

can be expected to cause flows to reach 2245-4355 m^3/s and during such events the model suggests that SSC could reach 212-256 mg/L. Again, under a future climate that saw increased frequency of high rainfall, these responses in river flow and SSC could be expected with increased frequency (i.e. extremely high flows and highly turbid water).

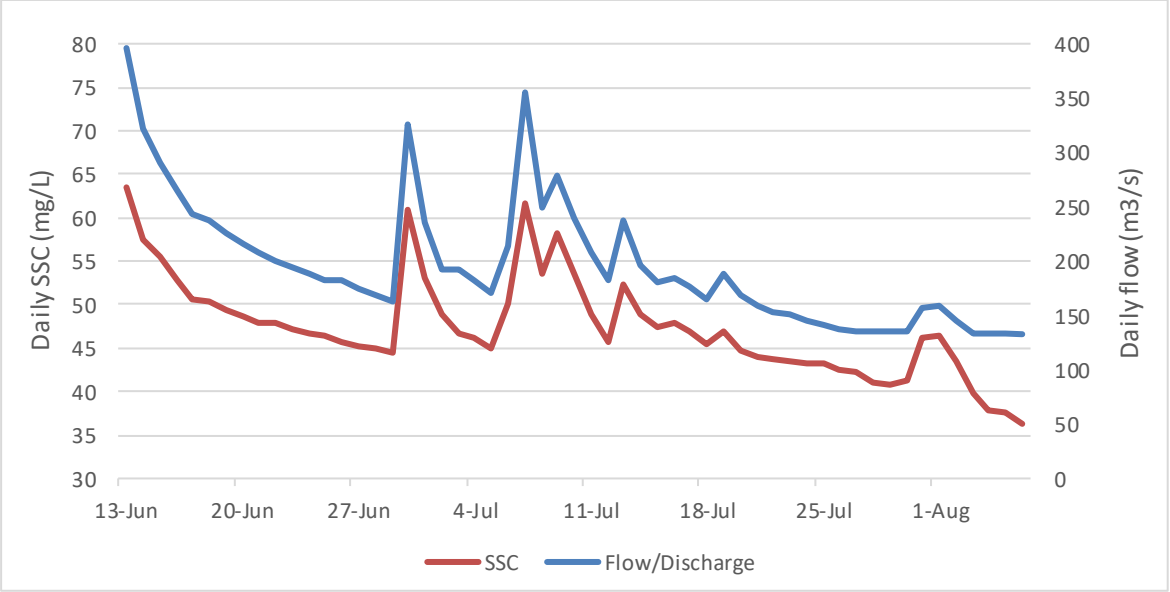

Figure 42. Flow and SSC during a period of sustained low precipitation in June and July 2014.

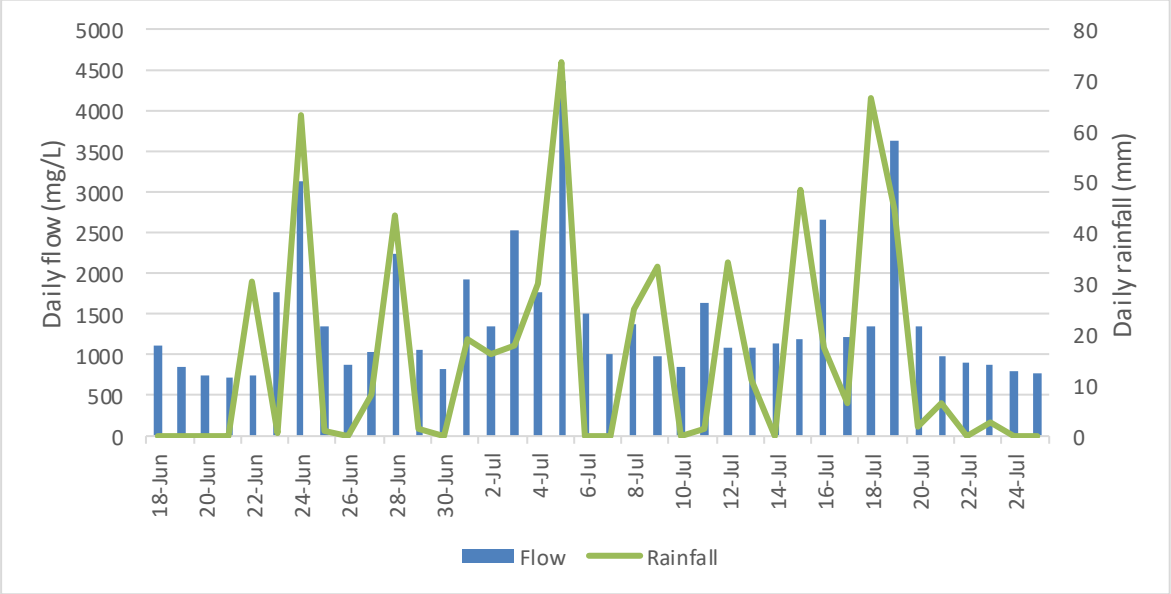

Figure 43. Rainfall and flow during a wet period in the year 2010.

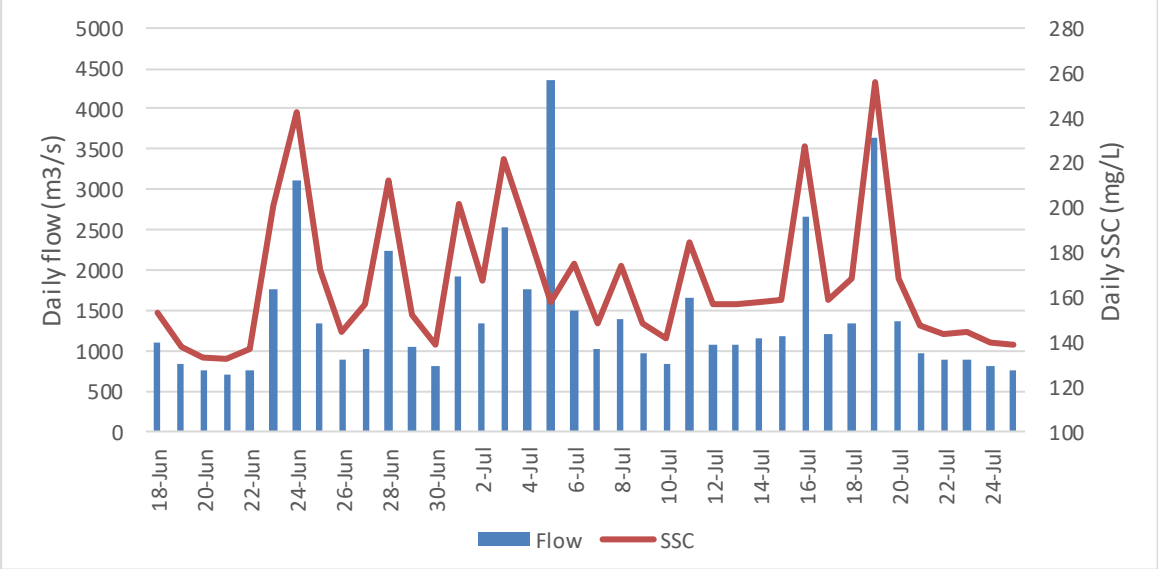

Figure 44. Daily flow and SSC during a sustained wet period in the year 2010.

5.5 Impact of the dam on flow and fine sediment loads

The operational regime of a dam determines the storage of water in the reservoir, sediment capture and release, as well as downstream flow patterns on daily and seasonal scales. One of the interesting findings from the dam simulations is that impacts of both the hydropower (HEP) and non-hydropower (Non-HEP) scenarios on flow are still visible 94 km downstream from the dam site, at the catchment outlet. The catchment area upstream from the dam site is 5599 km^2 which is 45.7% of the Baleh catchment area overall, and correspondingly the average daily flow measured at the dam site is 45.8% of that at the catchment outlet. The significant contribution of flow volume at the dam site likely explains why there are lasting effects of the dam on the flow at the catchment outlet.

The non-HEP regime produced long continuous periods at a low flow, which does not occur in the HEP regime or naturally in the Baleh. To further assess flow impacts, Figure 45 compares the two dam operational scenarios to baseline for the dam site and catchment outlet. At the dam site, the flow duration curves become less even and flatter; Q50 is hardly affected by the imposition of a HEP regime, but it increases substantially under a non-HEP regime. The low flows (percentiles 90, 95 and 99) are hardly affected. In general, the flow duration curve has recovered a more natural shape by the catchment outlet, though there are still some impacts in the lower flow percentiles (increased by the HEP scenario). Given that flow is one of the most important factors in the fluvial environment, the alteration of the magnitude and timing of high flows at the dam site will likely have a great effect on the structure, functioning, and dynamics of riverine ecosystems here (Junk et al., 1989; Poff et al., 1997).

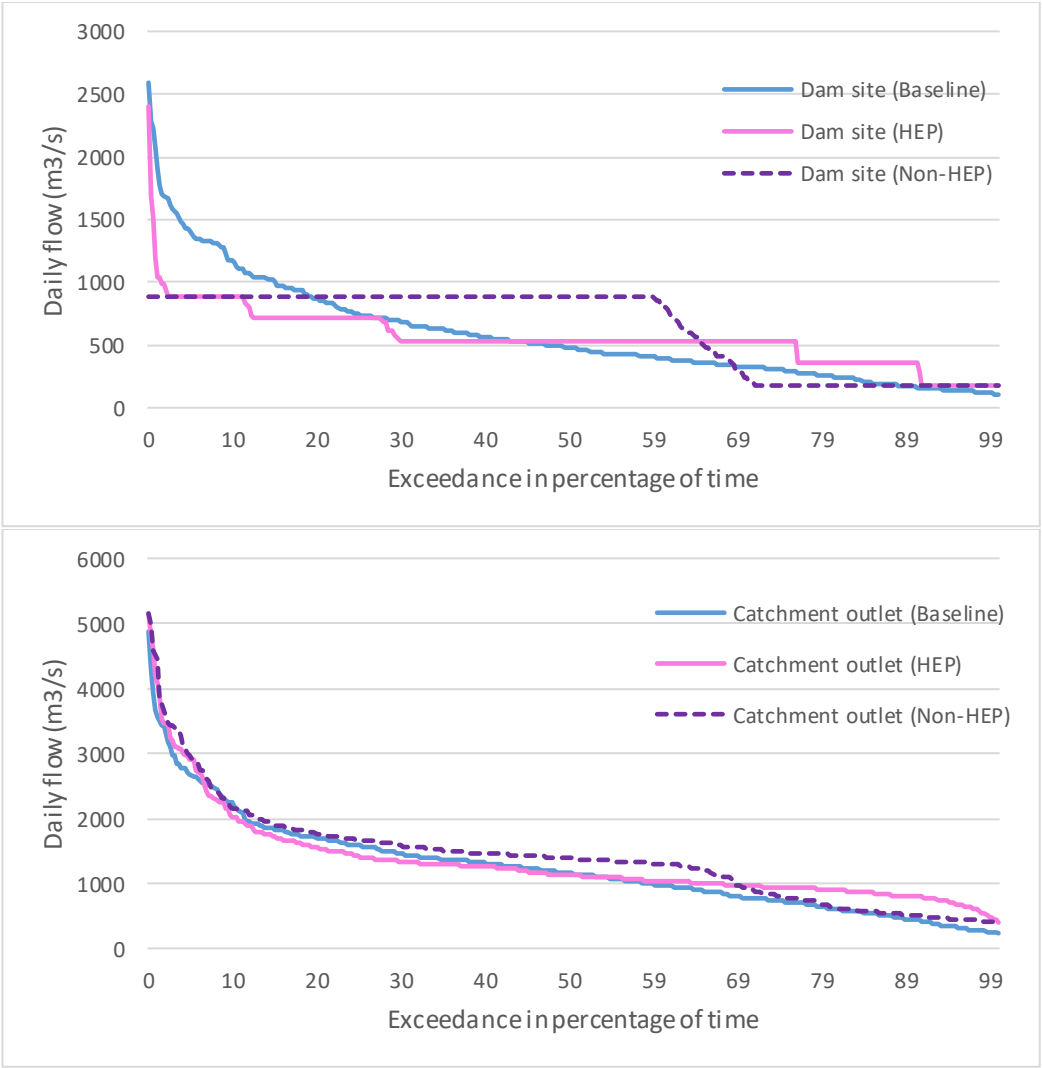

Figure 45 Top - Flow duration curves (FDC) comparing the baseline with the HEP and non-HEP scenario at the dam site (top) and catchment outlet (bottom). Only one of the randomisations of HEP was used as the representative.

A key issue in the Baleh is that at present (based on discussion with SEB, the funders of this project) the precise dam operational regime remains unclear; consequently, both modelled scenarios are hypothetical. The operation of hydroelectric power stations is driven by the demand for electricity so dams may produce different types of flow pulses at different times of the year, depending on this demand. These irregular discharges will adversely affect fishes and other aquatic organisms through downstream displacement, stranding, and spawning/rearing disruption (Ngor et al., 2018; Young et al., 2011). A study by Räsänen et al. (2012) on the hydrological impacts of the Lancang-Jiang hydropower dam cascade also reported higher overall flows at the most downstream point due to much higher dam releases during the wet season. The two dam operational regimes applied in the current study resulted in the volume of water being discharged into the mainstream of the Rajang increasing somewhat (for some flow percentiles). Räsänen et al. (2012) stressed that their findings were due to the parameters they used for their dam operations, and the same caveat applies to the current study – rather than the hypothetical scenarios, ideally impacts should be assessed for actual dam operational regimes.

Suspended sediment plays an important role in transporting nutrients, forming the riverbed landscape and creating or (in excessive amounts) causing a deterioration in ecological habitats (Junk et al., 1989). Baleh dam was predicted to trap about 95% of the sediment inflow from all the upstream reaches so there would be a drastic reduction in sediment loads at the reach directly downstream from the dam site and potentially a marked change in sediment supply to all the downstream reaches. The sediment load immediately downstream from the dam was very different for the HEP and Non-HEP scenarios. Based on Figure 36, the HEP scenario resulted in 'medium' daily sediment loads (391-645 tonnes) prevailing for most of the time (for 55% of the year) while the Non-HEP scenario had 'high' daily sediment loads (646-1154 tonnes) for most of the time (62% of the year).

The non-HEP scenario produced higher total annual sediment loads than the HEP scenario, which was expected since it released more sediment than the HEP scenario at the dam site. Since the dam was reducing the sediment supplied to the immediately downstream reach by around 95%, it was surprising that the daily simulated sediment loads at the catchment outlet with the dam in place were 4 to 10 times higher and the total annual sediment load was 4 times higher than the pre-dam, baseline conditions. The sediment-starved flows downstream of dams have a greater potential for bed incision and bank erosion (Gordon & Meentemeyer, 2006; Van Cappellen & Maavara, 2016) and these degradation processes may contribute to the higher downstream loads predicted for the Baleh. Critically though, these seemingly high loads may be artefacts of the short length of the SWAT simulations related to dam impacts on flows and sediment (i.e. 5 years with 2 for calibration and 3 for results); this timescale only provides insights into immediate, short term effects of the dam which may not represent the long term new 'equilibrium' state (see 5.7 for further discussion of this).

Varying the day of the HEP flow releases through the 50 randomisations used in SWAT did not have an effect on the overall patterns of sediment transport on an annual timescale. Thus, as far as overall sediment transport is concerned, the timing of the HEP releases is not critical. Figure 37 indicated however that the two scenarios had different implications for the temporal dynamics of sediment transport. There was a significant difference between the HEP and non-HEP scenarios in terms of accumulated frequencies (the HEP scenario higher percentage of total annual sediment accumulated in a smaller percentage of time). At the dam site, the HEP scenario was predicted to transport 50% of the load in 50% of the time. However, at the catchment outlet, simulations suggest that smaller frequencies of time carry a higher percentage of the load. This is indicative of the presence of flood events generated downstream from the dam that has a role in entraining and transporting sediment. It suggests an influence of tributaries entering between sites and how they play a role in the recovery of the river to a more "natural" state (Winton et al., 2019).

The combined impact of the dam under the HEP scenario and climate change was obvious in the daily flow values in the future (2030) at the catchment outlet as very high flows were drastically reduced (by 300-1400 m^3/s). However, for this scenario sediment load at the catchment outlet is predicted to be only slightly different (-4%) from the baseline value. This indicates a steady recovery of sediment supply from the various tributaries between the dam site and the catchment outlet.

5.6 Dam sedimentation

Reservoir sedimentation has always been a challenge for dam operators. Basson (2009) estimated an annual loss of 0.5 – 1% global dam storage volume. SEB included sediment yield estimates in their SEIA report for the Baleh dam. The report estimated 23.5 million tonnes of sediment retained in the dam per year with a trap efficiency of 97.3%. In comparison to SEB's estimation, SWAT predicts more than twice that amount between 2026 to 2031 (Table 21). Land cover change is expected to significantly increase sediment entering at the dam and increasing the amount of sediment stored by 580% as compared to the SEB value.

Table 21. Sediment deposited in the dam under the low deforestation + climate change scenario (L1R2) for the focal years.

Year	2026-2031	2032-2036	2047-2051
Sediment deposited in the dam per year (tonnes)	50,940,190	84,477,940	160,014,844
Percentage difference to SEB's estimation	+116%	+259%	+580%

Assuming a constant rate of sediment accumulation for the years 2037-2046 based on 2031-2036, the sediment accumulation in the dam was extracted from the SWAT model runs (Figure 46). SWAT predicted that approximately 5.5% of the dam would be filled with sediment in 25 years with low deforestation rates and climate change. This is not of major concern as it only contributes to 0.22% accumulated per year and will most likely not reduce the water storage capacity of the dam too significantly even in 2085 (50 years post-dam). The very large size of the reservoir (approximately 100 km long) likely limited the rate of storage capacity reduction.

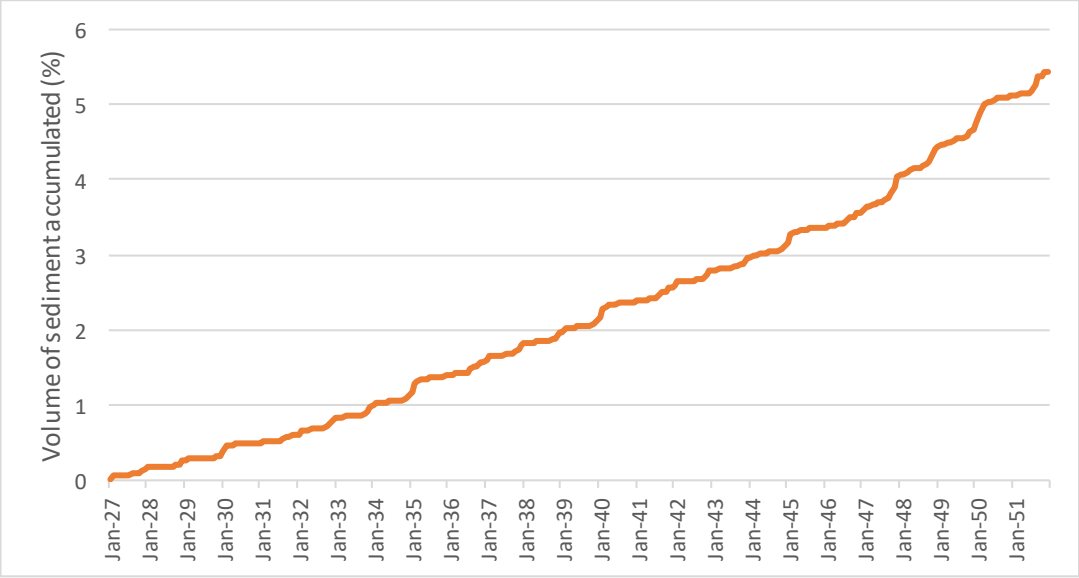

Figure 46. Sediment accumulation in the Baleh dam from 2027-2051. Volume is expressed as a percentage of the dam maximum capacity.

5.7 Long term adjustment in the Baleh river

At present (i.e. baseline, pre-dam conditions) there appears to be a reduction in sediment load in the first 23 km downstream from the dam site (i.e. sediment is lower at the point 23 km downstream than at point 0 km, at the dam site). In terms of the sediment budget of this section of the river, it seems that more sediment enters than exits this section, indicating net accumulation. This lack of competence may be due to physical conditions such as a low slope which causes sediment to be deposited rather than being transported downstream to the next reach. Similarly, channel geometry could differ from upstream (becoming wider) and this would reduce flow velocities and limit transport capacity. When the dam is incorporated in the SWAT model, due to sediment trapping, the load at point 0 km (dam site) is reduced to only around 5 % of the baseline level. However, the model suggests that with the dam in place, the sediment load has 'recovered' to its baseline value by 23 km downstream. Both dam operational scenarios result in higher mean flows, and together with the 'hungry water' effect caused by sediment trapping by the dam, may increase channel erosion associated with prevailing flows. This may explain the 'recovered' sediment load by 23 km.

Channel changes downstream from dams are spatially and chronologically complex. The behaviour of river channels below dams varies based on the degree of flood regulation and differs along the same river (Wolman, 1967). Different final states for rivers below dams are to be expected from different combinations of changes in flow regime and sediment loads along with variable rates and temporal sequences of changes (Petts & Gurnell, 2005). Figure 47 illustrates the hypothetical trajectory of fluvial metamorphosis following the installation and operation of a dam. There are three main stages: the natural regime state (N), the relaxation period (R1), and the adjusted regime state (A). The relaxation period can be separated into a reaction phase (Ra) and an adjustment phase (Ad).

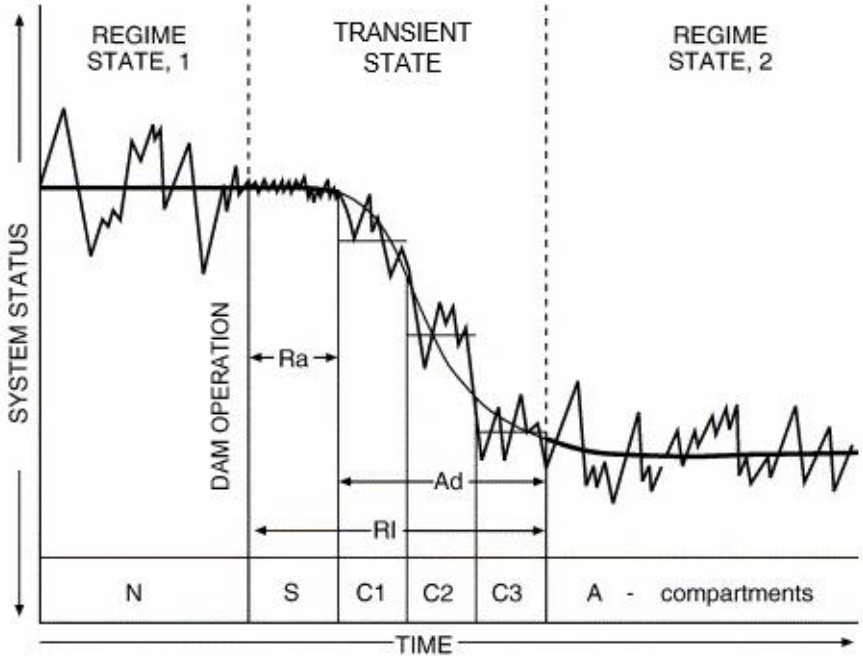

Figure 47. Trajectory and timeline of fluvial metamorphosis (Petts & Gurnell, 2005).

A detailed analysis of 21 dams in the United States found that channel degradation is at its peak once erosion begins soon after dam construction and experiences a gradual decline with time (Williams & Wolman, 1984). According to Petts & Gurnell (2005), a relaxation period of less than 10 years could be expected from environments with sand-bed channels, fast vegetation establishment and growth, and high sediment loads. Riparian vegetation (i.e. riparian trees and shrubs) have been suggested to play an active role in channel change through flow resistance and fine sediment deposition which promotes the succession towards a new post-dam steady-state (Gurnell & Petts, 2002). In other situations, it may take more than 100 years for a channel to achieve the adjusted regime state. These authors argued in this seminal paper that relaxation times vary between different climate regions and that downstream recovery distance in a given catchment depends on the number and dynamics of tributaries delivering water and sediments to the main stem.

Taking into account the high variability of relaxation times, rates of response and the direction of change, it is not unexpected that researchers are not able to predict the exact responses of river channels downstream from dams. Petts & Gurnell (2005) recommended that a period of 10-30 years be used for studies modelling the downstream effects of dams to capture the sequences of transient states which will evolve in response to the variation in flow and sediment loads in each reach and eventually arrive at the adjusted regime state. The SWAT model in this study has not been run continuously (i.e. future sediment predictions are short term runs, based on only the first 5 years of operation as described above in 5.5). Thus, the sediment yield predictions do not take into account the possible cumulative effect of successive years under a new flow and sediment supply regime following dam closure. To accurately examine the long term effects of the dam (up to 2050 as has been done for climate and land cover change), further modelling work will need to be undertaken to run the 25 years continuously. The value of this exercise will depend critically on the climate and land-cover scenarios used for the model runs, as flow and sediment inputs from downstream tributaries are key to the pace and spatial extent of relaxation and the adjusted state.

5.8 Limitations and future work

There are some limitations in this study that need to be acknowledged. Cloudiness in Borneo (as with tropical regions generally) affects the availability of multi-temporal cloud-free satellite images. This issue was addressed as best as possible with the use of image compositing algorithms. The incompleteness of the measured rainfall and temperature data obtained from the government meant that there were only 5 years of recent continuous data available to be used for the SWAT models. Reliable public domain climate datasets were used to fill the other data gaps so that the SWAT model can be run.

A key constraint for SWAT was that there is no continuous sediment data that could be used for calibration and validation (C&V) of the sediment output. Nevertheless, the predicted values of SSC (load divided by discharge) were consistent with an empirical assessment of SSC during a field survey in November 2019 (mainly undertaken for the purpose and landcover accuracy assessment) and broadly comparable with some historic SEB data (detailed in Methods). It is notable however that the C&V with flow data had a good performance, equalling or improving on those in published papers (Amirabadizadeh et al., 2018; Tan et al., 2015; Tarigan et al., 2018).

The future land cover and climate scenarios created for this study were informed by published literature. However, as published values for climate and land cover change in the region vary enormously, some judgement was needed to choose the more plausible ones (especially because it was impractical to run models covering all possible projections for both climate and land cover, along with different dam scenarios). Clearly, the SWAT simulation results are specific to the scenarios chosen and the effects observed on flow and sediment may not be extrapolated to other scenarios (e.g. some of the more extreme climate scenarios considered by Amin et al. (2016).

Last but not least, the absence of a definitive planned flow release regime for the Baleh dam that can be used as an input for the simulations caused uncertainties in this study. Hydropower dams operate by timing water releases to meet power production needs so there would need to be a projection of future electricity demand on a daily basis from SEB in order to improve on the scenarios modelled here. Therefore, while conclusions from the SWAT simulations are best considered to provide preliminary insights into flow and sediment dynamics, it is unlikely that more realistic scenarios can be devised at present. Further work will need to be done with SEB to fine-tune the simulations once the dam has started operating and its release regime is known.

References

Abbaspour, K. C. (2012). User manual for SWAT-CUP, SWAT calibration, and uncertainty analysis programs. *Swiss Federal Institute of Aquatic Science and Technology, Eawag, Duebendorf, Switzerland*, 93. https://swat.tamu.edu/media/114860/usermanual_swatcup.pdf

Abbaspour, K. C., Yang, J., Maximov, I., Siber, R., Bogner, K., Mieleitner, J., Zobrist, J., & Srinivasan, R. (2007). Modelling hydrology and water quality in the pre-alpine/alpine Thur watershed using SWAT. *Journal of Hydrology*, *333*(2–4), 413–430. https://doi.org/10.1016/j.jhydrol.2006.09.014

Abdullah, R. G. (2017). Accessibility and development. A case study from rural sarawak, Malaysia. *International Journal of Business and Society*, *18*(S4), 791–799.

Abu Bakar, Z. A., Madon, M., & Muhamad, A. J. (2007). Deep-marine sedimentary facies in the Belaga Formation (Cretaceous-Eocene), Sarawak: Observations from new outcrops in the Sibu and Tatau areas. *Bulletin of the Geological Society of Malaysia*, *53*, 35–45. https://doi.org/10.7186/bgsm53200707

Achard, F., Eva, H. D., Stibig, H. J., Mayaux, P., Gallego, J., Richards, T., & Malingreau, J. P. (2002). Determination of deforestation rates of the world's humid tropical forests. *Science*, *297*(5583), 999–1002. https://doi.org/10.1126/science.1070656

Alamgir, M., Campbell, M. J., Sloan, S., Engert, J., Word, J., & Laurance, W. F. (2020). Emerging challenges for sustainable development and forest conservation in Sarawak, Borneo. *PLoS ONE*, *15*(3). https://doi.org/10.1371/journal.pone.0229614

Amin, M. Z. M., Shaaban, A. J., Ohara, N., Kavvas, M. L., Chen, Z. Q., Kure, S., & Jang, S. (2016). Climate change assessment of water resources in sabah and sarawak, malaysia, based on dynamically-downscaled gcm projections using a regional hydroclimate model. *Journal of Hydrologic Engineering*, *21*(1), 05015015. https://doi.org/10.1061/(ASCE)HE.1943-5584.0001242

Amirabadizadeh, M., Halim, A., Feng, Y., & Wayayok, A. (2018). Assessment of impacts of future climate change on water resources of the Hulu Langat basin using the SWAT model. *Water Harvesting Research*, *2*(2), 13–29. www.jwhr.birjand.ac.ir

Arnold, J. G., Srinivasan, R., Muttiah, R. S., & Williams, J. R. (1998). Large area hydrologic modeling and assessment part I: Model development. *Journal of the American Water Resources Association*, *34*(1), 73–89. https://doi.org/10.1111/j.1752-1688.1998.tb05961.x

Askari, M., Tanaka, T., Setiawan, B., & Saptomo, S. (2008). Infiltration characteristics of tropical soil based on water retention data. *Journal Of Japan Society Of Hydrology And Water Resources*, *21*(3), 215-227. https://doi.org/10.3178/jjshwr.21.215

Athukorala, P., & Narayanan, S. (2018). Economic corridors and regional development: The Malaysian experience. *World Development*, *106*, 1-14. https://doi.org/10.1016/j.worlddev.2018.01.009

Basson, G. R. (2009). Management of siltation in existing and new reservoirs. *General Report Q. 89, Proceedings (on CD) of the 23rd Congress of the Int. Commission on Large Dams CIGB-ICOLD*.

Brander, L., Tai, B., Crossman, N., & Yeo, B. H. (2018). *Natural Capital Valuation using primary data research methods in Baleh, Sarawak Heart of Borneo Project area*.

Breiman, L. (2001). Random forests. *Machine Learning*, *45*(1), 5–32. https://doi.org/10.1023/A:1010933404324

Bryan, J. E., Shearman, P. L., Asner, G. P., Knapp, D. E., Aoro, G., & Lokes, B. (2013). Extreme differences in forest degradation in Borneo: Comparing practices in Sarawak, Sabah, and Brunei. *PLoS ONE*, *8*(7). https://doi.org/10.1371/journal.pone.0069679

Chang, C., Tseng, W., Hsu, H., Keenlyside, N., & Tsuang, B. (2015). The Madden-Julian Oscillation in a warmer world. *Geophysical Research Letters*, *42*(14), 6034-6042. https://doi.org/10.1002/2015gl065095

Cheng, Y., Yu, L., Cracknell, A. P., & Gong, P. (2016). Oil palm mapping using Landsat and PALSAR: A case study in Malaysia. *International Journal of Remote Sensing*, *37*(22), 5431–5442. https://doi.org/10.1080/01431161.2016.1241448

Cleophas, F., Musta, B., Puah, M. ., & Bidin, K. (2017). Runoff and soil erosion in selectively-logged over forest, Danum Valley Sabah, Malaysia. *Transactions on Science and Technology*, *4*(4), 449–459.

Cushman, S. A., Macdonald, E. A., Landguth, E. L., Malhi, Y., & Macdonald, D. W. (2017). Multiple-scale prediction of forest loss risk across Borneo. *Landscape Ecology*, *32*(8), 1581–1598. https://doi.org/10.1007/s10980-017-0520-0

Devia, G. K., Ganasri, B. P., & Dwarakish, G. S. (2015). A review on hydrological models. *Aquatic Procedia*, *4*, 1001–1007. https://doi.org/10.1016/j.aqpro.2015.02.126

Diong, J. Y., Yip, W. S., MatAdam, M. K., Chang, N. K., Yunus, F., & Abdullah, M. H. (2015). The definitions of the southwest monsoon climatological onset and withdrawal over Malaysian region. *Malaysian Meteorological Department*, *3*, 1–30. https://www.researchgate.net/publication/325314115

Douglas, I., Greer, T., Bidin, K., & Spilsbury, M. (1993). Impacts of rainforest logging on river systems and communities in Malaysia and Kalimantan. *Global Ecology & Biogeography Letters*, *3*(4–6), 245–252. https://doi.org/10.2307/2997773

Duan, Z., Tuo, Y., Liu, J., Gao, H., Song, X., Zhang, Z., Yang, L., & Mekonnen, D. F. (2019). Hydrological evaluation of open-access precipitation and air temperature datasets using SWAT in a poorly gauged basin in Ethiopia. *Journal of Hydrology*, *569*, 612–626. https://doi.org/10.1016/j.jhydrol.2018.12.026

Dudgeon, D. (1992). Endangered ecosystems: A review of the conservation status of tropical Asian rivers. *Hydrobiologia*, *248*(3), 167–191. https://doi.org/10.1007/BF00006146

Energy Commission. (2020). *Malaysia energy statistics handbook 2020*. Putrajaya.

Gaveau, D. L. A., Sloan, S., Molidena, E., Yaen, H., Sheil, D., Abram, N. K., Ancrenaz, M., Nasi, R., Quinones, M., Wielaard, N., & Meijaard, E. (2014). Four decades of forest persistence, clearance and logging on Borneo. *PLoS ONE*, *9*(7). https://doi.org/10.1371/journal.pone.0101654

Gaveau, D., Sheil, D., Husnayaen, Salim, M., Arjasakusuma, S., & Ancrenaz, M. et al. (2016). Rapid conversions and avoided deforestation: Examining four decades of industrial plantation expansion in Borneo. *Scientific Reports*, *6*(1). https://doi.org/10.1038/srep32017

Gomyo, M., & Koichiro, K. (2009). Spatial and temporal variations in rainfall and the ENSO-rainfall relationship over Sarawak, Malaysian Borneo. *Scientific Online Letters on the Atmosphere*, *5*, 41–44. https://doi.org/10.2151/sola.2009-011

Gordon, E., & Meentemeyer, R. K. (2006). Effects of dam operation and land use on stream channel morphology and riparian vegetation. *Geomorphology*, *82*(3–4), 412–429. https://doi.org/10.1016/j.geomorph.2006.06.001

Gorelick, N., Hancher, M., Dixon, M., Ilyushchenko, S., Thau, D., & Moore, R. (2017). Google Earth Engine: Planetary-scale geospatial analysis for everyone. *Remote Sensing of Environment*, *202*, 18–27. https://doi.org/10.1016/j.rse.2017.06.031

Gupta, H. V., Sorooshian, S., & Yapo, P. O. (1999). Status of automatic calibration for hydrologic models: Comparison with multilevel expert calibration. *Journal of Hydrologic Engineering*, *4*(2), 135–143. https://doi.org/10.1061/(asce)1084-0699(1999)4:2(135)

Gurnell, A. M., & Petts, G. E. (2002). Island-dominated landscapes of large floodplain rivers, a European perspective. *Freshwater Biology*, *47*(4), 581–600. https://doi.org/10.1046/j.1365-2427.2002.00923.x

Haddeland, I., Heinke, J., Biemans, H., Eisner, S., Flörke, M., Hanasaki, N., Konzmann, M., Ludwig, F., Masaki, Y., Schewe, J., Stacke, T., Tessler, Z. D., Wada, Y., & Wisser, D. (2014). Global water resources affected by human interventions and climate change. *Proceedings of the National Academy of Sciences of the United States of America*, *111*(9), 3251–3256. https://doi.org/10.1073/pnas.1222475110

Hall, F. G., Strebel, D. E., Nickeson, J. E., & Goetz, S. J. (1991). Radiometric rectification: Toward a common radiometric response among multidate, multisensor images. *Remote Sensing of Environment*, *35*(1), 11–27. https://doi.org/10.1016/0034-4257(91)90062-B

Hansen, M. C., Potapov, P. V., Moore, R., Hancher, M., Turubanova, S. A., Tyukavina, A., Thau, D., Stehman, S. V., Goetz, S. J., Loveland, T. R., Kommareddy, A., Egorov, A., Chini, L., Justice, C. O., & Townshend, J. R. G. (2013). High-resolution global maps of 21st-century forest cover change. *Science*, *342*(6160), 850–853. https://doi.org/10.1126/science.1244693

Hidayat, R., & Kizu, S. (2010). Influence of the Madden-Julian Oscillation on Indonesian rainfall variability in austral summer. *International Journal of Climatology*, *30*(12), 1816–1825. https://doi.org/10.1002/joc.2005

Hon, J., & Shibata, S. (2013). A review on land use in the Malaysian state of Sarawak, Borneo and recommendations for wildlife conservation inside production forest environment. *Borneo Journal of Resource Science and Technology*, *3*(2), 22–35. https://doi.org/10.33736/bjrst.244.2013

Hu, Y., & Hu, Y. (2019). Land cover changes and their driving mechanisms in Central Asia from 2001 to 2017 supported by Google Earth Engine. *Remote Sensing*, *11*(5). https://doi.org/10.3390/rs11050554

Hurni, K., Schneider, A., Heinimann, A., Nong, D. H., & Fox, J. (2017). Mapping the expansion of

boom crops in Mainland Southeast Asia using dense time stacks of landsat data. *Remote Sensing*, *9*(4), 320. https://doi.org/10.3390/rs9040320

IPCC. (2007). Summary for policymakers. In: Climate Change 2007: The physical science basis. Contribution of working group I to the fourth assessment report of the Intergovernmental Panel on Climate Change. In *Cambridge University Press, Cambridge, United Kingdom and New York, NY, USA.* https://doi.org/10.1038/446727a

Issaka, S., & Ashraf, M. A. (2017). Impact of soil erosion and degradation on water quality: A review. *Geology, Ecology, and Landscapes*, *1*(1), 1–11. https://doi.org/10.1080/24749508.2017.1301053

Jadczyszyn, J., & Niedzwiecki, J. (2005). Relation of saturated hydraulic conductivity to soil losses. *Polish Journal of Environmental Studies*, *14*(4), 431–435. https://www.researchgate.net/publication/273138184_Relation_of_saturated_hydraulic_conductivity_to_soil_losses

Jhonnerie, R., Siregar, V. P., Nababan, B., Prasetyo, L. B., & Wouthuyzen, S. (2015). Random forest classification for mangrove land cover mapping using Landsat 5 TM and ALOS PALSAR imageries. *Procedia Environmental Sciences*, *24*, 215–221. https://doi.org/10.1016/j.proenv.2015.03.028

Junk, W. J., Bayley, P. B., & Sparks, R. E. (1989). The flood pulse concept in river-floodplain systems. In D. P. Dodge (Ed.), *Proceedings of the International Large River Symposium* (pp. 110–127). Ca. Sepc. Publ. Fish. Aquat. Sci.

Khoi, D. N., & Suetsugi, T. (2014). Impact of climate and land-use changes on hydrological processes and sediment yield - a case study of the Be River catchment, Vietnam. *Hydrological Sciences Journal*, *59*(5), 1095–1108. https://doi.org/10.1080/02626667.2013.819433

Kondolf, G. M. (1997). Hungry water: Effects of dams and gravel mining on river channels. *Environmental Management*, *21*(4), 533–551. https://doi.org/10.1007/s002679900048

Kondolf, G. M., Rubin, Z. K., & Minear, J. T. (2014). Dams on the Mekong: Cumulative sediment starvation. *Water Resources Research*, *50*, 5158–5169. https://doi.org/10.1002/2013WR014979.

Kummu, M., & Sarkkula, J. (2008). Impact of the Mekong River flow alteration on the Tonle Sap flood pulse. *AMBIO: A Journal Of The Human Environment*, *37*(3), 185-192. https://doi.org/10.1579/0044-7447(2008)37[185:iotmrf]2.0.co;2

Kundzewicz, Z. W. (2008). Climate change impacts on the hydrological cycle. *Ecohydrology and Hydrobiology*, *8*(2–4), 195–203. https://doi.org/10.2478/v10104-009-0015-y

Kundzewicz, Z. W., Mata, L. J., Arnell, N. W., Döll, P., Kabat, B., Jimenez, B., Miller, K. A., Oki, T., Sen, Z., & Shiklomanov, I. A. (2007). Freshwater resources and their management. *Climate Change 2007: Impacts, Adaptation and Vulnerability. Contribution OfWorking Group II to the Fourth Assessment Report of the Intergovernmental Panel on Climate Change*, *December 2016*, 173–210.

Landsat 8. Landsat Science | A joint NASA/USGS Earth observation program. (2021). Retrieved 11 March 2022, from https://landsat.gsfc.nasa.gov/satellites/landsat-8/.

Lauri, H., Räsänen, T. A., & Kummu, M. (2014). Using reanalysis and remotely sensed temperature and precipitation data for hydrological modeling in monsoon climate: Mekong River case study. *Journal of Hydrometeorology*, *15*(4), 1532–1545. https://doi.org/10.1175/jhm-d-13-084.1

Li, P., Feng, Z., & Xiao, C. (2018). Acquisition probability differences in cloud coverage of the available Landsat observations over mainland Southeast Asia from 1986 to 2015. *International Journal of Digital Earth*, *11*(5), 437–450. https://doi.org/10.1080/17538947.2017.1327619

Li, X., Xiao, Q., Niu, J., Dymond, S., van Doorn, N. S., Yu, X., Xie, B., Lv, X., Zhang, K., & Li, J. (2016). Process-based rainfall interception by small trees in Northern China: The effect of rainfall traits and crown structure characteristics. *Agricultural and Forest Meteorology*, *218–219*, 65–73. https://doi.org/10.1016/j.agrformet.2015.11.017

Liew, Y. S., Sim, S. F., Ling, T. Y., Nyanti, L., & Grinang, J. (2020). Relationships between water quality and dissolved metal concentrations in a tropical river under the impacts of land use, incorporating multiple linear regression (MLR). *AACL Bioflux*, *13*(2), 470–480. http://www.bioflux.com.ro/aacl

Lim, S., Marzin, C., Xavier, P., Chang, C., & Timbal, B. (2017). Impacts of Boreal Winter Monsoon Cold Surges and the Interaction with MJO on Southeast Asia Rainfall. *Journal Of Climate*, *30*(11), 4267-4281. https://doi.org/10.1175/jcli-d-16-0546.1

Ling, T. Y., Soo, C. L., Heng, T. L. E., Nyanti, L., Sim, S. F., & Grinang, J. (2016). Physicochemical characteristics of river water downstream of a large tropical hydroelectric dam. *Journal of Chemistry*, *2016*. https://doi.org/10.1155/2016/7895234

Ling, T. Y., Soo, C. L., Kho, C. P., Nyanti, L., Sim, S. F., Lee, K. S. P., & Ganyai, T. (2019). Changes in water and sediment quality of a river being impounded and differences among functional zones of the new large tropical hydroelectric reservoir. *Polish Journal of Environmental Studies*, *28*(6), 4271–4285. https://doi.org/10.15244/pjoes/97397

Ling, T. Y., Soo, C. L., Sivalingam, J. R., Nyanti, L., Sim, S. F., & Grinang, J. (2016). Assessment of the water and sediment quality of tropical forest streams in upper reaches of the Baleh River, Sarawak, Malaysia, subjected to logging activities. *Journal of Chemistry*, *2016*. https://doi.org/10.1155/2016/8503931

Loh, J. Le, Tangang, F., Juneng, L., Hein, D., & Lee, D. I. (2016). Projected rainfall and temperature changes over Malaysia at the end of the 21st century based on PRECIS modelling system. *Asia-Pacific Journal of Atmospheric Sciences*, *52*(2), 191–208. https://doi.org/10.1007/s13143-016-0019-7

Markham, B. L., Storey, J. C., Williams, D. L., & Irons, J. R. (2004). Landsat sensor performance: History and current status. *IEEE TRANSACTIONS ON GEOSCIENCE AND REMOTE SENSING*, *42*(12). https://doi.org/10.1109/TGRS.2004.840720

Mas, J. F. (1999). Monitoring land-cover changes: A comparison of change detection techniques. *International Journal of Remote Sensing*, *20*(1), 139–152. http://www.tandf.co.uk/JNLS/res.htm

Miettinen, J., Shi, C., & Liew, S. C. (2019). Towards automated 10–30 m resolution land cover mapping in insular South-East Asia. *Geocarto International*, *34*(4), 443–457.

https://doi.org/10.1080/10106049.2017.1408700

Mohd-Azlan, J., Yi, M. C. K., Lip, B., & Hon, J. (2019). Camera trapping of wildlife in the newly established Baleh National Park, Sarawak. *Journal of Sustainability Science and Management*, *14*(4), 51–64.

Moriasi, D. N., Gitau, M. W., Pai, N., Daggupati, P., Gitau, M. W., Member, A., & Moriasi, D. N. (2015). Hydrologic and water quality models: Performance measures and evaluation criteria. *Transactions of the ASABE*, *58*(6), 1763–1785. https://doi.org/10.13031/trans.58.10715

Muli, A., Yee Ling, T.-, Sim, S.-F., & Grinang, J. (2019). Macroinvertebrates of the tributaries of Upper Baleh River, Sarawak. *Borneo Journal of Resource Science and Technology*, *9*(1), 26–35. https://doi.org/10.33736/bjrst.1582.2019

Nash, J. E., & Sutcliffe, J. V. (1970). River flow forecasting through conceptual models part I - A discussion of principles. *Journal of Hydrology*, *10*(3), 282–290. https://doi.org/10.1016/0022-1694(70)90255-6

Neitsch, S. L., Arnold, J. G., Kiniry, J. R., & Williams, J. R. (2011). *Soil and Water Assessment Tool Theoretical Documentation Version 2009*.

Ngor, P., Legendre, P., Oberdorff, T., & Lek, S. (2018). Flow alterations by dams shaped fish assemblage dynamics in the complex Mekong-3S river system. *Ecological Indicators*, *88*, 103-114. https://doi.org/10.1016/j.ecolind.2018.01.023

Nilsson, C., Reidy, C., Dynesius, M., & Revenga, C. (2005). Fragmentation and Flow Regulation of the World's Large River Systems. *Science*, *308*(5720), 405-408. https://doi.org/10.1126/science.1107887

Nyanti, L., Idris, N. E., Bolhen, H., Grinang, J., Ling, T. Y., Sim, S.-F., Soo, C.-L., Ganyai, T., & Suan Ping, K. L.-. (2019). Fish assemblages, growth pattern and environmental factors in Upper Baleh River, Kapit, Sarawak. *Borneo Journal of Resource Science and Technology*, *9*(1), 14–25. https://doi.org/10.33736/bjrst.1581.2019

Oliphant, A. J., Thenkabail, P. S., Teluguntla, P., Xiong, J., Gumma, M. K., Congalton, R. G., & Yadav, K. (2019). Mapping cropland extent of Southeast and Northeast Asia using multi-year time-series Landsat 30-m data using a random forest classifier on the Google Earth Engine Cloud. *International Journal of Applied Earth Observation and Geoinformation*, *81*, 110–124. https://doi.org/10.1016/j.jag.2018.11.014

Ouyang, W., Hao, F., Skidmore, A. K., & Toxopeus, A. G. (2010). Soil erosion and sediment yield and their relationships with vegetation cover in upper stream of the Yellow River. *Science of the Total Environment*, *409*(2), 396–403. https://doi.org/10.1016/j.scitotenv.2010.10.020

Öztürk, M., Copty, N. K., & Saysel, A. K. (2013). Modeling the impact of land use change on the hydrology of a rural watershed. *Journal of Hydrology*, *497*, 97–109. https://doi.org/10.1016/j.jhydrol.2013.05.022

Persoon, G., & Osseweijer, M. (2008). *Reflections on the heart of Borneo*. Tropenbos International.

Petts, G. E., & Gurnell, A. M. (2005). Dams and geomorphology: Research progress and future directions. *Geomorphology*, *71*(1–2), 27–47. https://doi.org/10.1016/j.geomorph.2004.02.015

Pimple, U., Simonetti, D., Sitthi, A., Pungkul, S., Leadprathom, K., Skupek, H., Som-ard, J., Gond, V., & Towprayoon, S. (2018). Google Earth Engine based three decadal Landsat Imagery analysis for mapping of mangrove forests and its surroundings in the Trat province of Thailand. *Journal of Computer and Communications*, *06*(01), 247–264. https://doi.org/10.4236/jcc.2018.61025

Poff, N. L., Allan, J. D., Bain, M. B., Karr, J. R., Prestegaard, K. L., Richter, B. D., Sparks, R. E., & Stromberg, J. C. (1997). The natural flow regime. *BioScience*, *47*(11), 769–784. https://doi.org/10.2307/1313099

Rafiei Emam, A., Kappas, M., Fassnacht, S., & Linh, N. H. K. (2018). Uncertainty analysis of hydrological modeling in a tropical area using different algorithms. *Frontiers of Earth Science*, *12*(4), 661–671. https://doi.org/10.1007/s11707-018-0695-y

Räsänen, T., Koponen, J., Lauri, H., & Kummu, M. (2012). Downstream hydrological impacts of hydropower development in the Upper Mekong Basin. *Water Resources Management*, *26*(12), 3495-3513. https://doi.org/10.1007/s11269-012-0087-0

Sa'adi, Z., Shahid, S., Chung, E. S., & Ismail, T. bin. (2017). Projection of spatial and temporal changes of rainfall in Sarawak of Borneo Island using statistical downscaling of CMIP5 models. *Atmospheric Research*, *197*. https://doi.org/10.1016/j.atmosres.2017.08.002

Sa'adi, Z., Shahid, S., Ismail, T., Chung, E. S., & Wang, X. J. (2017). Distributional changes in rainfall and river flow in Sarawak, Malaysia. *Asia-Pacific Journal of Atmospheric Sciences*, *53*(4), 489–500. https://doi.org/10.1007/s13143-017-0051-2

Shivhare, N., Dikshit, P. K. S., & Dwivedi, S. B. (2018). A comparison of SWAT model calibration techniques for hydrological modeling in the Ganga River Watershed. *Engineering*, *4*(5), 643–652. https://doi.org/10.1016/j.eng.2018.08.012

Sim, S. F., Ling, T. Y., Nyanti, L., Gerunsin, N., Wong, Y. E., & Kho, L. P. (2016). Assessment of heavy metals in water, sediment, and fishes of a large tropical hydroelectric dam in Sarawak, Malaysia. *Journal of Chemistry*, *2016*. https://doi.org/10.1155/2016/8923183

Singh, A. (1989). Review Article: Digital change detection techniques using remotely-sensed data. *International Journal of Remote Sensing*, *10*(6), 989–1003. https://doi.org/10.1080/01431168908903939

Sodhi, N. S., Koh, L. P., Brook, B. W., & Ng, P. K. L. (2004). Southeast Asian biodiversity: An impending disaster. In *Trends in Ecology and Evolution* (Vol. 19, Issue 12, pp. 654–660). Elsevier. https://doi.org/10.1016/j.tree.2004.09.006

Sternberg, R. (2010). Hydropower's future, the environment, and global electricity systems. *Renewable and Sustainable Energy Reviews*, *14*(2), 713–723. https://doi.org/10.1016/J.RSER.2009.08.016

Sovacool, B. K., & Bulan, L. C. (2012). Energy security and hydropower development in Malaysia: The drivers and challenges facing the Sarawak Corridor of Renewable Energy (SCORE). *Renewable Energy*, *40*(1), 113–129. https://doi.org/10.1016/j.renene.2011.09.032

Stibig, H. J., Achard, F., Carboni, S., Raši, R., & Miettinen, J. (2014). Change in tropical forest cover of Southeast Asia from 1990 to 2010. *Biogeosciences*, *11*(2), 247–258. https://doi.org/10.5194/bg-11-247-2014

Syvitski, J. P. M., Cohen, S., Kettner, A. J., & Brakenridge, G. R. (2014). How important and different are tropical rivers? - An overview. *Geomorphology*, *227*, 5–17. https://doi.org/10.1016/j.geomorph.2014.02.029

Tan, M. L., Gassman, P. W., & Cracknell, A. P. (2017). Assessment of three long-term gridded climate products for hydro-climatic simulations in tropical river basins. *Water (Switzerland)*, *9*(3). https://doi.org/10.3390/w9030229

Tan, M. L., Gassman, P. W., Srinivasan, R., Arnold, J. G., & Yang, X. Y. (2019). A review of SWAT studies in Southeast Asia: Applications, challenges and future directions. In *Water (Switzerland)* (Vol. 11, Issue 5, pp. 1–25). https://doi.org/10.3390/w11050914

Tan, M. L., Ibrahim, A. L., Yusop, Z., Duan, Z., & Ling, L. (2015). Impacts of land-use and climate variability on hydrological components in the Johor River basin, Malaysia. *Hydrological Sciences Journal*, *60*(5), 873–889. https://doi.org/10.1080/02626667.2014.967246

Tarigan, S., Wiegand, K., Sunarti, & Slamet, B. (2018). Minimum forest cover required for sustainable water flow regulation of a watershed: A case study in Jambi Province, Indonesia. *Hydrology and Earth System Sciences*, *22*(1), 581–594. https://doi.org/10.5194/hess-22-581-2018

Tie, Y. L. (1982). *Soil classification in Sarawak*. Soils Division, Dept. of Agriculture.

Townshend, J. R., Masek, J. G., Huang, C., Vermote, E. F., Gao, F., Channan, S., Sexton, J. O., Feng, M., Narasimhan, R., Kim, D., Song, K., Song, D., Song, X. P., Noojipady, P., Tan, B., Hansen, M. C., Li, M., & Wolfe, R. E. (2012). Global characterization and monitoring of forest cover using Landsat data: Opportunities and challenges. *International Journal of Digital Earth*, *5*(5), 373–397. https://doi.org/10.1080/17538947.2012.713190

Tuen, A. A., Sapian, A. F., Ismail, K., Peter, C., Haba, M. H. A.-H., & Lee, C. C. (2018). Avifauna in logged-over forest of Upper Baleh, Sarawak. *Borneo Journal of Resource Science and Technology*, *8*(2), 66–74. https://doi.org/10.33736/bjrst.1197.2018

Valentin, C., Agus, F., Alamban, R., Boosaner, A., Bricquet, J. P., Chaplot, V., de Guzman, T., de Rouw, A., Janeau, J. L., Orange, D., Phachomphonh, K., Do Duy Phai, Podwojewski, P., Ribolzi, O., Silvera, N., Subagyono, K., Thiébaux, J. P., Tran Duc Toan, & Vadari, T. (2008). Runoff and sediment losses from 27 upland catchments in Southeast Asia: Impact of rapid land use changes and conservation practices. *Agriculture, Ecosystems and Environment*, *128*(4), 225–238. https://doi.org/10.1016/j.agee.2008.06.004

Van Cappellen, P., & Maavara, T. (2016). Rivers in the Anthropocene: Global scale modifications of riverine nutrient fluxes by damming. *Ecohydrology and Hydrobiology*, *16*(2), 106–111. https://doi.org/10.1016/j.ecohyd.2016.04.001

Vijith, H., Hurmain, A., & Dodge-Wan, D. (2018). Impacts of land use changes and land cover alteration on soil erosion rates and vulnerability of tropical mountain ranges in Borneo. *Remote Sensing Applications: Society and Environment*, *12*, 57–69. https://doi.org/10.1016/j.rsase.2018.09.003

Walling, D. (2011). Human impact on the sediment loads of Asian rivers. In *Sediment Problems and Sediment Management in Asian River Basins*. Hyderabad, India; IAHS Publ.

Wera, F. A., Ling, T. Y., Nyanti, L., Sim, S. F., & Grinang, J. (2019). Effects of opened and closed spillway operations of a large tropical hydroelectric dam on the water quality of the downstream river. *Journal of Chemistry*, *2019*. https://doi.org/10.1155/2019/6567107

White, J. C., Wulder, M. A., Hobart, G. W., Luther, J. E., Hermosilla, T., Griffiths, P., Coops, N. C., Hall, R. J., Hostert, P., Dyk, A., & Guindon, L. (2014). Pixel-based image compositing for large-area dense time series applications and science. *Canadian Journal of Remote Sensing*, *40*(3), 192–212. https://doi.org/10.1080/07038992.2014.945827

Winemiller, K., McIntyre, P., Castello, L., Fluet-Chouinard, E., Giarrizzo, T., & Nam, S. et al. (2016). Balancing hydropower and biodiversity in the Amazon, Congo, and Mekong. *Science*, *351*(6269), 128-129. https://doi.org/10.1126/science.aac7082

Williams, G. P., & Wolman, M. G. (1984). Downstream effects of dams on alluvial rivers. *United States Geological Survey Professional Paper*, 1286.

Winton, R. S., Calamita, E., & Wehrli, B. (2019). Reviews and syntheses: Dams, water quality and tropical reservoir stratification. In *Biogeosciences* (Vol. 16, Issue 8, pp. 1657–1671). Copernicus GmbH. https://doi.org/10.5194/bg-16-1657-2019

Woldesenbet, T. A., Elagib, N. A., Ribbe, L., & Heinrich, J. (2017). Hydrological responses to land use/cover changes in the source region of the Upper Blue Nile Basin, Ethiopia. *Science of the Total Environment*, *575*, 724–741. https://doi.org/10.1016/j.scitotenv.2016.09.124

Wolman, M. G. (1967). Two problems involving river channels and their background observations. *Northwest. Univ. Stud. Geogr.*, *14*, 67–107.

Young, P., Cech, J., & Thompson, L. (2011). Hydropower-related pulsed-flow impacts on stream fishes: a brief review, conceptual model, knowledge gaps, and research needs. *Reviews In Fish Biology And Fisheries*, *21*(4), 713-731. https://doi.org/10.1007/s11160-011-9211-0

Zarfl, C., Lumsdon, A. E., Berlekamp, J., Tydecks, L., & Tockner, K. (2015). A global boom in hydropower dam construction. *Aquatic Sciences*, *77*(1), 161–170. https://doi.org/10.1007/s00027-014-0377-0

Appendix

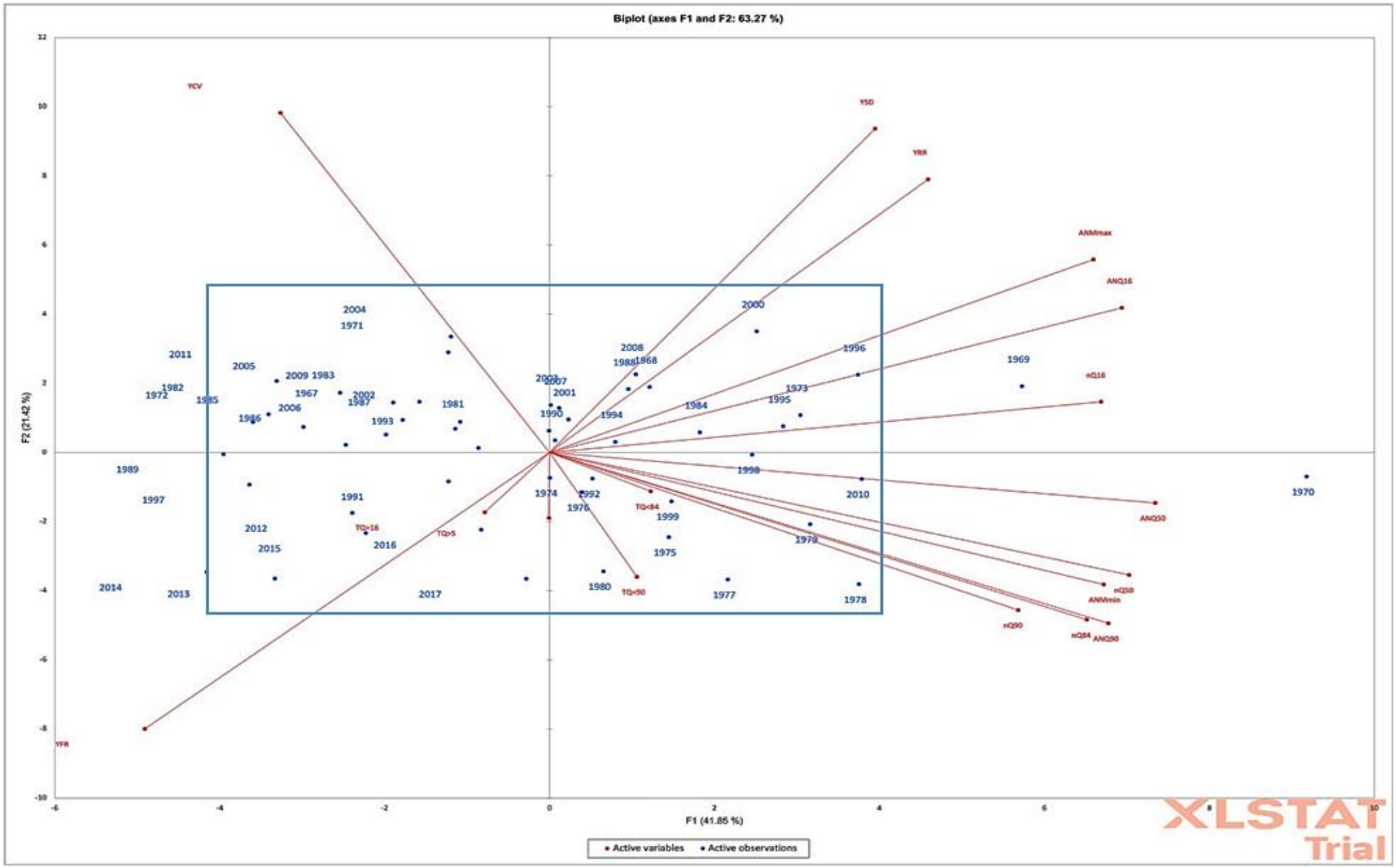

Figure A: Full size of Figure 4.

Table A. Total sediment yield values for all scenarios in focal years.

Scenarios	*Years used*	*1st-year total sediment yield (tonnes)*	*2nd-year total sediment yield (tonnes)*	*3rd-year total sediment yield (tonnes)*	*Average total sediment yield within 3 years (tonnes)*
Baseline	**2015, 2016, 2017**	107,616,218	149,233,451	102,663,629	119,837,766
2030 L1	**2029, 2030, 2031**	186,868,413	184,890,735	156,354,731	176,037,960
2030 L1R2		113,669,614	164,670,137	143,444,862	140,594,871
2030 L2		203,183,147	285,927,889	326,606,435	271,905,824
2030 L2R2		176,221,964	258,502,934	304,761,524	246,495,474
2035 L1	**2034, 2035, 2036**	194,736,099	259,588,989	254,298,223	236,207,770
2035 L1R2		165,452,701	227,686,911	218,200,590	203,780,068
2035 L2		431,250,469	524,239,494	618,323,429	524,604,464
2035 L2R2		371,865,364	460,944,557	545,068,968	459,292,963
2050 L1	**2049, 2050, 2051**	440,031,310	558,158,944	518,696,131	505,628,795
2050 L1R2		278,794,743	340,351,139	379,388,997	332,844,960
2050 L2		894,556,629	1,027,253,611	1,084,198,212	1,002,002,817
2050 L2R2		600,920,413	706,473,511	838,032,479	715,142,134

Table B. Observational data from 35 Tropical rivers obtained from Syvitski et al., (2014)

River	Country	Upstream Area (km^2)	Qavg (m^3/s)	Qs (Mt/yr)	Cs (Kg/m^3)	Yield ($T/km^2/yr$)
Amazon	Brazil	4618746	155430	1193	0.24	193
Congo	Congo	3475000	40223	43	0.03	12
Niger	Nigeria	2000000	4976	40	0.25	35
Orinoco	Brazil	939362	34500	173	0.16	180
Toncantins	Brazil	760000	11668	75	0.21	98
Sao Francisco	Brazil	510800	282	6.3	0.07	12
Volta	Ghana	394100	1212	19	0.49	48
Godavari	India	299320	3157	170	2.03	611
Magdalena	Columbia	251743	7530	220	0.65	868
Krishna	India	251355	1783	64	1.26	283
Mahanadi	India	142207	211	61	0.97	440
Chao Phraya	Thailand	141843	963	11	0.36	70
Fly	PNG	64413	5676	80	0.88	1146
Brahmani	India	52000	1135	20	0.56	383
Ca	Vietnam	27061	949	4	0.13	147
Tano	Ghana	15800	151	0.3	0.07	19
Cimanuk	Indonesia	4200	139	20	4.54	4738
Citanduy	Indonesia	3560	192	9.5	1.57	2666
Pamanga	Philippines	830	47	1	0.68	1205
Angat	Philippines	780	49	4.6	2.93	5862
Cilulung	India	600	30	4.8	5.03	7937
Cimuntur	Indonesia	580	30	1.9	2.01	3262
Grande	Puerto Rico	230	15	0.4	0.89	1739
Durabo	Puerto Rico	160	8	0.3	1.05	1875
Waikele	Hawaii	116	1	0.1	2.81	1147
Baleh (baseline)	Malaysia	12250	1159	3.6	0.09	296